Universitá degli Studi di Napoli Federico II

PhD in Fundamental and Applied Physics
XXIV cycle

Jamming transition in thermal and non-thermal systems

Candidate:
Raffaele Pastore

pastore@na.infn.it

Tutors:
Prof. Antonio Coniglio

Dr. Massimo Pica Ciamarra

29 Novembre 2011

"Immortale é chi accetta l'istante.
Chi non conosce piú un domani."

Cesare Pavese

"L'essentiel est invisible
pour le yeux."

Antoine de Saint Exupéry

A mio zio Angelo,
modello ineguagliabile di
umanitá e cultura,
che ancora vive...

A Chi ha aperto i miei occhi
e l' anima alla vita...
donandomi istanti di immortalitá.

Preface

"The Bishop, with the reliquary in his hand, walked slowly backward and forward in front of the alter, with rhythmical movements he raised the coagulated blood up high, between the two gold framed glass panels, as if he were cradling a child, a terrible new born fetish. The deacon shadowed the bishop's movements and with the light from candle illuminated the contents of the reliquary, the dry coagulated blood from behind. The bishop turned the reliquary slowly to the right and to the left, to show that the blood had not yet liquefied...then something happened that went beyond that party decorated fetish, and the wining women, and the blood that in the end begun to liquefy inside the reliquary, so that the bishop triumphantly raised it with a undulating and rhythmical movement, showing that the vial had filled with liquefied blood...something different. In the chapel, the women that awaited he miracle had begun to shout, then suddenly to clamour and applaud, because the show had succeeded...But apart from that something very different had happened inside us kneeling in front of the altar staring at the glass panel in which the liquefied blood re-boiled. Within us...Something real beyond resistance, suspicions and superstitions...We had understood that not only that which can be controlled exists. There is also that which cannot be proven, that cannot be checked...There is still another possibility."

In this piece from his romance 'Saint Januarius blood', the great hungarian writer Sandor Marai vividly describes a dramatic and ancient rite which takes place in Naples twice a year, in honour of the patron saint.

In scientific terms, the liquefaction of the blood, under the oscillations of bishop, is an example of a transition known as Jamming (more precisely Unjamming transition, as the first name is referred to the inverse, liquid-solid, transformation). The fact that this is associated to a miracle by the popular culture may sound as consolatory for many researchers working in this field. At the same time, the scientific appeal produced by this intriguing phenomenon, in its wide occurrence, resembles the feeling of believers toward the Saint's relic... Indeed, despite a great deal of efforts, the Jamming is still

source of several open questions.

Fortunately, not all material samples are so special as the blood of a Saint, and jamming systems usually exhibit a more reproducible phenomenology...

This thesis try to shed some light on the 'mysterious' nature of this phenomenon.

Contents

Chapter 1

Introduction

Liquid-Solid transitions are usually associated to crystallization and onset of order in the structure of a material. However, crystallization is not the only mechanism to pass from a liquid to a solid state, and probably it is not the most widespread. Indeed, many physical systems are able to transform from a fluid-like state to a solid-like state, both having a disordered internal structure. For instance, this transition occurs in molecular liquids and colloids upon varying thermodynamic variables, such as temperature and density, or in granular materials and foams when the applied stress is lowered, or when internal variables, such as the inter-particle friction, are changed.

These are some of the many faces of a very general paradigm, known as Jamming. The present framework in this field has been mainly developed along two lines, which concern thermal and non-thermal systems, respectively. These systems represent opposite but complementary aspects of the transition: in one case we are dealing with molecular systems, where the temperature plays a central role, in the other case, instead, constituents particles are object so large to be insensitive to thermal effects. In this Thesis we focus on two topics which are representative of the thermal and non-thermal case, respectively Jamming of simple liquids, also known as glass transition, and Jamming of granular materials.

Glass transition is a long debated question in condensed matter physics. In the last decades several models has been proposed, also inspired by previous advances in theory of critical phenomena and mean-field systems. However, a global understanding of this phenomenon is still far to reach.

In particular, when a liquid is cooled below the melting temperature fast enough to avoid crystallization, its relaxation time increases by many orders of magnitude, until it overcomes any experimentally available time-scale: then we get a glass. Understanding such a dramatic growth of relaxation time, when the temperature is lowered, is the main challenge in this field.

Experimental evidences and theoretical models predict the emergence of Dynamic Heterogeneities (DHs), i.e. clusters of particles dynamically correlated during times and over lengths, whose typical size grows on approaching the glassy phase. It is largely accepted that large relaxation time and large cluster life-times are not juxtaposed phenomena, but they are strictly related in glass forming liquids. However, this point is still elusive and structure and dynamics of DHs need to be investigated to clarify their relation with the structural relaxation process. Thus, in this work we will study:

- structure and evolution of dynamical clusters

- to what extent DHs are tangled with structural relaxation

To this aim, we have investigated via Monte Carlo simulations the 'Kob-Andersen model'. This is a popular glass former model, implemented on a cubic lattice, and based on the idea that glassy dynamics essentially results from a frustrated kinetics.

We find that, contrary to current expectations, relaxation process and DHs are characterized by different time-scales. This implies that they have a distinct physical origin. We provide a geometrical interpretation of the relaxation processes, and of the different observed time-scales. Indeed, we show that the relaxation time is related to a reverse percolation transition, whereas the emergence of dynamical clusters is related to the spatial correlation created by the motion of diffusing defects.

With respect to glasses, granular materials are a recent challenge in condensed matter physics. In this systems, the temperature plays no role and the particle interactions are strongly dissipative. These peculiarities make the problem completely different from those provided by classical statistical mechanics, so that the present understanding in this field still holds at a phenomenological level.

In granular materials Jamming essentially arises as a rheological effect. In response to an external stress, loose granular systems flow as a liquid, while, at high density, they deform as an elastic solid. Jamming marks the edge between this two limiting regimes, and systems near the transition exhibit very peculiar mechanical properties. For systems of soft frictionless spheres, in the limit of small applied stress, the transition is sharply defined: the system is found in a liquid-like or solid-like depending on the density and stress values. For more realistic system, the onset of Jamming may be no more sharp and different time-scales possibly affect the state of the systems, inducing transient regimes. In this case, the phenomenology is much more

complex and still poorly investigated. In particular, here we ask in which way the presence of inter-particle friction influences the transition.

To this aim, we have investigated, via molecular dynamic simulations, a system of soft frictional spheres at constant volume and subject to a constant external shear stress.

We find that, in the presence of friction, new rheological regimes appear, where the systems transiently flow before jamming. We describe this rich phenomenology introducing a jamming phase diagram with axes density, shear stress, and friction coefficient. We show that the resulting jammed states are characterized by different mechanical and structural properties. Between the observed regimes, a particularly intriguing case stands out: it is characterized by extremely long processes, with a diverging timescale, whereby a suspension first flows but then suddenly jams. We described a possible dynamical mechanism able to explain the observed behaviour.

1.1 Plan of the work

The work is organized as follow.

Chapter 2: Here we provide a preliminary discussion of the Jamming, where we define the transition in its generality. In Sec. 2.1 we introduce the jamming phase diagram as an useful tools to describe the behaviour of different systems, and we discuss the concept of Universality, according to which Jamming transition has general aspects that are insensitive to system details. In Sec. 2.2 we briefly describe the basic phenomenology of several jamming materials.

Chapter 3: We focus on the main topics of this work, namely glass transition and jamming of granular materials. Sec. 3.1 describes the main experimental and numerical facts regarding the behaviour of glass forming liquids. Sec. 3.2 is devoted to granular materials, starting from the simplest case of soft frictionless sphere at zero stress, where the jamming transition is well defined, and extending the discussion to the case of more realistic systems. Finally we illustrates the concept of 'fragile matter', which has been claimed to capture the peculiarity of mechanical properties observed in jammed granular materials

Chapter 4: Here we review the present understanding of glass transition. Sec. 4.1 describe experimental and numerical evidences supporting the existence of Dynamic Heterogeneities and describe a largely accepted scenario for their role in glassy dynamics. In Sec. 4.2 we describe the most quoted theoretical model for Jamming, particularly focusing on Mode Coupling Theory, Random First Order Theory and Facilitation.

Chapter 5: Here we illustrate our results on the Kob-Andersen Model. In Sec. 5.1 we describe the investigated model. Sec. 5.2 focuses on the dynamic correlation function we use to monitor the relaxation, namely the persistence. Sec. 5.3 is devoted to the behaviour of Dynamic Heterogeneities. In Sec. 5.4 we give a geometrical interpretation of Dynamic Heterogeneities and relaxation processes in terms of diffusing defects and of a reverse dynamical percolation.
This chapter is based on Ref. (a) and (b).

Chapter 6: Here we illustrate our results on the Jamming transition of frictional granular material. In Sec. 6.1 we describe the investigated system and the numerical procedures. Sec. 6.2 illustrates the different dynamical regimes observed. This phenomenology is conveniently described by the 3-dimensional jamming phase diagram presented in Sec. 6.3. In Sec. 6.4 we discuss the mechanical properties of the jammed states obtained in the different regimes. In Sec. 6.5 we focus on an intriguing regime which is present in the jamming phase diagram, we named as 'Flow & Jam' regime.
This chapter is based on Ref. (c), (d) and (e).

Chapter 7: Finally, we summarizes our results and sketch some possible future developments of this work.

The results presented in this Thesis have been published in the following papers:

(a) R. Pastore, M. Pica Ciamarra, A. de Candia and A. Coniglio, *Dynamical Correlation Length and Relaxation Processes in a Glass Former*, Physical Review Letters 107, 065703 (2011).

(b) A. Coniglio, T. Abete, A. de Candia, E. Del Gado, A. Fierro, R. Pastore and M. Pica Ciamarra, *Geometrical characterization of dynamical heteorgeneities in chemical gels, colloidal gels and colloidal glasses*, accepted in Proceedings of the International School of Physics 'E. Fermi', Course CLXXVI - 'Complex materials in physics and biology'.

(c) M. Pica Ciamarra, R. Pastore, M. Nicodemi and A. Coniglio, *Jamming phase diagram for frictional particles*, Physical Review E 84, 041308 (2011).

(d) R. Pastore, M. Pica Ciamarra and A. Coniglio, *'Flow & Jam' of frictional athermal systems under shear stress*, Philosophical Magazine 91,13, 2006 (2011).

(e) R. Pastore, M. Pica Ciamarra and A. Coniglio, *Mechanical response of jammed granular materials and the question of 'fragility'*, to appear in Granular Matter.

Chapter 2

Jamming

The Jamming is a non-equilibrium transition form a fluid-like to a disorder solid-like state, occurring in many materials by varying the system control parameters.

This is a general definition, but the world "Jamming" may be found in literature with different meanings. In facts, historically it has been first used mainly to indicate the zero temperature limit of the glass transition; only later the term gets the wider significance we adopt here and which includes the glass transition as a particular case. We will stress this topic in the next section dealing with the concept of universality and jamming phase diagram.

A fundamental precursor of the transition is represented by a slowing-down of the dynamics, where relaxation time and viscosity dramatically increase. In general, jammed systems show special mechanical properties, that are distinctive in respect of ordinary solids.

In order to avoid confusion, we want to point out that the Jamming strongly differs from the thermodynamic liquid-crystal transition. In fact, one mainly observes a dynamical phenomenon where the system gets trapped in a small region of phase space without chance to escape, at least for times comparable with typical experimental time-scales.

Understanding the Jamming transition is a fundamental challenge in many different fields including soft matter physics, processing advanced materials, transport processes of industrial nature and geophysics, where, for example, the Jamming is involved in mechanisms of faults generating earthquakes. This wide interest is motivated by the fact that Jamming occurs in material as different as simple liquids, colloids, granular materials, emulsions and bubbles. These materials, when jammed, give rise for example to glasses, gels, jammed grains, compressed emulsions and foams. Fig. 2.1 makes this concept more concrete by showing several examples of jamming materials usually met in the everyday life.

Figure 2.1: Examples of common jammed materials: (a) Granular media, consisting of solid grains in gas or vacuum. (b) Toothpaste, a dense packing of (colloidal) particles in fluid. (c) Mayonnaise, an emulsion consisting of a dense packing of (oil) droplets in an immiscible fluid. (d) Shaving foam, a dense packing of gas bubbles in fluid (from Ref. [2]).

2.1 Universality and jamming phase diagram

Now one may ask in which way these systems can pass from a liquid to a jammed phase: in general the relevant control parameters of the transition are the temperature, the density, and the intensity of an external stress (or "load" more in general). Interestingly, the properties observed on varying the control parameters suggest that Jamming transitions share an universal nature not strongly dependendent on microscopic details of specific materials. Inspired by this idea, Liu and Nagel sketched a 3-dimensional jamming phase diagram, reproduced in Fig. 2.2 which has on its axes the main control parameters. Such a diagram is just of a speculative kind and all its suggestion cannot be taken in a strictly quantitative sense, but, citing the authors, it has the merit of *"bring together several different types of behaviour under one rubric"*. The diagram stresses that for high density, low temperature and small external stress, a volume exists where systems are in a jammed state. The surface of this volume represents the boundaries of the transition. Note that the zero-load plane coincides with the domain investigated for simple liquids, and the intersection of the jamming surface with this plane represents the glass transition line. Analogously, in the zero-temperature plane we recover the case of non-thermal systems, i.e. whose constituent particles are too large to be sensitive to the temperature: this is the case, for

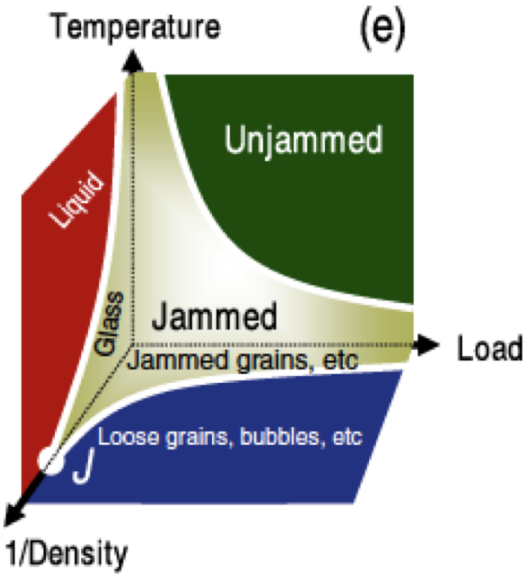

Figure 2.2: Speculative jamming phase diagram proposed by Liu and Nagel (from Ref. [2]).

example, of frictionless granular materials and foams. Here the intersection with the jamming surface is the yield stress line in the zero-temperature limit. By increasing the stress, the threshold density also increases. More in general, the shape of the jamming surface provides a reciprocal dependence for the threshold values of temperature, density and stress. This suggests that, for example, a glass may have a lower glass transition temperature under high shear stress and a jammed granular material may have a lower yield stress when forced in random motions, able to mimic thermal fluctuations.

2.1.1 Universality: "pro" and "contra"

After Liu and Nagel, the use of phase diagrams has become widespread in the community working on the jamming transition and their proposal has been intensively investigated.

In particular Trappe et al. [3] obtained a jamming phase diagram for attractive colloids, based on experimental measurements: a liquid colloid is transformed into a jammed solid by increasing the volume fraction, increasing the attractive energy (we will see in Sec. 2.2.2 that for attractive systems it corresponds to lower T), or decreasing the external shear stress. In each case, an almost identical phase transition has been reached and the structures

optically observed appear very similar, both on the fluid and solid side. This jamming phase diagram confirms that the concept of jamming may be fairly extended to the behaviour of different systems, highlighting the similarity between gelation and glass transition.

O'Hern et al. [24] identified a special point on the density axis where, in the zero-load and zero-temperature limit, frictionless jamming materials behaves in the same way. This point, known as *point-J*, seems to be really universal and it seems to control the location of the jamming surface. Near point-J, frictionless system may be modeled as a spheres system, no matter if hard or soft. In fact, in the limit of low temperature and stress, the involved energy are so small that hard and soft spheres are indistinguishable, although a particular choose may be motivated by computational chances. Under this condition, spheres models jam near the value already known for the random close packing (*rcp*). In reality, it should be more correct to say that point-J provides a precise definition for the elusive concept of *rcp* and not the opposite: we will clarify this point later when we deal with the behaviour at point-J in more details.

However, the experimental jamming surface of Ref.[3] shows everywhere a curvature which is opposite respect the one originally provided by Liu and Nagel and diverges at each corner as a consequence of particular details of attractive colloids. In general, now it seems to be clear that the shape of the entire jamming surface depends, at least quantitatively, by the specific system. A precise experimental location of the surface may be hard to define, particularly in the context of glasses, where, approaching the jamming transition, the relaxation time may increase too rapid for providing a reliable extrapolation of the divergence. Moreover, beyond temperature, density and stress, other parameters can in some case influence the transition: for example, for non-thermal systems, the presence of inter-particle friction plays an important role.

Summarizing, we can conclude that the jamming transition is a powerful concept in the understanding of apparently diverse fluid to solid transformation found in very different systems. For concrete applications, the use of jamming phase diagram is generally able to highlight the parameters that should be changed to get a desired response.

2.2 Jamming materials

Jamming occurs in wide variety of physical systems in response to the variation of some control parameters. In this section we will briefly review the main categories of jamming materials introducing a little bit of phenomenol-

ogy and focusing on control parameters and protocols used to get the transition.

2.2.1 Simple Liquids

Between jamming systems, a special case is represented by simple liquids. Unlike the other jamming materials, here we are dealing with monophase systems whose elemental constituents are molecules, so that, they are homogeneous also at scales smaller than nanometers. Because of these peculiarities, jamming of simple liquids is rather known as *glass transition* and in the past it has been perceived as a independent enough research field.

Glasses, the jammed states of simple liquids, are amorphous solids lacking the periodicity of crystals [4]. The most relevant control parameter to get a glass from a simple liquids are the temperature and the cooling rate. As any student book of physics teaches, lowering the temperature of a liquid below a certain value T_m , a first order phase transition to the crystal occurs: T_m is the melting temperature and the crystal represents the stable phase below it. Nevertheless in practice the situation is more complex: in fact, by cooling the liquid fast enough, it is possible to get the liquid phase also below T_m, avoiding crystallization. Such protocol is known as *supercooling*, and the liquid phase obtained below T_m as *supercooled liquid* or *glass-former liquid*.

Upon supercooling below T_m, the dynamics rapidly slows down as molecules rearrange so slowly that they are not able to explore phase space in the time allowed by the cooling rates[6]. Accordingly the structure of the liquid appears frozen on time scales which are larger and larger as the temperature is lowered; as a consequence longer and longer experiments are needed to understand whether the sample is really a liquid. In more quantitative terms, in a small range of temperature relaxation times and viscosities are found to increase of several orders of magnitude, a growth which seems dramatic if compared with the small increase occurring above T_m. In particular, by lowering the temperature below a value T_g, as much as one can wait, it becomes not possible to observe the liquid flowing, ...then, a glass has been obtained.

T_g is known as the *glass temperature* and it has been operatively defined as the point where the relaxation time exceeds any realistic experimental timescales. The value of T_g depends on the material and it is found to slightly increase for slower cooling rate. However as general rule we can state that $T_g \simeq T_m$. Here we have introduced some basics about the phenomenology of the glass transition, although these topics will be extensively discussed in Chap. 3.1.

2.2.2 Colloids

Colloidal systems are widespread in their occurrence and have a fundamental importance in many fields from the biological to the technological ones. Like the term "Jamming", also the term colloids is used in literature with a large range of meanings. In its wider definition a colloid consists in a disperse phase distributed uniformly inside a continuous medium. No matter the nature of the disperse phase and of the dispersion medium, which may be gas, liquid or solid. The only constraint concern with the dispersed particles sizes, which must range between the nm and the μm, i.e larger than the molecular scale but typically small enough to feel brownian effects. Using this definition, almost all materials, we will treat in the following paragraphs, may be classified as colloids. While we will devote to other types of dispersion later, here we refer to colloid in its narrow sense of a dispersion of compact and solid particles in a liquid medium, i.e. materials which can be modeled as systems of brownian spheres in a liquid.

The most relevant control parameter of colloidal systems is the density of the disperse phase, which is set explicitly by its volume fraction ϕ. At low volume fraction colloids behaves like liquids, but increasing the volume fraction they jam in *gels*, if attractive interaction are present, or in *colloidal glasses*. A gel just forms at small volume fraction of the order of 10^{-1}: in facts, its weight is mainly due to a liquid matrix, while its rigidity arises from a stress-bearing backbone of colloidal particles. In particular, in this section we will deal with a *physical gels*, to distinguish it from the *chemical gels*, where the bonds are irreversible due to their chemical origin. If able to remain liquid at higher volume fraction (about $\phi = 0.5$), colloids mimic the behaviour of atomic systems [9], whereby colloidal particles are the counterparts of atoms on a larger scale (and interestingly optically observable): eventually they may order in colloidal crystal, but, if crystallization is avoided, colloidal glasses are formed.

Let we do a slightly more detailed discussion: the difference between gel-forming and glass-forming colloids consists in the interaction between particles. Repulsive forces always dominate at very short inter-particle distance. When short-ranged attraction, set by a potential U, is also present, the particles will form clusters. As bonds between particles have a physical origin, the clusters are of a dynamical kind, i.e. they are formed and destroyed continuously, but their life-time rapidly grows with ϕ. As the volume fraction reaches a critical threshold ϕ_j a percolating cluster forms, whose relaxation time exceeds the experimental time-scales [8]. At this point we get a gel: it is solid as the percolating cluster behaves as a stress-bearing backbone . The critical volume fraction ϕ_j decreases as the energy U increases and the

temperature decreases. From this point of view, what is really important becomes the competition between the potential which tends to aggregate and the brownian motion which instead tends to restore fluidity. Consequently, the relevant control parameter is the ratio $\frac{K_BT}{U}$. Also the presence of an external shear stress σ affects the formation of a solid cluster, shifting ϕ_j to higher values with increasing σ. In general, a sufficient large stress will cause the gel to yield and flow; thus the yield stress, σ_y may be considered the third control parameters for jamming of attractive colloids, together with ϕ_j and $\frac{U}{K_BT}$ [3].

If U is set to zero, gels cannot exist and solid response arises only as a consequence of more compact structures. If the volume fraction is slowly increased crystal forms and progressively grows in phase coexistence with liquid, until that the sample is completely crystallized [9]. However, rapidly increasing ϕ and high polydispersity (which may be defined as the standard deviation of the particle size distribution divided by its mean) slow down crystal nucleation. Then, if crystallization is avoided, the particles remain frozen in a glass, very similar to molecular glasses except for the larger length scales and the weaker energy involved. Such systems are very well approximated by a hard-spheres system [11] which jams at the *rcp*, $\phi_c = \phi_{rcp} = 0.63$. In this case T just rescales the typical relaxation times, thus becoming marginal, while the volume fraction remains the only relevant control parameter for colloidal glass forming.

2.2.3 Polymers

In this paragraph, we are dealing with the case of polymers solved in liquids: polymers may link each other via chemical bonds, which can be consider as *permanent* or *irreversible*, as their bonding energy is larger than thermal K_BT and stress energies typically involved. Jamming of such materials, known as *chemical gelation* or *sol-gel transition*, transforms a solution of polymeric molecules, the sol, from a viscous liquid to an elastic disordered solid, the gel [10].

Increasing the density of the solved phase, polymers aggregate to form macropolymers, which can be considered statical clusters, as the nature of the bonds does not allow for a dynamic rearrangement. This results in a critical increase of the viscosity accompanied by a slowing down of the relaxation dynamics. When a critical value for the density ϕ_j is reached, the onset of the elastic response corresponds to the constitution inside the sol of a macroscopic polymeric structure [12, 13] which spans the whole system. Percolation is considered as the basic model for the transition [14] and the macromolecular stress-bearing structure in these systems is a percolating

network of permanent bonds.

As thermal effects are not able to inhibit chemical bonding, temperature is not a relevant control parameters but only rescales the typical relaxation times as in the case of hard spheres glasses. Also the intensity of the applied stress does not play an important role. Thus, also in this case, the density is the only important control parameter: from this point of view chemical gels and hard spheres systems represent two opposite limits. In the former Jamming already occurs at very small density of the order of $\phi_j = 10^{-2}$ as a results of the strong chemical attractions, while in the latter the transition occurs at very high density, just due to geometrical constraints and repulsions. Finally, the case of attractive colloids, where bonds have a finite life-time, is in between these two extremes.

We want only mention that chemical bonds is not an essential ingredient to get Jamming in polymeric materials as very different mechanisms may be involved. For instance, long polymers in the state of melt or of concentrated solution tend to geometrically entangle [15] in a network whose relaxation time becomes increasingly larger.

2.2.4 Emulsion and Foams

Here we consider both emulsions consisting of droplets of one liquid dispersed in another immiscible liquid, and, foams, which are dispersions of gas bubbles in a liquid. In spite of their different phase composition, these materials present large similarities in the basic properties and have a very rich rheology, useful for industrial applications. First, the droplets/bubbles sizes are such that thermal effects can be typically neglected (except for the case of *microemulsions* not considered here). On the one hand, dissipative effects are important. On the other hand, here we are dealing with system which are not conservative: number and volume fraction of the droplets/bubbles may spontaneously evolve in time due to processes, such as coalescence, Ostwald ripening and water drainage [16], which can be neglected only on small time scales.

Composition, microscopic structure, interfacial interactions and polydispersity are fundamental in determining the rheology of these materials [17]. The volume fraction ϕ of droplets/bubbles and the yield stress σ_y of the jammed states are the more relevant control parameters. By increasing ϕ, the liquid layers that separates nearby droplets/bubbles are thinner and thinner, until that they become a film . During the flow, high local shear rates are created in these films, which results in relatively high viscous dissipation of energy. The bubble/droplet deformability leads to non-linear dependences of the film thickness and of the resulting flow characteristics of foams and

emulsions on the applied shear stress [18].

A jamming transition is found from a simple viscous liquid to an elastic solid when the volume fraction increases up to a threshold ϕ_j, which, in the limit of low stress, is very close to the random close packing of hard spheres [19]. In general, foam bubbles, as well as emulsion droplets may be rather approximated as soft spheres, a system which is paradigmatic in the fields of the Jamming transition. In facts, the elastic interaction between droplets/bubbles are suitably modeled as a linear spring, while static friction is absent and only a velocity dependent viscous friction is present under flow [20].

2.2.5 Granular materials

Granular materials, like sands and powder, are ubiquitous in nature and represent the most treated materials in industrial processes. They are becoming a paradigmatic example of complex systems. We devote to the Jamming of granular materials the second part of Chap. 3.2. In this paragraph we just mention some basic and general aspects (see [21] [22] for a nice reviews).

Granular materials are assemblies of solid particles eventually dispersed in a liquid (wet) or in a gas (dry) phase. The typical particle size d larger than one μm is the main characteristic, which sets a sharp distinction with colloids and makes granular media the most representative case of non-thermal system. In facts, the thermal energy $K_B T$ is always smaller than the characteristic energy scale mgd, i.e. the work needed to shift a particle of an height equal to its linear size under the effect of its weight. This implies that temperature and brownian motions play no role. Usually, the interactions are limited to contact forces, such as non-elastic collisions and frictions. From the non conservative nature of these forces, an other important property arises: granular materials are dissipative systems, i.e. they tend to dissipate in time the kinetic energy they have at disposal. Thus, in order to actively investigate the dynamics, energy must be continuously introduced from the outside, for example by means of vibrations or stresses. This is why the intensity of the external load together with the volume fraction ϕ are the main control parameters of the rheology of granular media. In particular at low volume fraction (well below the rcp) and in absence of gravitation ($g = 0$), granular materials behave as a fluid, although very special, also in the limit of zero stress. Increasing ϕ until a critical value ϕ_j, the system jams in a solid-like state: in these conditions, crowding of grains results in a network of contact forces which balances the external stress. The critical value for the volume fraction depends on the stress, $\phi_j = \phi_j(\sigma)$, as clarified by the zero temperature plane of the jamming phase diagram of Fig.2.2. In

facts, increasing the stress favors the flow, shifting ϕ_j to larger values. Other characteristics, such as polydispersity and particle shape, may play a role in the rheology. In this work, we will show that also friction influences the Jamming of granular media, as a further control parameter.

In the case frictionless particles, in the limit of zero applied stress, granular systems jams at the *rcp* of hard spheres [24].

Moreover, simple models of chains of hard spheres have inspired the idea that jammed granular media represents a new class of solids, known as *fragile matter* [23], that cannot be considered as an elastic body also for small stresses. In facts, based on these models, jammed grains can support also a large applied stress in the direction of the force which has driven the system to jam, but the chains break and the system restarts flowing, if even an infinitesimal force is applied in a different direction. In order to avoid such a paradoxical consequence, it has been suggested that soft spheres are more suitable to model the behaviour of granular materials: allowing the particles to deform, in facts, give raise to a macroscopic elastic response, at least for small enough stresses [1]. Although the idea of fragility is able to capture some of the physics of this materials, such as strong anisotropy, in this work, we will show that for realistic granular systems it clearly fails.

Chapter 3

Supercooled liquids and Granular materials

In this chapter we describe in more details the phenomenology and some basics questions concerning glass formers and dense granular materials.

3.1 Supercooled liquids at equilibrium

A wide variety of liquids, supercooled below the glass transition temperature T_g , form glasses. T_g is operatively defined as the temperature where the relaxation times exceeds the experimental time. Typical values of cooling rate used in laboratory experiments are $0.1 - 100\ K/min$ and, as a general rule, the cooling rate must be large enough to avoid crystallization; we remind to Chap. 3 of Ref. [6] for a discussion on the mechanisms and the conditions that allow to avoid nucleation and growth of crystals. Here we only remark that for temperature below the melting temperature T_m the typical time for crystallization may be sensibly larger than relaxation times. In this case, between T_m and T_g, the system can equilibrate in an *equilibrium* supercooled liquid. The distinct nature of glass and supercooled liquid phases need to be clarified also to avoid confusion in the terminology.

Below T_m we are always dealing with a metastable phase: for time long enough the system crystallizes. Nevertheless, on shorter time-scales, we refer to *supercooled liquid* or to *glass-forming liquids* to indicate a liquid phase which is at equilibrium, not in the thermodynamic meaning, but in the sense that time-translation invariance (TTI) (and thus the dynamical fluctuation dissipation theorem) holds. Under these conditions the only observable accounting for metastability is the explicit crystallization of the sample.

Below T_g relaxation times are too large to equilibrate the system and TTI

is broken: the word *glass* indicates the resulting out of equilibrium material.

Summarizing, in the equilibrium metastable phase the typical time for crystallization is larger than our experimental time but the relaxation time is still shorter , whereas in an off-equilibrium glass also the relaxation time of the substance is too large compared to our experimental time. Here we suppose that above T_g is always possible to equilibrate our liquid on supercooling and we will focus on the equilibrium case disregarding the topics strictly related with the field of glasses.

3.1.1 A more precise definition of T_g

The operative definition of glass transition temperature, T_g, introduces a dependence on the available experimental time t_{exp}, and thus on the cooling rate. Indeed, T_g decreases with the cooling rate. However, as we will see in the next section, the relaxation time is extremely sensitive to the temperature, so that changes in the cooling rate causes a negligible variation of T_g. Thus, T_g can be defined as the temperature where the relaxation time τ overcomes a conventional threshold, of the order of the experimental time-scales. Say [25]:

$$\tau(T_g) \simeq 10^2 - 10^3 Sec. \tag{3.1}$$

τ can be extracted from the temporal decay of density fluctuations.

The *Maxwell relation*, $\eta = G_\infty \tau$, which relates the viscosity η to the relaxation time τ via the insatntaneous shear modulus G_∞, allows for an alternative definition of T_g. Indeed, since $G_\infty \simeq 10^{10} - 10^{11} dyne/cm^2$ and its value does not vary considerably in the supercooling regimes, η and τ are proportional and we can define T_g as the temperature where :

$$\eta(T_g) \simeq 10^{13} Poise. \tag{3.2}$$

Note that around the melting temperature typical values are $\tau \simeq 10^{-12} Sec.$ and $\eta \simeq 10^{-2} Poise$. This means that at the glass transition $T_g \simeq 2/3 T_m$ these quantities grow about of 14 orders of magnitude!

While we can do almost nothing to get equilibrium liquids below T_g, by contrast, in some circumstances the system fall out of equilibrium well above T_g due to limited experimental time. This occurs, for example, in numerical simulations of liquids, that, compared to real experiments, can cover a much smaller time intervals. In this case, in facts, the fundamental constraint is imposed by the CPU time, rather than by the simulated 'real' time of the liquid.

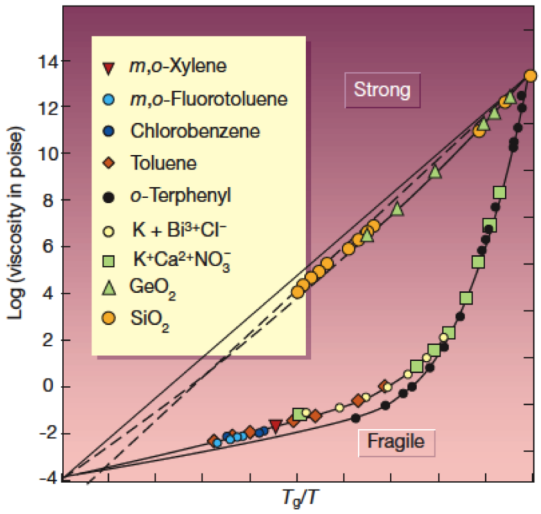

Figure 3.1: **Angell's plot.** Logarithm of the viscosity vs. rescaled inverse temperature for different liquids. The extreme case of purely Arrhenius behaviour and strongly super-Arrhenius behaviour corresponds to strong and fragile liquids respectively. From Ref. [4].

3.1.2 Behaviour of the viscosity: the Angell's plot

Given the definition of Eq. 3.2 of T_g, Angell [26] proposed a plot for reporting in a compact way viscosities data of different supercooled liquids: He suggested to plot the logarithm of the viscosity as a function of T_g/T. In this way all viscosity curves will have the same value (that is $10^{13} Poise$) at the point $T_g/T = 1$.

The *Angel's plot* of Fig. 3.1 clarifies that different liquids display two different behaviours. The simplest case consists in a straight line indicating an 'Arrhenius behaviour':

$$\eta = Ae^{\frac{\Delta E}{k_B T}} \tag{3.3}$$

where A and ΔE are temperature independent and k_B is the Boltzmann's constant. Glass-formers of this kind are usually known as *strong liquids* [27]. The behaviour of Eq. 3.3 suggests a simple relaxation mechanism, when ΔE is interpreted as the energy barrier to break locally a chemical bond. Thus, the value of the energy is insensitive to the temperature and may be easily estimated by measuring the slope of the straight lines in Fig. 3.1. Typical examples of strong liquids are SiO_2 (window glass) and GeO_2.

Other substances, instead, deviate substantially from the Arrhenius be-

haviour, their viscosities increasing steeply as the temperature is lowered. These systems are known as *fragile liquids* [27] and include o-terphenyl and toluene.

For strong systems it seems that at T_g really nothing particular happens, apart the viscosity hitting 10^{13} Poise; in this case, one may argue that the definition of T_g has purely practical implications, and nothing more. On the other hand, in fragile liquids the viscosity increases sharper on approaching T_g, suggesting relevant changes in the dynamics. For this reason, fragile liquids are the most interesting glass-formers, and many of the questions about glassy systems concern their properties. If a strong glass-former may be interpreted simply as a very viscous liquid, this seems to be inappropriate for fragile liquids, which seems to require a deeper explanation. For instance, if one tries to define an effective energy barrier ΔE for fragile glass-formers using the slope of the curves in Fig. 3.1 , then one finds that this ΔE is not constant (as for strong liquids) but it increases when the temperature decreases. Accordingly this behaviour is known as *super-Arrhenius* behaviour. It seems that the slowing down is not only due to the decreasing thermal energy (as in strong liquids), but also some structural change seems to occur, which make the energy barrier higher and higher. This suggests that the glass formation for fragile liquids is a collective phenomenon involving more and more particles as the temperature decreases . This interpretation is also supported by the fact that a good fit to the relaxation time or the viscosity is given by the Vogel-Fulcher-Tamman law (VFT):

$$\eta = A \exp[B/(T - T_0)] \tag{3.4}$$

where A, B and T_0 are temperature independent. This law suggests a divergence of the relaxation time, where a phase transition takes place at a finite temperature $T_0 < T_g$. Moreover other comparably good fits have been proposed as alternative to Eq. 3.4 . However note that although the relaxation time increases by 14 orders of magnitude, the increase of its logarithm (and therefore of the effective activation energy) is very modest, and experimental data do not allow to unambiguously determine the true underlying functional law without any reasonable doubt [28].

3.1.3 The temperature and entropy crisis

The previous arguments suggest that a thermodynamic phase transition may occur at a finite temperature T_0, although it is inhibited by a kinetic transition located at the higher temperature T_g. In other words, the experimentally observed glass transition should be interpreted as the signature of an

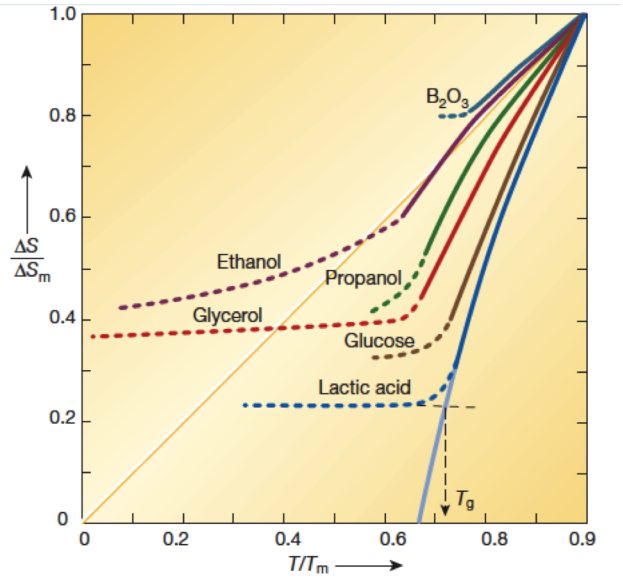

Figure 3.2: For different supercooled liquids, dependence of the excess entropy as a function of the temperature normalized by their value at the melting point. For a typical example of strong and fragile liquids data are extrapolated below the glass transition. From Ref. [4].

underlying ideal glass transition, which, in facts, is not observable. Some thermodynamic hints support this scenario. The crystal represents the stable phase below T_m as it has a free energy density lower than the liquid. But what about the entropy? At T_m the entropy of the liquid is larger than that of the crystal, but it decreases faster on cooling. The derivative of the entropy, the specific heat, is , in fact, larger in the liquid phase. Let us define the excess entropy $\Delta S(T)$,

$$\Delta S(T) = S_{liq}(T) - S_{cry}(T), \tag{3.5}$$

as the difference between the liquid and the crystal entropy at temperature T. Then, $\Delta S(T)$ is expected to decrease as the temperature decreases.

To compare the behaviours of different liquids, proposed [] to normalize the data plotting $\Delta S(T)/S(T_m)$ vs T/T_m.

Fig. 3.2 shows that at the glass transition $T_g/T_m \simeq 2/3$, ΔS does not vanishes. However, suggested to extrapolate equilibrium data at lower temperature. Using this extrapolation, it is found that in many systems the curves vanish at a finite temperature

$$\Delta S(T_k) = 0, \tag{3.6}$$

where T_k is called the *temperature*. In particular, as Fig. 3.2 demonstrates, $T_k \simeq 0$ for strong glasses and, $T_k > 0$ for fragile glasses. In addition, one finds T_k to be very close to T_0, the temperature at which a VFT fit (see Eq. 3.4) diverges. The extrapolation leads to the conclusion that $S_{liq}(T) < S_{cry}(T)$ for $T < T_k$. This phenomenon is known as *entropy crisis* or *'s paradox*. From these observations, immediately ruled out the most naive interpretation of T_k , i.e. that it could be the locus of a continuous transition from the liquid to the crystal phase. Additionally, the quantity ΔS may be identified with the the so-called configurational entropy, S_c, which quantifies the number of metastable states. A popular physical picture due to Goldstein [30] (see Sec. 4.2.1)is that close to T_g the system explores a part of the energy landscape (or configuration space) which is full of minima separated by barriers that increase when temperature decreases. The dynamic evolution in the energy landscape would then consist in a rather short equilibration inside the minima followed by jumps between different minima. At T_g the barriers have become so large that the system remains trapped in one minimum, identified as one of the possible microscopic amorphous configurations of a glass. Following this interpretation, one can split the entropy into two parts. A first contribution is due to the fast relaxation inside one minimum: this may be interpreted as a vibrational term of the entropy, thus expected to be similar to the entropy of the crystal. On the other hand, The second contribution is the configurational entropy, i.e. the term that counts the number of metastable states, $S_c = log(N_{metastable})$, and is expected to be similar to the excess entropy $\Delta S \simeq S_c$. Within this approximation T_K corresponds to the temperature at which the configurational entropy vanishes and where just a single non-crystalline state exists. This would lead to a discontinuity (a downward jump) of the specific heat and would truly correspond to a thermodynamic phase transition.

However the interpretation suffers of several contraddictions. First, we must stress that there is no reason why the entropy of the liquid should be larger than that of the crystal. As a matter of fact, the crystallization transition for hard spheres takes place precisely because the crystal becomes the state with the largest entropy at sufficiently high density [33]. Moreover, the liquid-crystal free-energy difference does not decrease when lowering the temperature [], so that any (reasonable) extrapolation does not indicate that the free energies of the two phases converges to each other. This seems to strongly invalidate the 's hypotesys, which would require converging free-energies and similar values of T_k for different observables, which is not the

case.

3.1.4 Static correlation

At this stage two remarks seems to be appropriate: First, all the distinctive properties of glass formers we discussed so far are essentially quantitative, such as the sharp increase of viscosities and relaxation times. Now we ask if there is any qualitative characteristic which allows a clear identification of glass-formers. In other words, taking a snapshot of a sample and looking at it, can we easily understand whether our sample is a deeply supercooled liquid rather than a usual liquid? Second, the presence of a sharply increasing relaxation time, and, may be, of a singularity in the specific heat, should suggest a similarity between the glass transition and the theory of critical phenomena, where a diverging relaxation time and a singularity in the thermodynamics is accompanied by a diverging correlation length. Under this perspective, a likely candidate providing a qualitative feature of the glass transition, should be the presence of a correlation length which rapidly increases as the temperature is lowered.

The simplest way to characterize a liquid is to consider the radial distribution function, $g(r)$ [31, 32]. The radial distribution function $g(r)$ allows to easily distinguish different phases (gas, liquid, crystal) of a particle system: the higher the degree of order in the system, the more structured in term of peaks is the $g(r)$. For instance, in a gas there is only the drop of probability at very low r due to the hard core of the particles, and no peaks at all, since there is no structure. In a liquid $g(r)$ is also zero at small r whereas at larger r the function steeply rises in correspondence to the first layer (or shell) of particles around the focal one; at even larger r there are some weaker, although still well defined, peaks corresponding to the various shells around the focal particle. In the liquid there is no long range order, so that the height of the peaks decreases as r increases. In a crystal, by contrast, there are not decaying sharp peaks because long range order sets in. Typically $g(r)$ is not directly accessible in experiments, whereas it can be extracted by the static structure factor $S(k)$. $S(k)$, in fact, can be measured by inelastic scattering and is related to the radial distribution function by a simple Fourier integral [31, 32],

$$S(k) = 1 + 4\pi\rho \int_0^\infty dr r^2 \frac{sin(kr)}{kr}(g(r) - 1), \tag{3.7}$$

and it provides in momentum space k the same kind of structural information as $g(r)$.

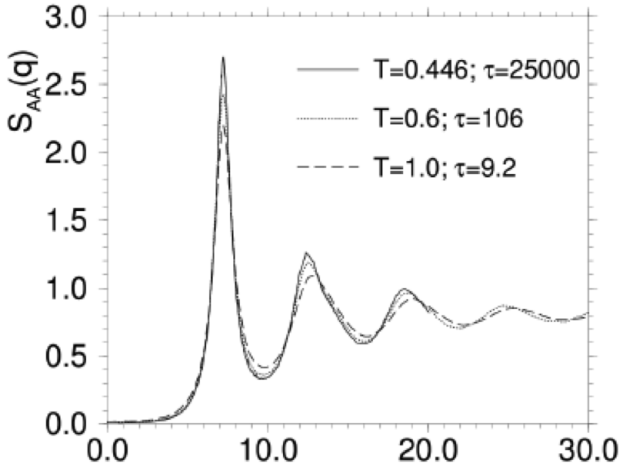

Figure 3.3: Structure factor in a Lennard-Jones liquid at three different temperatures. The relaxation time increases by almost 4 orders of magnitude, while the structure factor shows no particular change. From Ref. [34].

Results for the temperature dependence of $S(k)$ in the liquid and supercooled regime are shown in Fig. 3.3.

As the temperature is lowered, $S(k)$ exhibits very small changes in the shape of the peaks, whereby the relaxation time increases of orders of magnitude [35]. Other usual correlation function behaves in the same way, so that we can conclude that standard structural quantities do not allow to distinguish whether a sample is a supercooled liquid or not.

Nevertheless it has been proposed that the central point is not the real lack of a diverging length but consists in the choose of a suitable correlation function. Indeed, there is the debated possibility that a different correlation function may allow to extract a correlation length growing on approaching the transition [36, 6].

3.1.5 Non-exponential relaxation of dynamical correlation function

The glass transition we actually observe is a purely dynamical transition, and therefore if something new happens approaching T_g, the dynamics should detect it. On the other hand, the quest for finding a statical signature is motivated by the idea that dynamic and static observables are expected to

be related, as it occurs in critical phenomena of slowing-down. However, we have seen that for glass formers, this seems not to be a trivial syllogism.

For this reason, it is natural to search a quantitative signature of glassiness looking directly at the dynamics. Going back to the previous metaphor, one expects that a collection of at least two snapshots at two different times are necessaries to individuate a glass former sample, whereas a single snapshot is not enough. Instead of considering static correlation functions, one needs to investigate *dynamic* or *two-times correlation functions*. It is not a case, in facts, that the viscosity, which marks the onset of glassiness, is the integral over time of a dynamic correlation functions, namely the shear relaxation function. The same is true for the diffusion coefficient, related to the time integral of the velocity-velocity correlation function. However, an integral encloses an entire function into a single number, thus loosing a lot of informations. Hence, it seems a good idea to study the dynamic correlation functions, rather than their integrals, to see whether they show some qualitative signature of T_g. In general a correlation function is given by:

$$C(t_1, t_2) = \langle o(r, t_1) o(r, t_2) \rangle, \tag{3.8}$$

where $o(r, t)$ is a quantity, observed at time t and in the position r. Here we are assuming the system to be homogeneous, so that $C(t)$ does not depend on r. Moreover, in equilibrium system, time translation invariance holds and the correlation function only depends on $t = t_1 - t_2$ so that $C(t_1, t_2) = C(t)$ and Eq. 3.8 becomes:

$$C(t) = \langle o(r, 0) o(r, t) \rangle. \tag{3.9}$$

In liquids, a typical choice for $C(t)$ is the *intermediate scattering function* $F(k, t)$ [31], which is experimentally accessible and represents the dynamical counterpart of the structure factor $S(k)$. In this case, $o(r, t)$ is the Fourier transform of the density fluctuation, $\delta\rho(r, t) = exp[-ik \cdot rt])$, at fixed momentum k. Here $k = 2\pi/\lambda$ fixes the probing length-scale at values of the order of the wave-length λ. In general $o(r, t)$ can be any meaningful observable which depends both on space and time, and the decay of $C(t)$ allow to estimate the time-scale over which correlations within the system relax. In high temperature liquids, after a very short-time ballistic regime (for Newtonian dynamics) where particles move freely with no mutual interactions, the decays takes an exponential form, which is representative of a dissipative regime:

$$C(t) = C_0 exp[-t/\tau]. \tag{3.10}$$

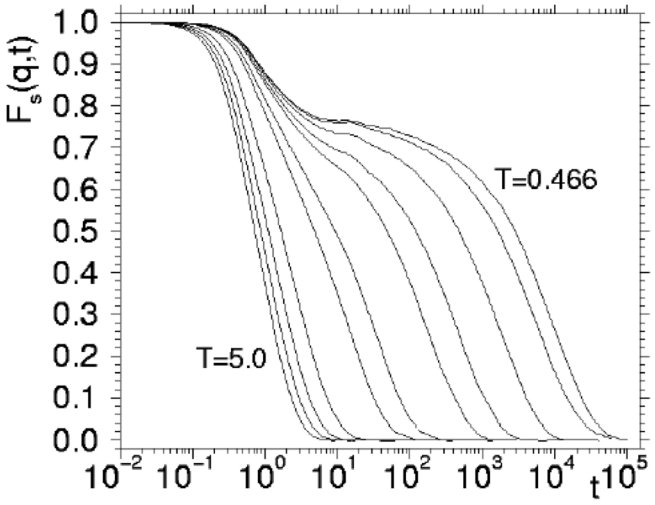

Figure 3.4: The dynamic correlation function $C(t)$ in a Lennard-Jones system. In this case, $C(t)$ is the self part of the intermediate scattering function $F_s(q,t)$ (see Sec. 4.1.2), evaluated at the value of q where the static structure factor has the main peak. At high temperatures the decay is exponential, but when the temperature get close to T_g a plateau is formed and relaxation proceeds in two steps. From Ref. [39].

Here τ is a relaxation time which in principle depends on the particular observable o. However, it is natural to expect that at high T there is only one intrinsic time scale in the system, for example the shear relaxation time, and that all the other time scales are a simple rescaling of it. In supercooled liquids, the typical relaxation time grows very sharply by lowering the temperature, so that the decay of $C(t)$ becomes increasingly slower on approaching T_g. Therefore, from a quantitative point of view, the dynamic correlation function differs significantly from the structural correlation function, which shows no dramatic temperature dependence close to T_g.

Indeed, Fig. 3.4 shows that also the qualitative shape of $C(t)$ exhibits a clear change approaching T_g: in a log-time representation a plateau emerges at low temperature, where the decay is no longer purely exponential [38, 39]. This type of decay is known as *two steps relaxation*, and it is the qualitative fingerprint of glassy systems.

Let us describe more carefully the shape of the correlation function at low T (Fig. 3.4): the time-scale over which the correlation function reaches the plateau is almost insensitive to T , whereas the length of the plateau, i.e. the time needed to leave the plateau, becomes larger the lower the temperature.

In the presence of such two steps relaxation process, the relaxation time , $\tau$is defined as that where $C(t)$ reaches a conventional small threshold value, as

$$C(\tau) = 1/e. \tag{3.11}$$

The shape of $C(t)$, however, clearly shows that two times are necessary for describing the decay. Roughly speaking, we can say that there is a fast process related to the approach to the plateau, and a slow process related to the decay from the plateau. The fast process is weakly dependent on T , while the slow process depends strongly on the temperature. Conventionally, these two processes are called, respectively, β (fast) and α (slow) relaxation. The relaxation time τ characteristic of glass formers relaxation is the one of the α relaxation, i.e. the time of the longest relaxation processes. Moreover, it is evident a separation between the two timescales, which is sharper the lower the temperature. This separation of times scales is the qualitative landmark of glassiness.

The value of $C(t)$ accounts for the degree of relaxation reached by the system at time t. In this sense, $C(t)$ may be considered as the dynamical order parameter of the relaxation process. To formalize this point, one can introduce a time-dependent scalar field:

$$\phi(r,t) = o(r,0)o(r,t). \tag{3.12}$$

Using Eq. 3.12 in Eq. 3.9, $C(t)$ can be written as the average of such field,

$$C(t) = \langle \phi(r,t) \rangle. \tag{3.13}$$

In this form, $C(t)$, looks indeed like an ordered parameter. Moreover, we can introduce the function $\Phi(t)$,

$$\Phi(t) = \frac{1}{V} \int_V d^3 r \phi(r,t), \tag{3.14}$$

which is clearly the bulk observable correspondent to the scalar field ϕ. Note that the average of $\Phi(t)$ is equal to the dynamical correlation function $C(t)$, indeed:

$$\langle \Phi(r,t) \rangle = \frac{1}{V} \int_V d^3 r \langle \phi(r,t) \rangle = \frac{1}{V} \int_V d^3 r C(t) = C(t). \tag{3.15}$$

These results will be useful in the next chapter, to deal with *four-point correlation functions* (Sec. 4.1.2).

3.1.6 Mean squared displacement and Violation of the Stokes-Einstein relation

Until now we approach the glass transition mainly dealing with macroscopic quantities, such as viscosity, relaxation time and entropy, which are easily accessible in experiments. In principle should be easier focus on a microscopic level. In this perspective, i.e. following the motion of single molecules, the question of the glass transition simply consists in understanding how the particles move in a liquid near to T_g. In practice, this underlies complicated experimental tasks: one should be able to resolve the dynamics of small objects (few Angstroms) on timescales of tens or hundreds of seconds, i.e. an enormous interval if compared to the typical time of molecular dynamics (picoseconds). On the one hand important insights can be inferred by experiment performed on systems with larger constituents, such as colloidal glasses and granular materials. On the other hand, computers furnish fundamental contributions, although numerical experiments are strongly constrained by the CPU times. Thus, if we were satisfied to stay in the moderately supercooled regime, numerical simulations allow to follow by construction the trajectory of each particle in the system. In this way, it is possible to investigate single particle dynamics, and to obtain new insights on the nature of the glass transition.

Consider, for example, the mean squared displacement (MSD) $\Delta r(t)$ of a tagged particle at time t:

$$\langle \Delta r^2(t) \rangle = \langle \frac{1}{N} \sum_{1}^{N} |r_i(t) - r_i(0)|^2 \rangle, \tag{3.16}$$

where $r_i(t)$ represents the position of particle i at time t in a system composed of N particles; the brackets indicate an ensemble average over initial conditions weighted with the Boltzmann distribution. For a liquid $\langle \Delta r^2(t) \rangle$ can be obtained by the diffusion equation for the density of a tagged particle. As a function of the time $< \Delta r^2(t) >$ is expected to vary ballistically $\langle \Delta r^2(t) \rangle \propto t^2$ for the early times where the particle experiments few collisions, and diffusively $\langle \Delta r^2(t) \rangle \propto D_s t$ at long times. Here D_s is the *self-diffusion coefficient* of the tagged particle. For liquids D_s may be directly linked to a macroscopic quantity such as the viscosity by using the Stokes-Einstein (SE) relation:

$$D_s \simeq \frac{T}{\eta}, \tag{3.17}$$

which predicts that the self-diffusion constant and the viscosity are inversely proportional at fixed temperature.

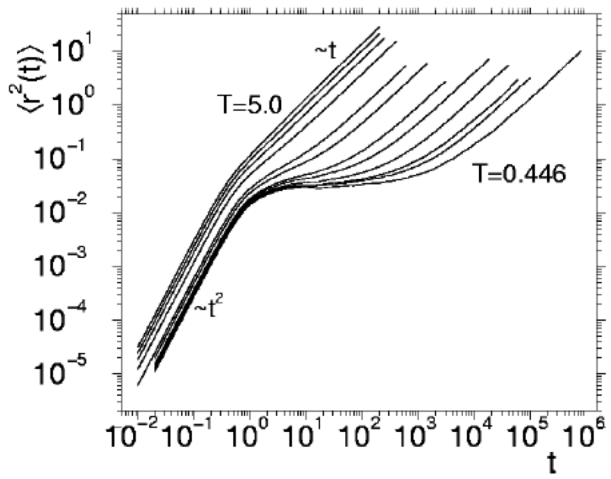

Figure 3.5: The mean square displacement (MSD) as a function of the logarithm of time in a Lennard-Jones system. At high temperature there is a crossover from ballistic transport to diffusion. At low temperatures the asymptotic behaviors are separated by a plateau. From Ref. [46].

Fig. 3.5 shows that the MSD also in supercooled liquids grows asymptotically linearly in time. However, the ballistic and the diffusive regime are separated by an intermediate plateau whose length increases by lowering the temperature.

This plateau is related to the behaviour of dynamic correlation function. In the time region of the plateau of the MSD, the tagged particle is definitely beyond the ballistic regime, but despite its many collisions with the other particles something prevents it from a standard diffusive motion, and the particle remains confined in a small region of space. If we look at the actual value of the MSD in correspondence of the plateau, we discover that it is quite small, well below the (square) inter-particle distance [46]. A nice interpretation uses the concept of a *cage*. The tagged particle is trapped in a cage formed by its neighboors: the plateau corresponds to the vibrations of the particle within the cage and diffusion is restored only when the particle escapes the cage. Note that, as we are watching things in log-time, after the particle has got out of the cage, it is effectively out of any cage. The time needed to get out of the cage corresponds to the α relaxation process, whereas the β relaxation is given by the particle vibrations within their local cages.

The concept of cage, although very useful, needs several remarks. First,

particles have neighbouring particles at all temperatures; what we would like to understand is why below a certain temperature, i.e. close to glassiness, the cage suddenly becomes stiff. Moreover, how the particle gets out of the cage after a certain time, and why this time increases by decreasing the temperature? In order to break a stiff cage, and thus to exit the plateau and to restore ergodicity, particles must rearrange. This can be done by either finding a rare 'hole' through the many energy barriers giving rise to the cage (a process that may be entropically costly, but energetically harmless), or by climbing up these barriers (energetically costly, but entropically harmless).

The cage description purely lives in real space. On the other hand, there are mean-field systems that have no real space structure at all, but where the plateau of the dynamical correlation function is anyway present at low temperatures. In these cases the cage effect cannot be the right interpretation, and the plateau is rather related to the persistence of the system in a local energy minimum.

Finally, note that although we described the escape from the cage as a single particle event, this is a simplistic view. As we shall see later on, dynamical relaxation is achieved through cooperative behaviour. Many particles must be dynamically correlated in order to unstuck from their local vibrational positions. Hence, one should rather say that it is the cage that collectively breaks up to free the particles, before another cage is formed. Understanding the nature of this collective rearrangement is one of the central questions related with the glass transition.

Now we turn to the diffusive behaviour. At relatively high temperature, it is found that D_s decreases by orders of magnitude when temperature decreases, and thus mirrors the behaviour of the (inverse) viscosity for real systems as provided by the SE relation 3.17. Closer to the glass transition, by contrast, the SE relation break down and D_s becomes several orders of magnitude larger than $\frac{T}{\eta}$ [42, 43, 44, 45]. In particular, the ratio $\frac{T}{D_s\eta}$ decreases sharply when the temperature is lowered close to T_g [42, 43]. This means that self diffusion coefficient and inverse viscosity have different functional dependence on T . So why structural relaxation are so sluggish, whereby self-diffusion is still relatively vital? We will try to give an answer in the next chapter, after we have introduced Dynamic Heterogeneities (see Sec. 4.1.1).

3.2 Jamming transition in granular materials

In this section we describe the Jamming transition of non-thermal systems, focusing on the behaviour of granular materials (see Sec.2.2.5).

First, we will discuss in detail the simplest case of soft frictionless spheres in the limit of zero applied stress. The seminal work of O'Hern et al. [24] laid the groundwork for much of what we understand about Jamming of these systems and it defines the point-J in the Jamming Phase Diagram of Fig. 2.2. Here the transition exhibits peculiar and well defined properties which seems to also control the region around it.

Then, we turn to describe the phenomenology of realistic granular materials, whereby Jamming occurs under finite applied stress and in the presence of friction.

Finally we will introduce the concept of 'fragile matter' [23], a central ideal for understanding the peculiar mechanical properties exhibited by jammed granular materials.

3.2.1 Point-J

The previous discussion about supercooled liquids clarifies that theories for jamming phenomena must explain the anomalous increase of the relaxation time observed on approaching the glass transition. At the same time, we have seen that the slow down itself poses experimental problems and makes it difficult to study the very phenomena being investigated.

For supercooled liquid the observed dynamical transition at T_g is related to the experimental time-scales: it is, in facts, not possible to go beyond T_g in order to investigate whether a transition with a 'self-defined' signature takes place at any finite temperature. Similar circumstances occur, for example, measuring the value of the yield stress, σ_y, in driven systems such as a foam: longer observations allow to detect the onset of flow at smaller applied stresses, thus returning a lower value of σ_y.

Summarizing, these transitions are therefore not sharp: the transition point depends on experimental time-scale and there is not a discontinuous jump as in first-order transition nor a clear divergence as in critical phenomena. Moreover, experiments have not been able to verify or refute the possibility that there is a underlying sharp transition.

One important advance in the study of Jamming is that, at least at point-J, the transition is sharp. In this simplified case the Jamming shows well defined properties, that are not only extension of previous results but contains new elements.

It is presently a subject of considerable controversy whether these insights will be relevant to more realistic systems and whether it will be useful to deal with the complexities of glass formation. However, the solid framework developed at point-J offers the hope that this understanding can be enlarged at least to the region around it [47].

The model

The framework of point-J has been developed for systems of soft frictionless spheres. In these model, temperature, gravity, and shear stress are set to zero. The interaction can be expressed as a function of a dimensionless penetration length, δ_{ij}, between two particles i and j:

$$\delta_{ij} = 1 - \frac{r_{ij}}{R_i + R_j}. \tag{3.18}$$

Here R_i and R_j denote the radii of the undeformed particles, while r_{ij} is their center-to-center distance, so that the two particles are in contact only if $\delta_{ij} \geq 0$. The particles interact via the following pairwise potentials:

$$\begin{aligned} V_{ij} &= \delta_{ij}^{\alpha} \;\; \delta_{ij} >= 0, \\ V_{ij} &= 0 \;\; \delta_{ij} <= 0. \end{aligned} \tag{3.19}$$

The exponent α set the type of contact interaction: for example, $\alpha = 2$ corresponds to harmonic repulsions, while $\alpha = 5/2$ give raise to 'Hertzian' repulsion, where contacts becomes stiffer for larger compressions.

Once the contact laws are given, one can generate packings using various different protocols, such as Molecular dynamics (MD) or Conjugate Gradient (CG). In particular CG, used in Ref. [24], is based on the fact that for frictionless particles, the interaction are conservative and stable packings correspond to minima of the elastic energy. This protocol aims to create configuration at $T = 0$ and a given volume fraction ϕ. To obtain such states, simulations start with a fixed number of particles, N, with the particle positions chosen completely at random (this corresponds to $T = \infty$) within a square or cubic box with side length L and periodic boundary conditions. Starting with randomly generated $T = \infty$ states guarantees that all phase space is equally sampled. Then CG allows to bring the system to the nearest potential-energy minimum by constantly moving downward on the potential energy surface. Each conjugate gradient energy minimization is terminated if, by successive iterations, the potential energy per particle deviates in a fixed small range. This procedure brings the system extremely close to $T = 0$.

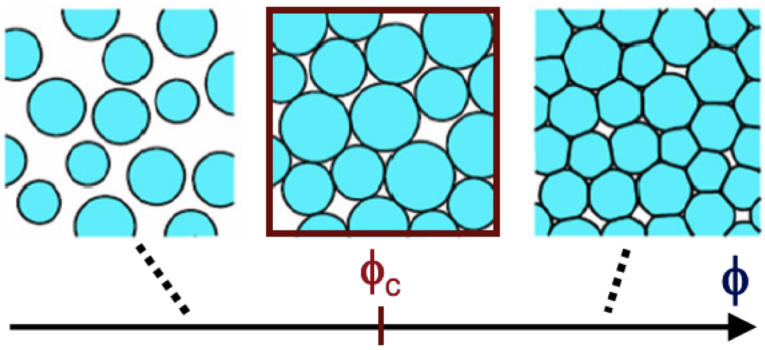

Figure 3.6: Typical packings of soft frictionless spheres as a function of volume fraction ϕ, below, at and above the threshold value, ϕ_c for the onset of Jamming. Left: unjammed system at low volume fraction -pressure is zero and there are no contacts. Middle: jammed system near ϕ_c: undeformed frictionless spheres just touching. Right: jammed system at high volume fraction -pressure has a finite value. From Ref. [2].

The properties of the resulting state are investigated slightly perturbing the system via compression, decompression or by applying a shear strain. After each infinitesimal perturbation, the CG is again used. Since this technique takes the system to the bottom of its local potential well, the quantities so measured are related to the static, or infinite-time ($t = \infty$) response of the configurations. By contrast, instantaneous responses can be investigated by measuring the response to a perturbation immediately after it has been applied (before minimizing the energy by the conjugate gradient technique).

Finally we note that, to avoid crystallization, two-dimensional packings are usually made polydisperse, and a popular choice is bidisperse packings where particles of radii 1 and 1.4 are mixed in equal amounts. In three dimensions, this is not necessary as monodisperse spheres then do not appear to order or crystallize for typically employed numerical packing generation techniques [2].

Evidence for sharp transition

Figure 3.6 shows typical configurations of soft frictionless particles for different values of the volume fraction, ϕ. At low density no contacts are present and particles are undeformed so that the potential energy, V, and the pressure, P are both zero. In response to an external stress, the systems behaves like a fluid, as each particle can move avoiding easily its neighbours.

By contrasts, at high volume fraction, particles experiments a large num-

ber of contacts which compress them and warrants mechanical stability in response to finite stresses: the system behaviour is elastic, as particles can deform but not move, due to the crowding around them. In this case, jammed granular materials can be treated as amorphous but well connected solids, where disorder essentially acts as a perturbation on the responses computed on a referencial ordered configuration. Accordingly one may use the approach of *effective medium theory* based on the *affine assumption*: particles locally follow the globally applied deformation field. More precisely, the strict definition of affine transformations states that three collinear particles remain collinear and that the ratio of their distances is preserved and affine transformations are, apart from rotations and translations, composed of uniform shear and compression or dilatation.

Nevertheless, the more interesting phenomenology occurs in between these two limiting cases. Indeed, an intermediate volume fraction, ϕ_c, which marks the onset of Jamming: at ϕ_c, particles are in contact (except for a few rattlers), but in a way that they just touch without deforming. Close to ϕ_c, effective medium theories clearly fails as affine assumptions no more hold [2]: in facts, the packing geometry is such that disorder cannot be treated as a small perturbation, but it is rather the 'essential'. In this 'ambiguous conditions', it becomes difficult to point out any 'a-priori' expectation about the mechanical properties of the system, and even to estimate whether the system is jammed or not.

Using the numerical protocols described above [1], O'Hern et al. [24] fix the jamming threshold ϕ_c as the volume fraction value where the static shear and bulk moduli simultaneously become nonzero. Although the value of ϕ_c changes on different realizations, its distribution becomes narrower as the system size increases. In particular, the width of the distribution, W, vanishes with the number of particles, N, as $W \propto N^{1/2}$.

Thus, in the thermodynamic limit, ϕ_c has a well defined value, which defines point-J. Moreover, this value corresponds to the volume fraction previously measured for the 'random close packing' (rcp). As the original concept of rcp is elusive and not suitable for mathematical definitions, the authors suggest that the framework developed at point-J represents a robust and highly reproducible possibility to fix the rcp value.

In addition, for all initial configurations, the properties of the jammed states behaves in the same way , when measured as a function of $\phi - \phi_c$. As we will discuss below, these behaviours includes scaling laws, discontinuous jumps and diverging length scales, suggesting that $\phi - \phi_c$ is a good control

[1] by using different protocols, such as molecular dynamics simulations, only negligible deviations on the value of ϕ_c have been measured [48, 49, 50, 51].

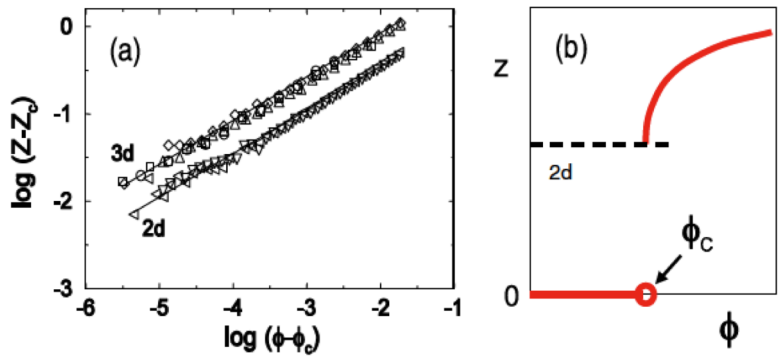

Figure 3.7: Panel a: excess number of contacts per particle $Z - Z_c$ for 3-dimensional (upper curve) and 2-dimensional systems with different potentials and polidispersity. Panel b: Schematic representation of the excess number of contacts as a function of the volume fraction ϕ. From Ref. [24, 2].

parameter. [2]

All these facts clarifies that Jamming at point-J takes the form of a sharp transition.

Contact number and Isostacity

Locking at Fig. 3.6 one can realize that a key parameter for packing is the average contact number per particle, Z. In fact, it is generally found that most mechanical properties of jammed granular materials depend sensitively on Z [2].

At point-J, Z exhibits a very peculiar behaviour: as schematically showed in Fig. 3.7b, at low volume fraction $Z = 0$, and it discontinuously jumps to a precise value at ϕ_c, $Z_c = 2d$, then increasing as the system is compressed. Fig. 3.7a shows that this increase gives raise to a power law scaling when the excess contact number, $Z - Z_c$, is plotted as a function of $\phi - \phi_c$ [170, 24, 2],

$$Z - Z_c = Z_0(\phi - \phi_c)^{\zeta}, \quad \zeta = 1/2 \tag{3.20}$$

where the value of ζ is insensitive to potentials, dimensionality and polydispersity, while the prefactor Z_0 depends on the dimensionality, and weakly on the degree of polydispersity . It is worth to mention that Z is computed by ignoring the rattlers particles with no contacts at all. The fraction of rattlers

[2]Other good parameter controlling the distance from the Jamming, may be the pressure P and the average overlap δ, which are both zero at the transition. They are found to be related by power law scaling, $P \propto \delta^{\alpha-1} \propto (\phi - \phi_c)^{\alpha-1}$ [2].

in the system is typically $\simeq 5\%$ near ϕ_c and do not depend on the system size, whereas it is found to decrease for increasing volume fraction.

The discontinuous jump in $Z(\phi)$ can be rationalized using the concept of *Isostacity*: at low density, $Z = 0$ since if particles are not forced to be in contact, they will push each other apart. In order to have any contact, a particle must be held in place by neighbors on all sides, so touching particles must belong to a cluster spanning the entire system. Accordingly, Z must jump discontinuously from $Z = 0$ to a nonzero value, Z_c, at the transition volume fraction, ϕ_c. For frictionless spheres, Z_c turns out to be the isostatic vale, i.e. the minimum possible value needed for mechanical stability. In fact, a mechanically stable system must have force balance on every particle, so that, for N spheres in the connected backbone in d dimensions, the number of equations that must be satisfied by the inter-particle forces is Nd. The number of these forces equals the total number of contact, which is $NZ/2$, since each contact is shared by two particles. The condition for mechanical equilibrium requires that the number of forces is at least equal to the number of equation, that is $NZ/2 \geq Nd$. The minimum contact number to have mechanical stability, $Z_c = 2d$, is by definition the isostatic number.

Moreover, we can consider that the amount of overlap between soft particle must vanish at the onset of Jamming. This introduces $NZ/2$ equations that must be satisfied by the dN particle coordinates. The only trivial solutions are when $d \geq Z/2$. Combining these two inequalities implies that at point-J , the contact number precisely equals $2d$ in agreement with the numerical results [47].

Mechanical responses

In Ref. [24] the nature of the static mechanical response are investigated and compared with those predicted by the effective medium theory. The static bulk and shear moduli and the pressure are found to scale as a power-law of $\phi - \phi_c$ with exponents that depend on the potential but not on dimensionality and polydispersity.

When $\phi \to \phi_c^+$, the pressure vanishes as:

$$p \propto (\phi - \phi_c)^{\psi}, \;\; \psi = \alpha - 1, \tag{3.21}$$

where α is the exponent characterizing the potential in Eq. 3.19. The bulk modulus, K, is related to the derivative of pressure with respect to volume fraction. Thus, it is expected to behaves as:

$$K \propto (\phi - \phi_c)^{\beta}, \;\; \beta = \alpha - 2, \tag{3.22}$$

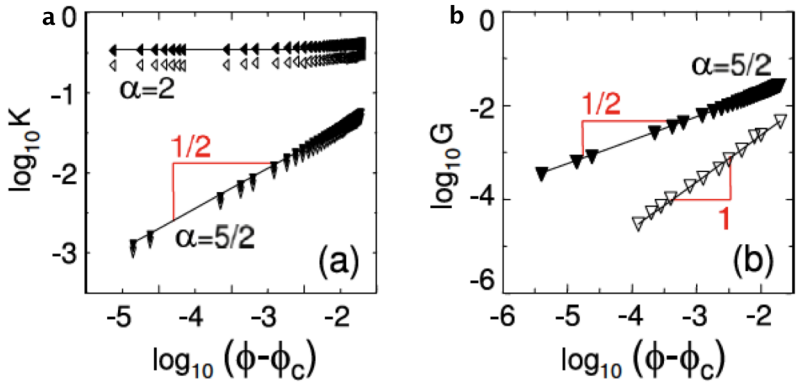

Figure 3.8: Bulk modulus K (panel a) and shear modulus G (panel b) as a function of $\phi - \phi_c$ for 2-dimensional bidisperse systems, with interaction potential $V_{ij} \propto \delta_{ij}^{\alpha}$ (see Eq. 3.19). The closed symbols denote moduli computed by imposing affine deformations, and the open symbols to the moduli calculated after the system has relaxed via CG. From Ref. [2] (adapted from [24]).

which is in very good agreement with the numerical results, as illustrated in Fig. 3.8a These power-laws are also provided by effective medium theory, suggesting that, under compression, systems at point-J do not strongly violates the affine assumptions. However, measuring the instantaneous bulk modulus, K_0, obtained by imposing an affine compression, it is found that $K < K_0$, as Fig.3.8a evidences.

By contrast under shear the response of the system deviates strongly by the effective medium behaviour. As shown in Fig.3.8b, the shear modulus G scale as:

$$G \propto (\phi - \phi_c)^{\gamma}, \;\; \gamma = \alpha - 3/2, \tag{3.23}$$

whereas for affine deformation $\gamma = \alpha - 2$ is expected. This discrepancy is confirmed by directly measuring the instantaneous shear modulus G_0 when an affine deformation is imposed. Indeed, Fig. 3.8b shows that $G_0 \propto (\phi - \phi_c)^{\alpha-2}$ and $G < G_0$.

Diverging length-scales

The signature of a diverging length-scale has been first grasped by O'Hern et al. [24], observing lack of self averaging near point-J, i.e. the average properties of a very large system are not the same as the average over an

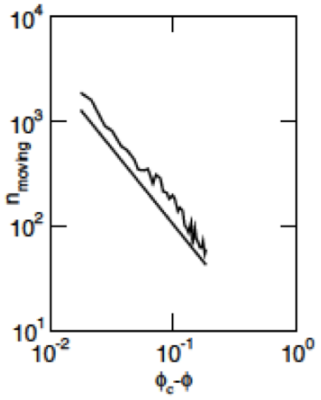

Figure 3.9: In response to the movement under a constant drive of a single probe disk trough a system of soft disks, total number of moving disks, n_{mov} as a function of $\phi_c - \phi$. The solid line is a power-law fit. From Ref. [53].

ensemble of many smaller system at the same volume fraction.

Later, several static length-scales has been recognized, which diverge by approaching point-J, although each one is defined only one side of the transition. Here we will introduce some of these lengths. We will use the notation ξ^+ and ξ^- to indicate a length-scale which diverges as $\phi \to \phi_c^+$ and $\phi \to \phi_c^-$ respectively.

Drocco et al. [53] investigated the jamming transition at point-J as a function of increasing volume fraction, $\phi \to \phi_c$, in a disordered two-dimensional assembly of disks (d=2). In particular, they measure the total number of moving disks, n_{mov}, and the transverse length of the moving region, ξ^-, when a single probe disk is pushed through the other disks. Upon increasing the packing density toward ϕ_c, power law divergences are found in the number of moving disks, $n_{mov} \propto (\phi_c - \phi)^\tau$ (see Fig. 3.9), with $\tau \simeq 1.3$, and in the spatial correlation length $\xi^- \propto (\phi_c - \phi)^\nu$, with $\nu \simeq 0.65$. Note that the values of the exponents are consistent with $\tau = d\nu$, which suggests that cluster of moving particles are compact object in 2-dimension. We also mention that Olsson and Teitel [54] have found a similar value for the exponent ν, although they investigated a different correlation length and a different numerical experiment: a 2-dimensional system flows in a steady state due to an external shear stress σ_{xy}, and ξ^- is extracted by the velocity-velocity correlation function, $g(x) = \langle v_y(x_i, y_i) v_y(x_i + x, y_i) \rangle$, where $v_y(x_i, y_i)$ is the velocity along the y-axis for a particle in position (x_i, y_i). In this case, point-J is approached as a function both of the volume fraction, $\phi \to \phi_c$ and the shear stress, $\sigma \to 0$.

Wyart et al. [55] suggested that the existence of isostacity at point-J implies the presence of a length-scale which diverges as point-J is approached from above. This idea is supported by the following theoretical arguments: if we cut a circular blob of radius l from a rigid material, the bubble should remain rigid. However for jammed granular materials, the rigidity (given by the shear modulus) is proportional to $Z - Z_c$. Thus, the circular blob has of the order of $l^d(Z - Z_c)$ excess contacts. By cutting it out, one breaks the contacts at the perimeter, which are of the order of $l^{d-1}Z$. If the number of broken contacts at the edge is larger than the number of excess contacts in the bulk, isostacity is violated and the resulting blob is not rigid but floppy: it can be deformed without energy cost. The smallest blob one can cut out without it being floppy is obtained when these numbers are equal, and represents the characteristic length-scale, $\xi^- \simeq Z/(Z - Z_c)$. Close to the jamming transition, $Z \simeq Z_c$ is essentially constant and so one obtains as a scaling relation that $\xi^- \propto (Z - Z_c)^{-1}$, which, as provided by Eq. 3.20, diverges at the transition as $(\phi - \phi_c)^{-\zeta}$.

Above point-J, the presence of large correlations clearly emerges when one focus on the forces between contacting particles. In particular, Fig. 3.10 evidences the presence of a characteristic length-scale in the response of the contact force networks: close to point-J, the scale up to which the response looks disordered becomes large. By studying the radial decay of fluctuations in response to the inflation of a single central particle, one extract a length ξ^+ which, as the theoretically derived length-scale, varies as $\xi^+ \propto (Z - Z_c)^{-1} \propto (\phi - \phi_c)^{-\zeta}$ [56]. This length-scale seems to be crucial in order to address a central question concerning the behaviour of granular materials, i.e. whether elasticity can describe a system response to, for example, point forcing. Indeed, observations by Ellenbroeck et al. [56] suggest that below ξ^- the response is dominated by fluctuations, and the deformation field can be seen as a distorted floppy mode, while at larger length-scales the response crosses over to elasticity.

Jamming at point-J as a mixed transition

Fig. 3.11 schematically summarizes the behaviour observed at point-J. As one can note, we are dealing with a sharp transition which exhibits very unusual properties with respect to both first-order and second-order phase transitions.

From the one hand, there is evidence of diverging length-scale and power-law scaling which resembles critical phenomena. On the other hand, the average number of contacts Z exhibits a discontinuous jump, as occurs in first order transitions. In addition, the values of the exponent in the power-

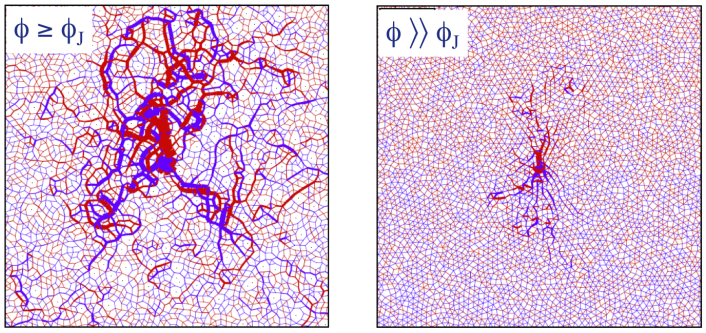

Figure 3.10: Divergence of a characteristic length-scale near jamming as observed in the fluctuations of contact forces of a system of soft disks. Blue (red) bonds correspond to increased (decreased) force in response to inflate a single particle in the center of the packing. Left: the system is very close to ϕ_c. Right: the system is strongly compressed above ϕ_c. From Ref. [56].

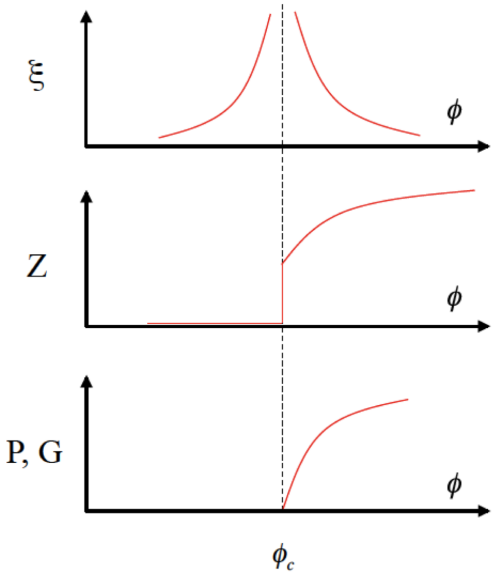

Figure 3.11: Schematic behaviour at point-J: there are diverging length-scales (upper panel), the number of contacts has a discontinuous jump at ϕ_c then increasing as a power-law of $\phi - \phi_c$ (central panel), while the mechanical responses continuously increase from zero as a power-law of $\phi - \phi_c$ (lower panel).

law scaling do not depend on the dimensionality, as in critical phenomena, but they can be sensitive to the interaction potential between grains.

Due to this nature, which joins properties of first and second order transition, Jamming at point-J has been classified as a *mixed transition*. Similar transitions, although rare, have been observed in other models. Remarkably, all of these models have been proposed for the glass transition or, more in general, in order to capture glassy dynamics [57, 58], in the mean-field limit. Also a particular percolation model, known as $k-corepercolation$ [59] displays the same behavior when implemented on the Bethe lattice (which correspond to the infinite-dimensional or mean field limit) [60]. A characteristic of k-core percolation is that it can be mapped on one class of models with glassy dynamics, namely kinetically constrained models (see Sec. 4.2.2). Thus, this percolation yield some insight into the connection kinetically constrained models and the Jamming transition [47].

3.2.2 Realistic granular systems

The development of a robust framework for the Jamming transition at point-J was possible because systems of frictionless soft spheres can be investigated cleanly at zero temperature and zero external stress. However realistic granular material are typically far enough from these 'asymptotic' systems and experiments are inevitably performed with frictional grains and under finite applied stresses. As anticipated in Sec.2.2.5, the action of a finite applied shear stress, σ, favors the fluid phase, shifting the onset of Jamming to higher values of the volume fraction, $\phi_j(\sigma) > \phi_c$. In other worlds, for volume fraction $\phi > \phi_c$, granular materials develop an yield stress σ_y, such that for $\sigma < \sigma_y$ the system responds as a solid, while it flows when $\sigma > \sigma_y$. By contrast, the presence of friction favors the solid phase, because it makes possible the existence of stable packing at volume fraction $\phi < \phi_c$.

Apart these very general facts, experiments reveal a complex and very rich phenomenology often characterized by transient regimes and different time and length scales. Many of these experiments are performed in a Couette cell, i.e. an annular shear cell submitted to a external shear stress and, possibly, to vibrations [61, 62, 63]. The rheology observed in the fluid phase comprises non-linear velocity profiles, shear bands, stick-slip behaviour, an ordering transition, possibly affected by hysteretic effects [62, 63]. As the volume fraction is increased, Jamming may suddenly occurs after the system flow for a finite time [61].

In this context, numerical simulations are still fundamental in order to stepwise increase the level of complexity, and focus on different emerging aspects of the rheology. Below we point out the main effect of friction and

stress close to the Jamming transition of soft spheres at zero temperature.

Jamming of frictional spheres

The crucial difference with the frictionless case is that both the threshold volume fraction ϕ_j and contact number Z_j are not sharply defined at the transtion. Indeed, both values depend on the friction coefficient, μ and on the preparation protocol, and are lower than for frictionless spheres [64, 65, 66, 190].

In the presence of friction, Jamming and isostaticity are not strictly entangled In the limit of zero stress, the contact number at Jamming, Z_j, can range from $d+1$ to $2d$, where $Z_\mu^{iso} = d+1$ is the isostatic value for frictional spheres. It is found that Z_j approaches Z_μ^{iso} in the limit of infinite friction and very slow equilibration of the packings [66, 190]. In all other cases, the number of contacts at Jamming is larger than the minimal number needed for force balance and rigidity, so that frictional packings of soft spheres at jamming are *hyperstatic*: $Z_j > Z_\mu^{iso}$. Hyperstaticity implies that, for packings of rigid, frictional spheres, the contact forces are not uniquely determined by the packing geometry, as was the case for the isostatic packings of rigid, frictionless spheres [2].

Effect of stress on the Jamming transition

For frictionless spheres and small shear stresses the transition at point-J still governs the behaviour of the viscosity. Indeed, quasistatic simulations at constant volume, show that for small shear stress the viscosity η seems to critically diverges at ϕ_c [54].

The scenario clearly changes at larger shear stress: MD simulations of 3-dimensional systems [68] show that the volume fraction where the viscosity diverges increase with the applied stress. In addition, hysteretic effects appears: a flowing or a jammed state can be found, depending on whether the system is prepared coming from the fluid or the jammed phase. In particular the volume fraction when the system unjams coming from the jammed phase, $\phi_u(\sigma)$, is larger than the volume fraction $\phi_j(\sigma)$ where the system jams coming from the fluid phase. However the deviation decrease when σ is lowered and becomes negligible at small stresses, where $\phi_j \simeq \phi_u \simeq \phi_c$, in agreement with the results of Ref. [54].

In the case of frictional spheres, MD simulations return much of the phenomenology observed in experiments: in particular, at finite shear stress, the system may flow for a long time in a steady state, but then suddenly jams [69].

3.2.3 Fragile matter

As we have mentioned, under the action of an anisotropic stress, granular systems may suddenly jam after a transient flow. Some years ago, Cates et al. [23] introduced the concept of 'fragile matter' to describe the mechanical properties of these jammed systems. Simple geometries of hard spheres have been proposed to capture the essential of this behaviour [70, 71]: under the effect of an an anisotropic stress, such as a shear stress, particles rearrange until they found a microscopic configuration able to sustain the stress itself. If the applied stress increases in modulus, then the system may possibly behave elastically, while flow is restored if even an infinitesimal force is applied in a different direction. In this sense, the systems are "fragile" and strongly differ from any ordinary visco-elastic or elasto-plastic materials.

The authors expect that slight particles deformability allow a macroscopic elastic response at least for small stresses, although they suggest that realistic granular materials may be very close to the fragile limit. However, this is still an open question.

Simulations of frictionless soft spheres under shear stress find that the system do not show transient flows which should give raise to fragile response: the system is either flowing in a steady state or jammed depending on the control parameters [68]. However transient flow appears in the presence of friction, leading to a rheology which seems to resemble previsions of sheared hard spheres models which originally contributed to inspire the idea of fragile matter [72]. Under these conditions, the solid response of granular material is still an open question. In particular it is not clear to what extent the concept of fragility may capture the properties of realistic system and whether these mechanical properties are peculiar to granular systems, or also found in different amorphous materials.

Chapter 4

Dynamical Heterogeneities and theoretical models

The presence of spatio-temporal fluctuations in the dynamics, known as Dynamical Heterogeneities (DHs), has been recently considered as a central aspect of the dynamics of jamming systems. Their existence has been inferred from experiments in liquids [74, 75], while clearer observation has been available on systems with larger constituents, such as colloids and granular media [77, 76, 78]. Computer simulations of spherical particles with simple pair potentials have been used as models for both colloidal and molecular systems, with dynamically heterogeneous behaviour clearly present in a variety of models. DH has also been investigated in a large number of more schematic lattice models, such as kinetically constrained or lattice glass models [147]. Finally in the last years, the concept of DH has been used beyond the field of the jamming transition, as a tool to characterize deformations and fracture in disordered media [80, 81].

Here we will mainly focus on the case of glass formers liquids: we begin the first section of this chapter, describing earlier numerical and experimental facts supporting the existence of DHs. This allows to clarify some intriguing general aspects of glass formers such as the non-exponential relaxation and the violation of the Stokes-Einstein (SE) relation (see Sec. 3.1.6). Later we will discuss the role of the dynamical correlation function, as a fundamental tool for a quantitative investigation of DH . As the concept of DH seems very promising to distinguish between competing theories, in the last section of this chapter we will introduce some theoretical models for the Jamming transition .

4.1 Dynamical Heterogeneities

A central problem in understanding the physics of glass formers arises from the importance of fluctuations in glassy systems. Liquid have disordered structure, where identical molecules are instantly immersed in different local environments. At high temperatures, these differences can be neglected, as different configurations are rapidly sampled: thus, the behaviour of the system may be derived by choosing a typical environment, which may be considered as the result of a time average. By contrasts, in the supercooled phase fluctuations slowly relax, making difficult to select a typical environment as a variety of different behaviors emerges.

The presence of such spatio-temporal fluctuations is generally known as Dynamical Heterogeneities, and is now considered as a central aspect of structural relaxation in disordered materials with slow dynamics.

A recent advance in this field points that the DHs play here the same role as the critical fluctuations in ordinary critical phenomena. However, the application of this idea to glassy systems has required substantial new insight into the nature of relevant fluctuations and observables. The reason is that here we are dealing with a dynamical problem, whereas the theory of usual critical phenomena has a thermodynamic nature as we discussed in the the previous chapter. If one analyses static snapshots of viscous liquids, there is little evidence of increasing fluctuations or heterogeneity, at least when analyzed using standard liquid state correlation functions. Instead of an ensemble of snapshots, one must apply the methods of critical phenomena to an ensemble of "collection of snapshots taken at different times" [121].

4.1.1 Earlier evidences

Our discussion on DH may surely begin with the deepening of a question which we have already mentioned in the previous section: the non-exponential relaxation of dynamical correlation functions (see Sec. 3.1.5). The deviation from exponential relaxation, in facts, is not only represented by the break-up of the decay into two steps (see Fig. 3.4); even the late relaxation is non-exponential. In particular, it is found that the Kohlraush-Williams-Watts stretched exponential form [135, 83],

$$C(t) = C_0 exp[-(t/\tau)^{\beta}], \;\; \beta < 1 \tag{4.1}$$

fits reasonably well the data. Here the exponent β decreases when the temperature is decreased, marking a larger and larger deviation from a standard exponential relaxation [84] . Moreover, two-step relaxation and the

stretchted exponential relaxation seem to be related: at higher T the exponent β approaches 1, and at the same time the whole two steps structure of the dynamical correlation function disappears, and the relaxation goes back to simple exponential.

Two natural, but fundamentally different, explanations has been proposed, i.e. (1) the *heterogeneous* and (2) the *homogeneous* hipotesys.

1) The relaxation is locally exponential, but different regions have different relaxation times. As global correlation or response functions are essentially an average over this spatial distribution of relaxation times, they results non-exponential.

2) The relaxation is essentially non-exponential , even at a local scale.

Although the two scenarios are not necessarily contradictory, it is now well established both numerically [85, 86, 107, 88] and experimentally [89, 75] that close to the glass transition the dynamics of real supercooled liquids is heterogeneous. It is possible to directly observe domains few nanometers away from each other with significantly different mobility and relaxation times.

Let us still consider two subsequent snapshots, taken at two instants of time separated by an interval t. We can now measure how much each particle moved in this time interval by computing the *Van Hove correlation function* $G(r,t)$. If t is very short, i.e. in the ballistic regime, we do not expect great variations of the particles mobility, because interaction with environment are still unimportant; similarly, if t is very large, much larger than the structural relaxation time τ, then we are averaging over a temporal window so large that ergodicity is restored; and we cannot observe differences once we take the ensemble average, and thus each particle will again have a similar mobility. By contrast, if t has an intermediate value, long enough to monitor particles interaction, but short enough not to restore statistical homogeneity, we see something very different: there are particles with mobility significantly higher, and lower, than the average. We will see later that the dynamics itself is able to select the time of maximum heterogeneity, which in general is close to the plateau regime of the dynamic relaxation function $C(t)$ [85, 86, 107, 88].

When we raise the temperature, the dynamical correlation function and, simultaneously, the MSD loose their plateau structure and dynamics becomes homogeneous, irrespective of the value t has.

This observation strongly suggests that the non-exponential relaxation of the dynamical correlation function is linked to heterogeneous dynamics. A clear and more direct confirmation of the heterogeneous character of the dynamics also stems from simulation studies. where single particle dynamics is resolved both in space and time [90]. Fig 4.1 shows that particle trajecto-

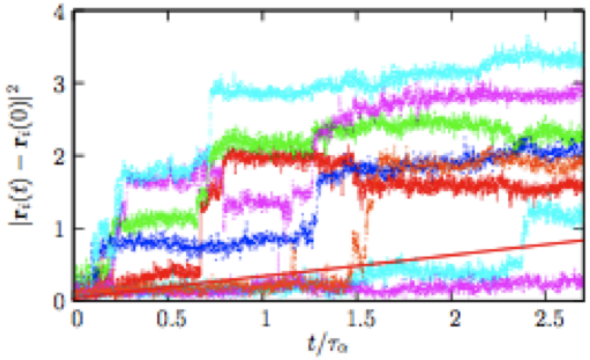

Figure 4.1: Time resolved squared displacements of individual particles in a Lennard-Jones systems. The time on the *x-axis* is rescaled by the structural relaxation time. The average is shown as a smooth full line. Trajectories are composed of long periods of time during which particles vibrate around fixed positions, separated by rapid jumps that are widely distributed in time, underlying the importance of dynamic fluctuations. From Ref. [90].

ries are strongly intermittent. Vibrations were previously suggested by the plateau observed at intermediate times in the mean-squared displacements of Fig. 3.5, but the existence of jumps that are clearly statistically widely distributed in time cannot be obtained from averaged quantities only. The fluctuations in Fig. 4.1 suggest, and direct measurements confirm, the importance played by fluctuations around the averaged dynamical behaviour.

The phenomena described above, clearly show that the dynamics is spatially heterogeneous. However, they in principle do not clarify whether this is related to purely local fluctuations or, instead, there are clusters of particle dynamically correlated over increasingly large regions. This point can be unveiled trough spatially resolved measurement, where one tries to probe a small enough number of dynamically correlated regions, and detect their dynamics. For instance, using Atomic Force Microscopy techniques, the polarization fluctuations in a volume of size of few tens of nanometers has been measured close to T_g[91] in a supercooled polymeric liquid (PVAc). Indeed, the signals reveal that the dynamics is very intermittent in time: it switches between moments with intense activity, and moments with no dynamics at all, suggesting that extended regions of space indeed transiently behave as fast and slow regions. A much smoother signal would have been measured if particles with similar mobility were not clustered.

In general experiments of this kind are quite difficult: while important information are reached about the typical life-time of the dynamic hetero-

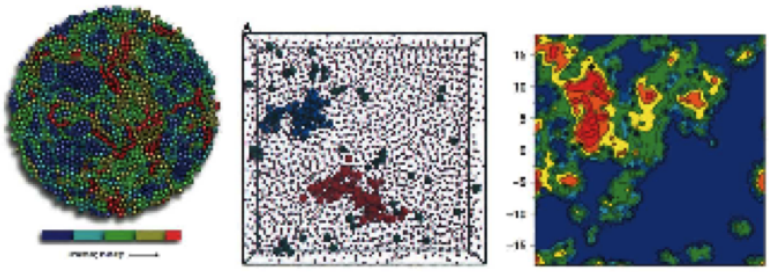

Figure 4.2: Three examples of dynamical heterogeneity. In all cases, the figures highlights the clustering of particles with similar mobility. (Left, from Ref. [76]) Granular fluid of ball bearings, with a colour scale showing a range of mobility increasing from blue to red. (Centre, from Ref. [77]) Colloidal hard sphere suspension, with most mobile particles highlighted. (Right, from Ref. [92]) Computer simulation of a two-dimensional system of repulsive disks. The color scheme indicates the presence of particles for which motion is reproducibly immobile or mobile, respectively from blue to red.

geneity, by contrast, the determination of a dynamic correlation length-scale is rather indirect and partial. Nevertheless, the outcome is that a non-trivial dynamic correlation length emerges at the glass transition, where it reaches a value of the order of about $\simeq 10$ molecule diameters [74].

In order to make more concrete such ideas in Fig. 4.2 we show several jamming systems [76, 77, 92] in which mobile and immobile particles can be identified in particular trajectories using different methods. Via a color scale we clearly see that particles with different mobilities do not appear randomly in space but are clustered. This observation suggests that structural relaxation is a cooperative dynamical process. Indeed, in its narrow definition DHs are clusters of particle dinamically correlareted. We must not forget that these clusters in glass-formers, are dynamical, not structural! They continuously form over a length-scale and relax after a life-time, whose typical values are found to increase by approaching the dynamical transition.

If we accept the evidences for spatio-temporal heterogeneities in the dynamics of glass former, we can try to answer to a previous question concerning with the decouplings between viscosity and diffusion coefficient: why close to T_g structural relaxation are so sluggish, whereby self-diffusion is still relatively vital? A natural explanation of this effect is that different observables probe differently the distribution of relaxation times [74]. In particular, diffusion is dominated by the fastest clusters whereas structural relaxation is

dominated by the slowest one. An unrealistic but instructive example is a model where there is a small, non-percolative subset of particles that are blocked forever, coexisting with a majority of mobile particles. In this case, the structure never relaxes but the self-diffusion coefficient is non-zero because of the mobile particles. Of course, in reality all particles will eventually diffuse. A slightly more realistic model was proposed in [45]. Suppose that there are just two kinds of clusters equally numerous, fast and slow ones, with relaxation time and diffusion coefficient respectively $\tau_{fast} << \tau_{slow}$ and $D_{fast} >> D_{slow}$. Note that in general $\eta \simeq \tau$ where τ is the (global) structural relaxation time. So, at fixed temperature T the SE relation 3.17 reduces to,

$$D \simeq \frac{1}{\tau}. \tag{4.2}$$

Thus, it is evident that the violation of SE relation corresponds also to a decoupling between diffusion coefficient and relaxation time. Let us supposed that in this case the SE relation is obeyed in each cluster, so that $D_{fast} \simeq 1/\tau_{fast}$ and $D_{slow} \simeq 1/\tau_{slow}$. Under these hypotheses, we have that the (global) observable relaxation time is $\tau \simeq \frac{\tau_{fast}+\tau_{slow}}{2} \simeq \tau_{slow}/2$, whereas a measurement of the diffusion coefficient returns $D \simeq \frac{D_{fast}+D_{slow}}{2} \simeq D_{slow}/2$. Thus, $D >> \frac{1}{\tau}$ and the SE relation results violated as expected. In general, decouplings of this kind may be explained considering that different observables are likely to probe different moments of the distribution of timescales. To conclude this point, we also mention that it has been shown that the SE equation 3.17 is restored when the diameter of the probe used to measure the diffusion coefficient increases [45]. This makes sense in terms of heterogeneous dynamics: when the probe is larger that the typical cluster size at a fixed temperature, we are averaging over many heterogeneities, thus washing out their influence.

4.1.2 Dynamical correlation functions

Until now we reported some basic facts supporting the existence and the fundamental role played by DHs in glassy systems. To go further, it has been necessary to develop tools allowing for the quantitative characterization and measure of spatio-temporal dynamical fluctuations. Recently, substantial progress in this direction was obtained trough the use of *four-point*, or, *two-time two-point correlation functions*. This type of dynamical correlation functions has been inspired by ideas previously introduced for spin glasses [93, 94].

The existence of clusters of highly mobile (or immobile) particles of size r suggests that the movement of particle i over the time interval t is correlated

to the movement of particle j at distance r from i, over the same time interval (provided that i and j belong to the same dynamical cluster, and t is smaller than the typical cluster life-time). For example, it may be that the only way for particle i to escape its 'cage' over a time t is to cooperate to a synchronous collective movement involving a certain number of particles; if particle j, at distance r from i participates to the same collective movement, there will be a correlation between the displacements of i and j. Hence, we need to measure the correlation between the displacements over a time interval t of particles at mutual distance r.

The concept of mobility connects directly to the physical picture of DHs and it is thus quite illuminating. However, the essential ingredient to measure spatio-temporal fluctuations in the dynamics is not really the mobility, but rather the fact that we are calculating a two-time two-point correlation function, in contrast with standard two-point functions, as $g(r)$. The two-time two-point nature simply derives from the fact that, to unveil cooperative dynamics, we must check what happens in two spatial locations, separated by r, at two different instants of time, separated by t. The correlation function can thus be defined using any reasonable observable $o(r,t)$, provided that we keep the four-point structure:

$$g_4(r,t) \propto \langle o(0,0)o(0,t)o(r,0)o(r,t)\rangle - \langle o(0,0)o(0,t)\rangle\langle o(r,0)o(r,t)\rangle, \quad (4.3)$$

where we assumed that TTI holds and the system is homogeneous . The correlation function g_4 depends both on space and time: it is expected to become increasingly long-ranged as the temperature is lowered, allowing to extract a time-dependent correlation length $\xi_4(t)$. $\xi_4(t)$ is provided to account for the typical linear extension of dynamical clusters at time t.

Alternatively, in order to characterize correlations, we can focus the space integral of $g_4(r,t)$. The dynamic susceptibility, $\chi_4(t)$, is by definition proportional to such integral:

$$\chi_4(t) \propto \int_V d^3r g_4(r,t). \quad (4.4)$$

Eq. 4.4 suggests that $\chi_4(t)$ represents an estimation for the volume of dynamical clusters at time t, i.e. the typical number $N_{corr}(t)$ of particles cooperating over the time scale t.

Four-point correlation functions and the order parameter

A clearer physical interpretation of g_4 and χ_4 is obtained by relating them to the two-time correlation function $C(t)$. As we point out in Sec. 3.1.5, the

most remarkable dynamical signature of the glass transition is indeed the non-exponential relaxation of $C(t)$: the lower the temperature, the longer $C(t)$ remains at the plateau.

To this aim, Let us recall the scalar field $\phi(x,t)$ and its bulk correspondent $\Phi(t)$ defined in Eq. 3.12 and Eq. 3.14 respectively, that by averaging directly return $C(t)$ (Eq. 3.13, Eq. 3.15). In particular by using Eq. 3.13 in Eq. 4.3, g_4 takes the form of the spatial correlation of the field ϕ,

$$g_4 \propto \langle \phi(0,t)\phi(r,t)\rangle - \langle \phi(0,t)\rangle\langle \phi(r,t)\rangle. \tag{4.5}$$

Therefore, g_4 formally mimics a two-point (spatial) correlation function associated with the order parameter, while the very four-point nature lies in the definition (3.12) of $\phi(t)$, which is itself a two-time function.

Similarly, by using Eq. 3.15, we can express $\chi_4(t)$ in term of the fluctuation of $\Phi(t)$, indeed

$$\begin{aligned}
\chi_4 \propto &= \int_V d^3 r g_4(r,t) \\
&= \int_V d^3 r \langle \phi(0,t)\phi(r,t)\rangle - \langle \phi(0,t)\rangle\langle \phi(r,t)\rangle = \\
&= \frac{1}{V}\int_V d^3 y \int_V d^3 x \langle \phi(x,t)\phi(y,t)\rangle - \langle \phi(x,t)\rangle\langle \phi(y,t)\rangle = \\
&= V(\langle \Phi(t)^2\rangle - \langle \Phi(t)\rangle^2).
\end{aligned} \tag{4.6}$$

Therefore, the dynamical susceptibility $\chi_4(t)$ measures the fluctuations of the dynamical order parameter.

Four-point functions in discrete space

In order to construct dynamical correlation function, it is often more convenient to focus on particle observables $o_i(t)$ that are discretely labelled trough a particle index i. In this case we get for the two-time correlation function $C(t)$:

$$C(t) = \frac{1}{N}\sum_{i=1}^{N} < o_i(0) o_i(t) >, \tag{4.7}$$

which is the discrete analogous of eq 3.1.5, being N the total number of particles in the system. Similarly Eq. 3.12 and Eq. 3.14 become respectively:

$$\phi_i(t) = o_i(0) o_i(t), \tag{4.8}$$

$$\Phi(t) = \frac{1}{N}\sum_{i=1}^{N}\phi_i(t), \tag{4.9}$$

so that, for the four point correlation function we have:

$$g_4(r = |i-j|, t)\langle\phi_i(t)\phi_j(t)\rangle - \langle\phi_i(t)\rangle\langle\phi_j(t)\rangle. \tag{4.10}$$

The volume integrals, wich in Eq. 4.4 relate g_4 and χ_4, is now substituted by a sum over particles:

$$\chi_4(t) \propto \frac{1}{N}\sum_{i=1}^{N}\sum_{j=1}^{N} g_4(|i-j|, t) \tag{4.11}$$

Finally, using Eq.s 4.11, 4.10 and 4.9, the relation 4.6 becomes:

$$\chi_4(t) \propto N(\langle\Phi(t)^2\rangle - \langle\Phi(t)\rangle^2), \tag{4.12}$$

whereas all the other relations of the previous section still holds in the discrete case.

Note that where the space is discretized, such as in lattice glass model, correlation functions can be expressed in therms of both a particle index, or a site index. In the last case sums run over the V sites of the system.

General behaviours

The four-point correlation function in glass formers have been the object of intense research effort, both experimental and numerical. Here we briefly summarize the main general results, that have an almost universal validity. We focus on the role played by the temperature, which is central for glass formers; However similar behaviours are found in other systems as response to other relevant control parameters such as the density.

$g_4(r, t)$ is expected increasingly long-ranged when the temperature is lowered. This is consistent with the behaviour of $\chi_4(t)$ shown in Fig. 4.3: it first grows, when t is in the ballistic and early β-regime, then it reaches a maximum at $t = t^*$, decreasing for larger times. The peak $\chi_4(t^*) = \chi_4^*$ confirms what we anticipated in the discussion on DH (cfr. 4.1.1). Clusters of dynamically correlated particles are transient in time. For times too short, correlation has still not formed because of the lacking of interactions among the particles; for times too long, by contrast, the time average equals the ensemble average restoring statistical homogeneity. It is only at intermediate times that dynamical correlations are relevant. The behaviour of $\chi_4(t)$ clarifies that there is a time t^* where the dynamics is maximally heterogeneous.

As expected from our previous discussion, one finds that $t^* \simeq \tau$, i.e. the order parameter fluctuations are largest when computed over a time window of the order of the relaxation time.

Now let us discuss in more details the expected relation between χ_4 and g_4. The susceptibility $\chi_4(t)$ is proportional to the space integral of the correlation function $g_4(r,t)$ (see Eq. 4.4). By analogy with critical phenomena, if the behaviour of g_4 is dominated by a dominant length-scale ξ_4, for r large enough, one may suppose a scaling form such as:

$$g_4(r,t) = \frac{A(t)F(r/\xi_4(t))}{r^{d-2+\eta}}, \tag{4.13}$$

where d is the dimensionality of the system, η ia an exponent characterizing the long-range decay, and $A(t)$ is an amplitude factor. Using this scaling for g_4 in Eq.4.4, one finds that:

$$\chi_4(t) \simeq A(t)\xi_4(t)^{d-\eta}. \tag{4.14}$$

Moreover, if $g_4(r,t)$ monotonically decreases in space, one expect to estimate $A(t) \simeq g_4(0,t)$ which is simply the variance of the scalar field $\phi(0,t)$. Finally, if the order of magnitude of the amplitude does not vary, Eq. 4.14 states that:

$$\chi_4(t) \simeq N_{corr}(t) \propto \xi_4(t)^{d-\eta}, \tag{4.15}$$

where $d-\eta = 3$ is expected for compact clusters. Thus, a large susceptibility implies a slower spatial decay of $g_4(r,t)$. This means that $g_4^*(r) = g_4(r,t^*)$ should be the slowest decaying correlation function, allowing to extract a value for the correlation length $\xi_4^* = \xi_4(t^*)$ which is the largest one at that temperature. In particular, as χ_4^* increases when the temperature decreases, one expects that the correlation function $g_4^*(r)$ is more long-ranged and that the maximum dynamical correlation length ξ_4^* increases by approaching the dynamical transition.

Numerical and experimental results

Direct measurements of $\chi_4(t)$ have been performed in colloids [95] and granular materials [76, 78] close to the colloidal and granular glass transitions, and in foams [96] and gels [97], where the dynamics is more easily spatially and temporally resolved. A major issue is that obtaining information on the behaviour of $\chi_4(t)$ and $g_4(r,t)$ from experiments on molecular systems is difficult. In molecular liquids, it remains a difficult task to resolve temporally the dynamics at the nanometer scale. Such measurements are

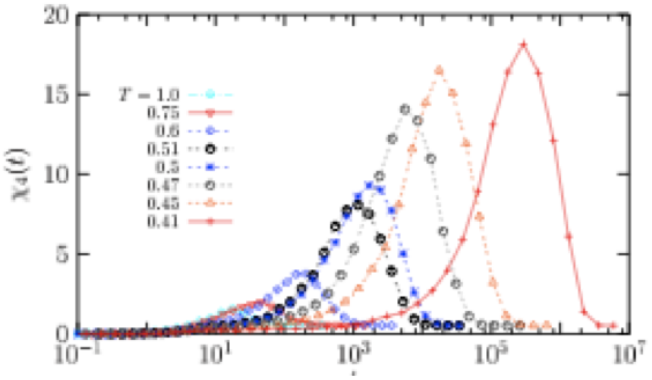

Figure 4.3: Time dependence of $\chi_4(t)$ computed from the fluctuations of the self part of the intermediate scattering function in a molecular dynamics simulation of a Lennard-Jones supercooled liquid. For each temperature, $\chi_4(t)$ has a maximum, which shifts to larger times and has a larger value when T is decreased, revealing the increasing length-scale of dynamic heterogeneity in supercooled liquids approaching the glass transition.From Ref. [102].

however important because numerical simulations and experiments on colloidal and granular systems can typically only be performed for relaxation times spanning at most $5-6$ decades. The function $\chi_4(t)$ has been measured by Molecular Dynamics, Brownian and Monte Carlo simulations in different liquids [98, 99, 100, 101, 102, 103, 105]. Moreover, its behaviour has been theoretically investigated using various theoretical perspectives, as described below in Sec. 4.2. A typical example is shown in Fig. 4.4, taken from Monte Carlo simulations of a simple Lennard-Jones supercooled liquid.

Fig. 4.4 clarifies that the time and temperature behaviour of $\chi_4(t)$ is very rich: the growth towards its peak value is composed of several time regimes, closely reflecting the broad spectrum of relaxation processes characterizing time correlation functions. An analogous behaviour is found in nearly all cases, as detailed in [106].

Similarly, the temperature evolution of χ_4, and in particular the peak height, can be quantitatively studied. In numerical simulations χ_4^* increases by at most 2 orders of magnitude from a high temperature value up to the lowest temperature at which the system can be equilibrated. In this range of temperature data seem to be compatible with a power law divergence of χ_4^* and t^* at a finite temperature close to the value provided by the *mode coupling theory*, which we will discuss in Sec. 4.2.1 [107, 99, 108, 100].

It is worth to mention that the behaviour of χ_4^* has been investigated in

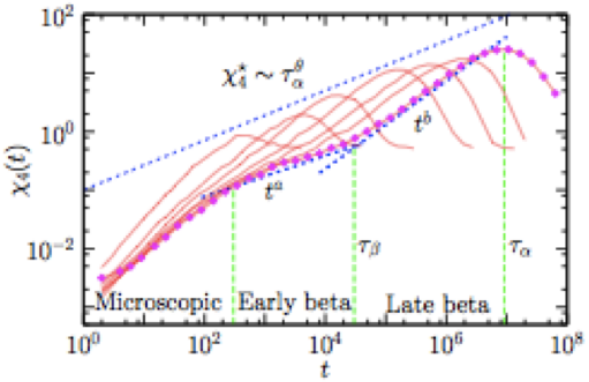

Figure 4.4: Time and temperature evolution of $\chi_4(t)$ computed by the spontaneous fluctuations of the intermediate scattering function in a Lennard-Jones supercooled liquid in Monte Carlo simulations. The growth of $\chi_4(t)$ is characterized by several distinct time regimes, mirroring the complexity of time correlation functions. Here τ_β and $\tau_\alpha = \tau$ indicate the time-boundary of the β-regimes and α-regimes respectively. Moreover, as the temperature is lowered, the peaks χ_4^* appear to increase as a power-law of the relaxation time $\tau_\alpha = \tau$. From Ref. [121].

a recent experiment very close to the jamming transition of colloids [109]. Surprisingly, these results show that the well known increase χ_4^* is followed by a sharp drop when the volume fraction is very close to the critical value.

As we anticipate, χ_4^* should provide a measure for the volume over which the dynamical processes relevant to structural relaxation at $t \simeq \tau$, are correlated. More direct evidences of a growing dynamical correlation length can be obtained by measuring directly $g_4(r,t)$. Indeed, the form of $g_4(r,t)$ has been checked to be roughly compatible with the scaling proposed in Eq. 4.13, so that the increase of the peak of $\chi_4(t)$ corresponds to a growing dynamic length-scale [99, 110, 100, 112, 111], as provided by Eq.4.15 . However, these measurements are difficult in computer simulations, because very large systems need to be simulated to determine ξ_4 unambiguously [113, 114].

Choosing observables and probing length-scales

As discussed above, one may define four-point correlation functions starting from any suitable observable. Indeed, many candidates have been considered.

For instance, a natural choice is to start from Eq. 3.12 and to take $\phi(k,r,t) = \delta\rho_k(t)\delta\rho_{-k}(0)$ as the autocorrelation of a single Fourier component of the density. In this case, $C(t)$ is just the intermediate scattering function

$F(k,t)$ (cfr 3.1.5).

Instead in computational studies, is more convenient to use $\phi_i(k,t) = e^{ik\cdot(r_i(t)-r_i(0)}$. As we will explain in the next chapter, in this case $C(t)$ becomes the self part $F_s(q,t)$ of $F(q,t)$. The definition of g_4 and χ_4 obtained in these ways are not equivalent. Differences between them were discussed in Ref. [100], where, anyway, it was concluded that they contain similar informations. From a physical point of view, what count is that as particle i moves away from its initial position $r_i(0)$, the function $\phi_i(q,t)$ decays from a value of unity, approaching zero when the particle has moved a distance a, which is the probing length scale of the used observable, (in the case of scattering functions a is of the order of the wave-length $\lambda = 2\pi/k$ associated to k).

Based on this physical interpretation, other choices for $\phi_i(t)$, including step functions, or smoothly decaying functions were used [98, 99, 100, 102]. As expected on physical grounds, constructing four-point correlation functions based on these choices again leads to qualitatively similar behaviours.

Yet another choice is to use a function $\phi_i(t)$ that depends not just on the positions at time zero and time t, but also on the whole history of the particle between these times. In particular, as we will do in the next chapter, one may use a "persistence" function which takes a value of unity if the particle remains in its initial position for all times between 0 and t; otherwise it takes the value zero. Again, one observes a broadly similar behaviour [115].

By contrast, the quantitative results strongly depend on the probe length scale a. Typically, if the probes length scale a is of the order of the particle diameter, $\phi(r,t)$measures local motion, and this is often the scale on which heterogeneity is most apparent. On the one hand, if the probes length scale increases, contributions to $\chi_4(t)$ come from pairs of particles that remain correlated over distances comparable to a and, typically, such correlations weaken as a increases, reducing $\chi_4(t)$ [115] . On the other hand, also if a is much smaller than the particle s size, $\chi_4(t)$ decreases, as short-scale motion corresponding to thermal vibrations are uncorrelated.

Therefore, $\chi_4(t)$ is usually maximal for a probe length scale comparable to the particle size, and it is fixed to a constant when comparing data at different temperatures or densities. An alternative choice is to adjust the probe length-scale a at different state points such that $\chi_4(t,a)$ reaches its absolute maximum, this can be very important for some systems like granular media close to the *jamming/rigidity* transition where the maximum is reached for values of a of order of fractions of the particle diameter [116, 117, 182].

Geometrical structure of dynamical clusters

We could conclude that a growing peak in χ_4 stands for the growth of a dynamic correlation length, as the glass transition is approached. Eq. 4.15 clarifies that, at time t, $\chi 4(t)$ can be interpreted as an estimate of the volume of dynamical clusters, while ξ_4 accounts for their linear dimensions. Similarly, the time $t*$, where correlations become maxima, is interpreted as the typical cluster life-time. Accordingly, $\chi 4^*$ and ξ_4^* represents the maximum volume and linear extension of these clusters.

However, this interpretation can be actually correct only if g_4 has a scaling form of the type provided by Eq. 4.13 where the amplitude $A(t)$ stays approximatively constant. However, it is not simple to check whether this is true, both in experiments and simulations. In contrast to χ_4, in fact, detailed measurements of g_4 are not easy , as dynamic correlations must be resolved in space over large distances. From the point of view of numerical simulations, where many measurements of χ_4 were reported, the main limitation to properly measure g_4 is the system size. Indeed, typical numbers extracted for the correlation length ξ_4 are modest, growing, say, from 1 to at most $5 - 10$. However such a small increase hides the fact that correlation functions only decays to zero for distances r that are several times larger than ξ_4. [1]

Some significative data has been obtained for lattice glass model, where measurements of $g_4(r, t)$ are somewhat easier than in molecular dynamics simulations. As we anticipated, often, one estimates the amplitude $A(t)$ in Eq. 4.13 to be equal to $g_4(0, t)$ In general, the work in this domain is broadly consistent with $\chi_4(t)/g_4(0, t)$ representing the number of particles involved in heterogeneous relaxation. In other words, 'direct' measurements seems to confirm that the increase of the peak of $\chi_4(t)$ corresponds, as expected, to a growing dynamic lengthscale $\xi_4(t)$ [110, 99, 102, 111].

Nevertheless the mentioned results of Ref. [109], showing a drop of the susceptibility very close to the Jamming, suggests that the relation between $\xi_4(t)$ and $\chi_4(t)$ shuould be more complex.

Finally we note, that the exponent $2-\eta$ in Eq. 4.15 may have more than one interpretation. If one assumes that a typical cluster has size $\xi_4(t)$ and contains $\xi_4(t)^{2-\eta}$ particles, then $2 - \eta$ is interpreted as a fractal dimension.

[1] Given that g_4 is accurately measured up to $r = L/2$ in a periodic system of linear size L, going to few ξ_4 (say, five times), when $\xi_4 \simeq 5$ requires systems containing at least $N \simeq L^3 \simeq (2 \cdot 5 \cdot 5)^3 \simeq 125000$ particles in three dimensions, assuming the density is near $\rho = 1$. Such large system sizes are not easily studied at low temperatures when relaxation times get very large, even with present day computers. However, these studies are of vital importance in that they allow the dynamical length scale $\xi_4(t)$ to be measured directly. Moreover, insights from such studies can then be used when inferring the behaviour of $\xi_4(t)$ from measurements of $\chi_4(t)$.

However, an alternative would be that clusters are all compact, but that the distribution of their sizes is rather broad. This uncertainty reflects the fact that four-point correlation functions involve averages over many clusters, so that they do not resolve details of cluster structure.

Until now, an exhaustive geometrical characterization of such dynamical clusters is still an open question in understanding the glass transition.

Final remarks

Concerning the role of DHs in the glassy physics, several key questions are still unanswered.

We have seen how direct measurements of growing dynamic correlation lengths have provided evidences in favor of the collective nature of the glass transition itself. This fact being now established, it remains to understand more quantitatively the connection between these growing correlation lengths and the increasing viscosity of liquids approaching the glass transition. In particular, it is not clear to what extent DHs and structural relaxation are related. For instance, the surprising drop of the susceptibility found in Ref. [109] could be addressed to a decoupling between DH and relaxation processes.

As we anticipated, direct experimental measurements of dynamic length-scales are still not available for molecular glass-formers, and are scarce even for colloidal materials. Thus, it would be useful to develop new experimental tools to resolve the dynamics of molecular glass-formers, while it is not yet clear whether molecular dynamics simulations of model systems have covered a broad enough range of timescales and are thus relevant to understand the physics of real glass-formers near the experimental glass transition temperature. We also have already pointed out that further work should be devoted to a better characterization of the geometry (and not only typical length-scale) of the dynamically heterogeneous regions.

4.2 Theories and predictions

In this section we provide an overview of several theoretical models for the glass transition. On the one hand a satisfactory and complete framework explaining the wide phenomenology of glass formers is still lacking. On the other hand, a variety of theoretical approaches have been proposed, providing fundamental contributions to understand different , although not resolutive, aspects.

Here we will deal with models able to furnish quantitative predictions

that can be easily compared with the experimental data. Moreover we don't discuss in great detail developments, limitations, and fails of the theories, but we will focus on the keystone ideas and on the predictions, specially when related with the topic of DHs, as they are propaedeutic for the results we will discuss in the next chapter.

The section is divided in two part: we first deal with model based on thermodynamics. In particular we will mention some earlier models that first introduced new concepts, resulting fundamental in designing the present scenario. Then we will focus, in fact, on the *Mode Coupling Theory* (MCT) and on the *Random First Order Theory* (RFOT) that are now considered the most quoted theories for describing the behaviour of glass formers in the moderately and deeply supercooled phase respectively.

We anticipate that many of these models assume the existence of a static length-scale ξ which grows approaching the glass transition. This may be surprising: we have stressed in the previous chapter that a length-scale of this kind is never been observed using standard correlation functions, and one may asks why these models are based on a fact which seems to disagree with the experimental evidences. Actually, the idea which leads this route is that a growing correlation length effectively exists in supercooled liquids, although it is not measurable with standard methods. Thus, this theories aim to understand what is the nature of this hipotetyc static correlation length in order to develop non-standard tools able to detect it.

In the second part of the present section, we will deal with models that conceive the glass transition as a purely dynamical phenomenon: here we will focus on the so called *Kinetically Constrained models* (KCM), and, we will discuss the diffusing defects paradigm.

4.2.1 Thermodynamic approach to the glass transition

Goldstein's scenario

In 1969 Goldstein [30] elaborated the first theoretical description for the equilibrium dynamics of supercooled liquids. The Goldstein's work introduced seminal ideas about the deeply supercooled phase, where activated processes are now recognized as the main mechanism for relaxation. Goldstein focuses on the evolution of the system in phase space. Over this space it is defined the total potential energy of the system, and the surface of this function is often called *potential energy landscape*. Each different configuration is represented by a point in the phase space, and the dynamics of the system may be viewed as the motion of this point over the potential energy landscape. The local minima of the potential energy corresponds to locally stable configurations of the particle system. We are interested in the local minima corresponding

to particles arrangement that are completely lacking long-range crystalline order. These are amorphous, or glassy, minima, and have a potential energy that is larger than the crystal one. Goldstein's idea is that at low enough temperatures a supercooled liquid explores the phase space mainly through 'activated jumps' between different amorphous minima, separated by potential energy barriers. In real space, the jump may be interpreted as the local rearrangement of a relatively small number n of particles localized in a limited region of space of linear size ξ, whereas the other particles are almost untouched by this process. In activation dominated dynamics, the relaxation time is expected to scale as :

$$\tau \propto \exp\left[\frac{\xi^{\psi}}{K_B T}\right], \tag{4.16}$$

where it is assumed that the energy barriers ΔE scales as some power of ξ,

$$\Delta E \propto \xi^{\psi}. \tag{4.17}$$

Note that the local nature of rearrangements is one of the central idea in the Goldstein's scenario: the number n of particles participating in the rearrangement sets the potential energy barrier separating two minima, and thus it scales as some power of n. It is natural to expect that the typical value of n increase by decreasing the temperature, so explaining the non-Arrhenius behaviour of the viscosity. Nevertheless, due to the local nature of the process, n remains always negligible compared to the size N of the entire system, so that barriers can be surpassed by means of the thermal energy fluctuations that are of the order of $K_B T$. When the temperature is increased, activation itself is a bad approximation of the true dynamics, as thermal energy becomes comparable and even higher than the typical potential energy barriers [122]. In this case it is clear that Goldstein's scenario must break down. Therefore, the break down of Goldstein's scenario marks a conceptually useful border, that is the temperature, say T_x, separating a low-T activated and viscous regime, from a high-T non-activated and fluid regime. Goldstein [30] estimated the value of the shear relaxation time at T_x, concluding that $\tau(T_x) \simeq 10^{-9} - 10^{8} Sec.$, which return a value for T_x intermediate between the glass and the melting temperature: $T_g < T_x < T_m$. Summarizing, the Goldstein's scenario introduces at least three important points:

1) The importance of the energy landscape for the dynamics of the system in phase space.

2) The local nature of activated processes.

3) The definition of a temperature above which activated dynamics no

more holds and any other relaxation mechanisms should dominate.

Adam-Gibbs-Di Marzio Theory
The first successful attempt to connect at the theoretical level the glass phenomenology to a thermodynamic transition is due to a series of papers published by Adam, Gibbs and Di Marzio between 1956 and 1965 [123, 124, 125]. Activation plays still a central role in the *Adam-Gibbs-Di Marzio Theory*(AGDM), which clearly relates some important topics of the glassy dynamics: energy barriers, the relaxation time the existence of static correlation length and the number of local minima in the energy landscape, i.e. the configurational entropy S_c.

The key idea is that at low temperature relaxation proceeds through the rearrangement of larger and larger regions of correlated particles, which the authors called *Cooperative Rearranging Regions* (CRR). The typical CRR is defined as the smallest region that can be rearranged independently from its surrounding. This means that different portions of one CRR cannot choose their own configuration independently from each other, and thus cannot contribute to the proliferation of the number of states available to the entire CRR.

How many states W the global system can be found in? Given that, by definition, different CRRs are weakly interacting with each other, the answer to this question is very simple, $W = \Omega^{N/n}$, where where N is the total number of particles in the system, and n the typical number of particles in each CRR. Thus, N/n is the total number of independent CRRs. The configurational entropy S_c is then the logarithmic density of the number of locally stable states $S_c = \frac{1}{N} log(W) = log(\Omega/N)$. Inverting this relation we finally obtain the behaviour of n as a function of the temperature: $n(T) = \frac{log(\Omega)}{S_c(T)}$. Now, supposed that $n \simeq \xi^d$ and that typical energy barriers ΔE are proportional n ($\psi = 1$ in Eq. 4.17), we have: $\Delta E \simeq \xi \simeq n \simeq 1/S_c$. Moreover for the relaxation time is expected: $\tau \simeq \exp(\frac{\Delta E}{K_B T})$. Thus, we can write that $\tau \simeq \exp(\frac{B}{TS_c(T)})$, where B contains all the constant factors. It is clear that in this case the explicit dependence of τ on the temperature is set by the functional form of $S_c(T)$. Further developments of the AGDM theory, in fact, predicts that at low temperature the configurational entropy behaves as

$$S_c \propto \frac{T_K - T}{T_K}, \tag{4.18}$$

which leads to the fragile behaviour of the relaxation time, in the form of a VFT law which diverge at the Kauzmann temperature T_K. Hence, in

AGDM view, the dynamic glass transition at T_g is nothing more than a mere precursor of the thermodynamic transition at T_K, which is, in this framework, the only relevant physical phenomenon.

p-spin model

A different thermodynamic scenario is provided by *Fully Connected Mean-Field Models* [126]: here each particle (or spin, or any other degree of freedom) interacts with all other particles, so that exiting a local energy minimum requires changing N degrees of freedom. In this case activation processes and local rearrangements are forbidden as thermal fluctuations cannot surpass the barrier .

Nevertheless there exists a class of spin glass models that shows a phenomenology strikingly similar to that of supercooled liquids. The *p-spin model* is the paradigm of such class [127]. It was proved that this particular model was described by a set of dynamical equations formally identical to those we will meet for MCT. This is a model where there is no underlying lattice, nor space structure at all, where each spin is equally close (or distant) to every other spin (this is at the origin of the name 'fully connected' or 'infinite dimensional' attributed to these models; by contrast, for the same reason, normal, non-mean-field systems are sometimes called 'finite dimensional' systems).

The correlation function of the p-spin model develops a plateau, giving rise to the two steps relaxation pattern, as in real liquids and in MCT. Unlike real liquids, however, but similar to MCT, the length of the plateau (and thus the relaxation time τ) diverges as a power law at a finite temperature T_c, called the dynamical transition in the spin-glass literature. The interesting thing is that no thermodynamic (static) divergence, nor anomaly takes place at T_c. What happens at T_c is that the system remains dynamically trapped within metastable states surrounded by infinite free energy barriers that the system cannot overcome by thermal activation . For this reason, in mean-field model metastable states have an infinite life-time and can be sharply defined. The system is therefore forbidden to restore ergodicity, and a true dynamical divergence occurs.

Mode Coupling Theory

MCT was formulated [129, 130] in the attempt to quantitatively describe the dynamical properties of supercooled liquids by determining the equations of motion for the dynamical correlation function of the density fluctuations.

The starting point of the method is the derivation of the following equation for the dynamical structure factor $F(k,t)$:

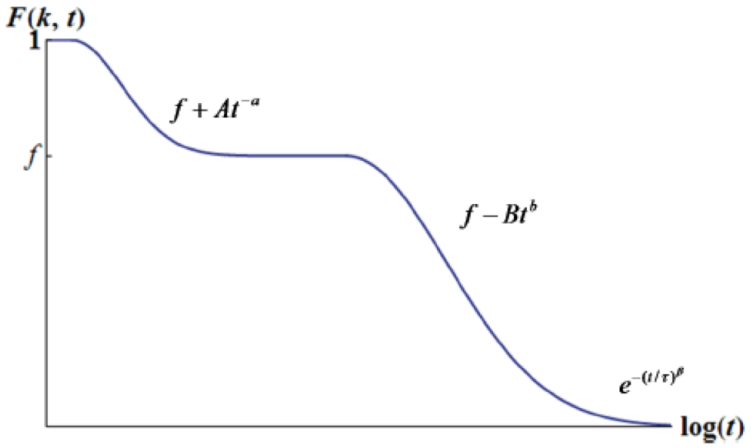

Figure 4.5: Schematic behavior of the Intermediate Scattering Function, $F(k,t)$, in the Mode Coupling Theory. From Ref. [131]

$$\frac{d^2F(k,t)}{dt^2} + \frac{k^2K_BT}{mS(k)}F(k,t) + \int_0^t dt^{'}M(k,t^{'})\frac{d}{dt}F(k,t-t^{'}) = 0. \qquad (4.19)$$

Here $M(k,t)$ is the *memory kernel* of a particle of mass m at temperature T, which is shown to corresponde to the variance of the random force acting on the density field [134]. Thus, $M(k,t)$ captures the effect of all degrees of freedom other than the density field on the density field itself. The physical idea motivating MCT is to focus on the slow part of the random force, so that only the bilinear density products contribute to $M(k,t)$and it can be expressed in terms of a four-point function. In a final approximation, this function is factorized as the product of two-point density functions $F(k,t)$, turning Eq. 4.19 into a self-consistent equation.

In this way, the only input of Eq. 4.19 is the static structure factor $S(k) = F(k,0)$ [135]. This may appear surprising, since we have seen that structural quantities do not show anything peculiar close to T_g. The central point here consists in the very nonlinear form of the the MCT equations: even a tiny change in the structural properties may cause a steep slow down of the dynamical relaxation.

At low temperature the MCT predicts correctly the two steps relaxation of the dynamical correlation function, developing a plateau whose length increases when the temperature is decreased. The theory provides the two step relaxation not only as a qualitative signature, but furnish a precise

quantitative prediction of the way the correlation function should arrive to and depart from the plateau, and thus it gives a precise description of both the β (fast) and α (slow) relaxation. These prediction agrees rather well with t experimental and numerical evidences [38, 39, 46, 133]. In particular, the decay to the plateau and the departure from it are characterized by power law behaviours. The exponent $0 < a < 0.5$ fixes the short time behavior, $F(k,t) \simeq f_0 + At^{-a}$, whereas the departure from the plateau is characterized by the so called *von Schweidler law*, $F(k,t) \simeq f_0 - Bt^{-b}$, where $0 < b < 1$. These exponents are related via the equation, $\frac{\Gamma^2(1-a)}{\Gamma(1-2a)} = \frac{\Gamma^2(1-b)}{\Gamma(1-2b)}$.

However the theory fails as the deeply supercooled phase is approached. MCT, in fact, predicts that the relaxation time diverges at a finite temperature, T_c in the form of a power-law:

$$\tau = \frac{1}{(T - T_c)^\gamma}, \tag{4.20}$$

with $\gamma = \frac{1}{2a} + \frac{1}{2b}$. If the divergence located by MCT were at very low temperature, well below T_g, we could not completely exclude its existence. However, this is not the case, and there is in fact evidence that such divergence is not present in experimental data, but it is rather an artifact of the theory.

Understanding why the MCT predicts an inexistent divergence is not easy, due to the fact that the theory has not a clear physical interpretation and that many of the approximation used are uncontrolled. However, inspired by the similarity with mentioned p-spin model, there is a common consensus that this happens because MCT does not take into account activated barrier crossings. The relaxation mechanism of MCT is something different from activation, even though it is not easy to understand its nature by a mere inspection of the MCT equations. As in the p-spin case, below T_c the MCT dynamical mechanism is completely stuck, so that the theory cannot go beyond T_c and it therefore locates a divergence here. A real liquid, by contrast, can switch from the MCT mechanism to activated barrier crossing, thus keeping the relaxation time finite, although sharply increasing with lowering the temperature.

Note that we have seen the Goldstein's scenario begins to hold at a temperature T_x where activation dominates the dynamics, whereas MCT works until a temperature T_c where activated precess are unimportant. This interesting consideration suggests:

$$T_x \simeq T_c, \tag{4.21}$$

meaning that Goldstein's and MCT scenario joins at this temperature, as they are based on complementary relaxation mechanisms. In fact, relation

in Eq. 4.21 has been verified by several investigations [136, 137]. The identification of the MCT transition temperature with Goldstein's crossover temperature has an important implication: even though one knows there is no real divergence, it is nevertheless very useful to extract T_c (typically via a power law fit of the data) as a reference temperature for a system approaching glassiness. In fact, from what we have discussed above one may conclude that the definition of $T_x \simeq T_c$ is more fundamental than that of T_g, which depends on an arbitrarily fixed time or viscosity scale (see Sec. 3.1.1).

In fact, it is now recognized that the MCT transition must be interpreted as an approximate theory of a crossover taking place in the dynamics. This clear limitation, together with its precise predictions, makes the MCT an useful starting point for investigation of the dynamics of moderately supercooled liquids.

Dynamic Heterogeneities in MCT

MCT has been introduced as a dynamical theory for two-time correlation functions. However, the recent surge of interest on DHs suggests that it could be interesting to develop an MCT approach also for four-point correlation functions. This developments allows for an impressive set of very detailed predictions starting from the form of the microscopic interaction between the particles.

$\chi_4(t)$ is predicted to grow with time with two distinct power laws, $\chi_4(t) \simeq t^a$ and $\chi_4(t) \simeq t^b$ in the time regimes respectively corresponding to the approach to, and departure from, the plateau. Here, a and b are the exponents found for the decay of the dynamical correlation function in the same regimes. These two power law regimes have been successfully identified in numerical works, with numerical values for the exponents a and b that are in reasonable agreement with numbers predicted by MCT [138, 105, 90]. At a times $t^* \simeq \tau$, the susceptibility is provided to reach its maximum χ_4^*, whose height diverges at T_c as $(T - T_c)^{-1}$. So that, using Eq. 4.20, one finally finds $\chi_4^* \simeq \tau^{-1/\gamma}$.

Thus, in MCT scenario, the divergence of relaxation time is accompanied by simultaneously diverging dynamical fluctuations. As occurs for the relaxation time, data obtained in the moderately supercooled regime are found to approximately follow an initial growth which is consistent with the MCT prediction, which break down at lower temperatures.

Random First Order Theory

The original version of the *Random First Order Theory* (RFOT), was formulated by Kirkpatrick, Thirumalai and Wolynes in the late 80s, in order to investigate the potential relationships between supercooled liquids and the

p-spin class of mean-field spin-glasses [139]. Later it was presented [140]. as a thermodynamic description of metastable states in supercooled liquids. This real space version of the theory is also known as the *Mosaic Theory*. The theory was strongly influenced by ideas proposed in the AGDM scenario, but it contains a key ingredients which promoted new important advances.

This is the idea of a surface tension which in a finite dimensional system marks the interfaces between two local configurations. In fact, if a finite dimensional system has many states, then different regions may be found in different states, the world 'states' means for local configurations which have the same bulk free-energy. Thus, it is reasonable that an energy cost is associated to the creation of the interface, due to the mismatch along the edge of the two such states. In particular, the free energy cost, ΔF_{cost}, to rearrange a surface of linear size R is

$$\Delta F_{cost} = Y R^{\theta}, \tag{4.22}$$

where in RFOT $theta \leq d-1$ is supposed, and consequently Y means for a "generalized" surface tension. In fact, while the usual definition of surface tension assumes that ΔF scales as R^{d-1}, this "a-priori" assumption seems to be too strong in the case of supercooled liquids.

The system dynamics is ruled by the competition between the surface tension, which tends to keep the system in its original state, and a drive to different state. In RFOT the thermodynamic drive to rearrange a droplet of linear size R is provided by the fact that such a region has an exponentially large number of available configurations. There is an entropic price that must be paid by the region to stay in just one of these many states, and this entropic price can be released if the rearrangement takes place by means of thermal fluctuations. In particular, the free energy gain, ΔF_{gain} is proportional to the total configuration entropy available for that region:

$$\Delta F_{gain} = T S_c(T) R^d. \tag{4.23}$$

For small R the cost dominates and there is no net thermodynamic gain in the formation of a droplet. Instead, for large R the entropic drive dominates; this occurs for any size R larger than a critical value ξ fixed by the balance of Eq. 4.22 and Eq. 4.23:

$$\xi(T) = \left(\frac{Y}{T S_c(T)} \right)^{\frac{1}{d-\theta}}. \tag{4.24}$$

Here ξ is the typical size of the rearranging regions and thus may be interpreted as a static correlation length. This size is inversely proportional to

the configurational entropy, although with a non trivial exponent, and in this respect we recover the most important result of the AGDM theory. Moreover, ξ is also proportional to the surface tension, and this is an ingredient that is completely absent in AGDM.

Further developments lead to the following expression for the relaxation time:

$$\tau = \propto \exp\left(\frac{Y^{\frac{d}{(d-\theta)}}}{T[TS_c(T)]^{\frac{\theta}{(d-\theta)}}}\right). \tag{4.25}$$

Therefore the RFOT does not provide directly the VFT law 3.4, because the precise dependence on S_c, and thus on T_k (see Eq. 4.18), is related to the exponent θ. In [140], however, it was claimed, using renormalization group arguments, that $\theta = d/2$. In this case, we recover the VFT behaviour. It is hard to say whether the claim $\theta = d/2$ is correct or not. However, as a matter of fact, different fits, obtained by Eq. 4.25, may work even better than VFT law.

As a remark, we want note that until now we have neglected a possible dependence of the surface tension Y on the temperature. In fact, at very low temperature it is reasonable to believe that Y does not vary strongly with T , and that it levels to some finite value. By contrast, at higher temperatures this assumption does not hold, and it is fair to consider $Y = Y(T)$. In particular, from the discussion in sec 4.2.1, we do not expect the multi-state scenario, we are adopting here, to hold also at high temperatures and we already suggested that states (whatever they are) become ill-defined above the Goldstein temperature $T_x = T_c$, whereby the MCT scenario appears more suitable. Thus, it is reasonable to suppose that the surface tension vanishes close to this crossover $Y(T_x) \simeq 0$. Finally, we mention that recent versions of RFOT suggests that, at fixed temperature, Y is not single-valued, but characterized by a continous distribution. This allows to overcome some disagreement between theory and observed phenomenology.

Dynamic Heterogeneities in RFOT

How do DHs emerge in thermodynamic picture designed by RFOT?

The basic idea in RFOT consists in the fact that regions of size smaller than $\xi(T)$ are ideal glasses: they cannot relax, as their state is, in fact, the only one allowed at that length-scale. Regions of size greater than $\xi(T)$ are liquid in the sense that they explore with time an exponentially large number of unrelated configurations.

Moreover, when a rearrangement takes place within one of this region, also know as *glassite*, the boundary conditions of the nearby region changes.

Thus, there is a substantial probability that a local rearrangement triggers, or facilitates, a similar event in a close region, possibly inducing an 'avalanche' process that extends over a dynamic correlation length $\xi_4(t) > \xi$. This is at the origin of DHs in RFOT. Note that in this case the static correlation length acts as a lower bound for the dynamical one. The dynamics on length scale less than ξ is, within RFOT, inherently cooperative, but the relation between the dynamic correlation length ξ_4, defined trough four-point correlation function, and the mosaic length ξ is not yet clear [141, 142].

If ξ_4 is of the order of a few glassites lengths ξ, then one expects that $\chi_4(\tau)$ should grow as some power of ξ. Assuming activated scaling (see Eq. 4.16), $log(\tau) \simeq \xi^{\psi}$, finally leads to $\chi_4(\tau) = log(\tau) \simeq \xi^{z}$, instead of a power-law relation predicted by MCT or other models. The crossover towards this logarithmic behaviour is not incompatible with the data [143]. However, the details of the crossover between the MCT and the RFOT regime are still very mysterious [144]. Despite of this, some claims have been made about the evolution of the shape of the dynamically correlated regions, that should change from stringy, fractal objects in the MCT regime to compact blobs at lower temperatures [145].

4.2.2 Facilitation: Kinetically constrained model and diffusing defects

The concept of *Facilitation* represents another approach to the glass transition, which has been extensively discussed in a recent review [146]. The underlying central idea is that, as very viscous liquids may be considered as almost solid, mobility is so sparse at any given time that any local relaxation event is likely to trigger, or 'facilitate' the relaxation of nearby regions after a time which is short compared to the macroscopic relaxation time but large compared to the microscopic one. Some degree of facilitation is surely present near the jamming transition, but the theoretical approach described in this section goes well beyond this simple observation and assumes that the system dynamics is mainly due to facilitation effects. This means that mobility cannot spontaneously arise in an immobile region of space, nor can it spontaneously disappear, but it is rather thought as a propagating entity.

KCMs are the result of implementing this concepts on lattice gas models and research on the facilitation approach to glassy dynamics has mainly consisted in the analysis of the physical behavior of these models. Motivation for this work largely stems from the observation that, despite their simplicity, KCMs are able to reproduce very well the phenomenology of real glass-formers, also concerning with the onset of DHs. Therefore, KCMs pro-

vide a simplified context to investigate glassy phenomena in details, or at least study one of their possible explanations.

At a theoretical level, KCMs and facilitated mechanisms have been rationalized in the diffusing defects picture, where defects generally represents the mobile regions that facilitate relaxation. Now this represents a very simple theoretical scenario for the glass transition, which is still able to furnish important quantitative or semi-quantitative predictions.

KCMs

All the theoretical scenarios we have discussed until now deal with a complex energy landscape. In MCT and p-spin models the many local energy stationary points directly lead to vitrification, whereas the sharp transition seems to be substituted by a smooth crossover when activated dynamics is taken into account.

However, an alternative view of the glass transition was sustained, stating that a complex energy landscape is not a necessary ingredient to have glassy phenomena. This is proven by the behaviour observed in KCMs [147]. These models typically consists in lattice gas filled with particles experimenting no other interaction apart from an hard-core repulsion which forbids the overlap. The system evolves following a given set of dynamical rules based on the local geometrical constraints of a single particle. In the most of KCMs the only control parameter is the density, which plays the role of an inverse temperature. This model is an attempt to capture the physics of a hard sphere system, and the fact that dynamics becomes slow at high density because the environment of each particle is very crowded.

The energy landscape doesn't represent a central ingredient at all, and it may be also trivial, i.e. with all the configuration allowed and available. As a consequence no thermodynamic transition can take place and the glassy behaviour is exclusively due to dynamical effects.

As a matter of fact, numerical simulations show that, as the density is increased, the dynamics becomes sluggish and heterogeneous, leading, in some cases, to a sharp dynamical transition of structural arrest. Although KCMs cannot approximate the behavior of glass-forming liquids in all regimes, they might still capture, at least on some range of time scales, the key dynamical aspects of real glass transitions.

In particular, KCMs may be divided in two classes. *Non-Cooperative* models display Arrhenius dynamic slowing down and are thus reminiscent of strong glass-formers. On the contrary, *Cooperative* models are able to reproduce the behaviour of fragile supercooled liquids, as they display a super-Arrhenius dependence of the structural relaxation time.

Diffusing Defects picture

A common feature of all KCMs is that their relaxation can be accurately described in terms of the motion of sparse defects. In Non-Cooperative models, such defects simply consist in empty sites able to diffuse, whereas in Cooperative models they can be formed by extended clusters moving in a cooperative manner, whose structure may be complex and nebulous.

As in facilitated systems, local relaxation at a given site occurs when it is visited by one such "defect", explaining structural relaxation is equivalent to explaining the defect dynamics. The amount of defects in a system may be characterized by their density ρ_d [106]. This quantity decreases as the density is increased: obviously the specific form of $\rho_d(\rho)$ will depend on the typical defect structure, which in turn depends on the dynamical rules. In the trivial case of freely diffusing lattice gas $\rho_d = 1 - \rho$, while for more complex KCMs ρ_d is provided to decrease as a faster law, possibly vanishing $\rho < 1$.

Defects diffuse anomalously with an exponent $1/x$ and a given diffusion coefficient D_d, which is also expected to be density dependent. Thus, $n_v(t) = (D_d t)^{d_f/x}$ is the number of distinct sites visited by a given defect at time t, and d_f is the fractal dimension of the walk. In the case of a 3-dimensional standard random walk, for example, we have $d_f = x = 2$ and $n_v(t) = D_d t$.

The relaxation time of the system can be reasonably defined as the time over which a finite fraction of the system, say $1/e$, has been visited by at least one defect. Supposeing that defect motions are weakly interacting, we can write $\rho_d n_v(\tau) = \rho_d (D_d \tau)^{d_f/x} = 1/e$, from which we find the following expression for the relaxation time:

$$\tau \propto \frac{1}{D_d(\rho)} \rho_d(\rho)^{-x/d_f}. \tag{4.26}$$

This expression suggests that when the density increases both the density of defects becomes small and their dynamics (captured by the diffusion coefficient) slows down dramatically, implying that the overall relaxation slows down in an activated, possibly super-Arrhenius manner.

Dynamic heterogeneities in KCMs

Another useful aspect of KCMs is that four-point spatial correlation functions can be studied in much greater detail than in molecular systems, to the point that scaling relations between timescales, lengthscales, and dynamic susceptibilities can be sometimes established [112, 106, 115, 138] . The type of scaling behaviour depends on the details of the model at hand. However, this behaviour may be still rationalized, at least at a qualitative level, in the diffusing defect paradigm.

In this scenario, the onset of DHs arise from the fact that a given defect creates a dynamical correlation between the sites that it progressively visits. As a consequence, the dynamical correlation length is expected to estimates the linear extension of the region visited after a time t, $\xi_4(t) \simeq (D_d t)^{1/x}$. This regime is provided to hold until regions explored by different defects interpenetrate. When this occurs the uncorrelated motion of the different defects destroys the correlation and ξ_4 starts to decrease. It is generally assumed that the time where the two regimes alternates should scale as the relaxation time τ.

Similarly, in the short times regime, the four-point susceptibility associated with ξ_4, is found to be the square of the volume visited by the same defect times the defect density, $\chi_4(t) \simeq \rho_d n_v(t)^2 = (D_d t)^{2d_f/x}$. When t is comparable to the relaxation time τ, the susceptibility reaches its maximum χ_4^*, and using Eq. 4.26 one finds $\chi_4(\tau) \simeq 1/\rho_d$ which, as expected, increases when increasing the density.

Chapter 5

Glassy dynamics in Kob-Andersen model

The main challenge in the field of supercooled liquids is the understanding of the rapid increase of the relaxation time and of the viscosity as the temperature decreases. Experimental evidences and theoretical models predicts the simultaneous emergence of DHs. Actually, the great interest for DHs is mainly motivated by the idea that large structural relaxation time and large spatio-temporal fluctuations of the dynamics are not only juxtaposed phenomena, but they are strictly related.

Summarizing the most quoted physical picture discussed in the previous chapter, such spatio-temporal fluctuations are interpreted as dynamically correlated clusters. By lowering the temperature the extension of these clusters grow and their cooperative rearrangement becomes more complicated. This results in a rapid increase of typical cluster life-time, which is in turn related to the structural relaxation time, at a macroscopic level.

From a quantitative point of view, the dynamical susceptibility $\chi_4(t)$, estimates the volume of dynamical clusters. Thus, χ_4 is expected to grow as some power of the dynamical correlation length; in particular $\chi_4(t) \propto \xi_4(t)^d$ for compact clusters in d dimensions, whereas a smaller exponent is expected if clusters have a fractal structure. This imply that the four-point correlation function $g_4(r,t)$ becomes progressively long-ranged as $\chi_4(t)$ grows. The time t^* where $\chi_4(t)$ reaches its maximum is also the time where correlations starts to decrease, and thus it is interpreted as an estimate of the typical cluster life-time. Then, the starting hipotesys is that DHs and relaxation are related, and one expects $t^* \propto \tau$.

We have seen that several experimental and numerical results seem to support this picture. However we must also warn that typically these results concern a limited range of temperatures and they often suffer of scarce statis-

tics. For this reasons, the relation between dynamical susceptibility and the cluster structure and, more in general, between relaxation processes and DHs remains elusive. For example, in order to unveil the precise relation between χ_4 and ξ_4 one needs to know the explicit form of $g_4(r,t)$, which is not an easy experimental task.

Such a state of the art motivates our work [131, 148]. In particular, we investigate via Monte Carlo simulation an andy glass former model, the popular 'Kob-Andersen model' (KA) , in order to:
- Perform a detailed study of DHs which comprises a direct inspection of $g_4(r,t)$ and $\xi_4(t)$.
- Provide a geometrical characterization of relaxation processes and DHs.

In this way we aim to clarify:
- In which way correlations and the dynamical susceptibility are related.
- To what extent DHs are tangled with relaxation.

This chapter is organized as follows. Sec. **??** is an introduction to the investigated system, where we discuss dynamical rules, numerical procedures and some previous results for glassy dynamics in the KA model. Results on the behviours of dynamical correlation function and DHs are described in Sec. **??**. In Sec.5.4 we provide a geometrical interpretation for DHs and relaxation processes.

5.1 Investigated system

5.1.1 Model

The Kob-Andersen model [149] is a kinetically constrained model (see Sec. 4.2.2), which consists in a cubic lattice of volume $V = L^3$ containing N particles. Periodic boundary conditions are imposed along the three x, y and z directions. The global density $\rho = N/V$ is the only control parameter and it plays the role of an inverse temperature in determining the glassy dynamics. No interactions between particles are present apart from an hard-core repulsion which prevents more than one particle to occupy the same lattice site: all microscopic configurations where the particles occupy N among the V available sites are allowed, isoenergetic and equiprobable. Thus, the model is characterized by a trivial energy landscape, where no thermodynamic transition is available and time translational invariance (TTI) holds in the dynamics.

These properties simplified numerical simulations, as no equilibration is

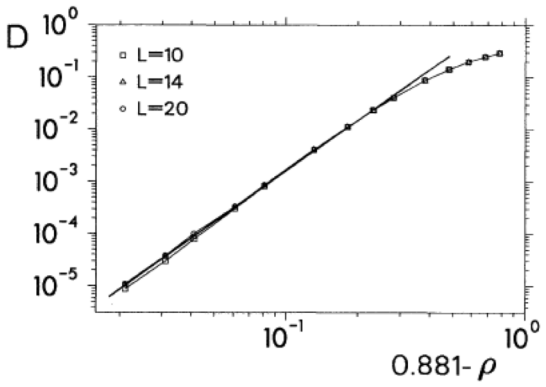

Figure 5.1: Diffusion coefficient D for three system sizes $L = 10, 14, 20$ as a function of $(\rho_{ka} - \rho)$. The straight line is a power law fit $D \propto (\rho_{ka} - \rho)^{3.1}$. From Ref. [149].

needed, allowing to investigate time-scales typically precluded to more complex glassy models. In fact, after generating a random initial configuration, we can immediately start the dynamics. The evolution of the system is set by the following dynamical rules:

1)Pick randomly a particle placed in a site r_i

2)Pick at random a site r_j between the six nearest neighbours of r_i

3) Check whether:a) r_j is empty. b) r_i has less than $m = 4$ occupied nearest neighbours. c) r_j has less than $m + 1$ occupied nearest neighbours.

4) If this three conditions are fulfilled, then let the particle in the site r_i moves in the site r_j. Otherwise, the particle remain in the site r_i.

5) Advance the clock of $1/N$ time unit and go back to 1).

This protocol may be thought as a trivial Monte Carlo simulation in which every configuration is equally probable, as it has the same energy.

The model we investigate and discuss so far is the original version introduced in [149], and also known as *Standard KA model*. However by changing the value of m, the dimensionality and the geometry of the lattice, several variations of the standard model have been introduced in literature [150].

5.1.2 Main previous results

Since its introduction in 1993, the KA model has been object of intense research. Here we mention the basic phenomenology and the results relevant

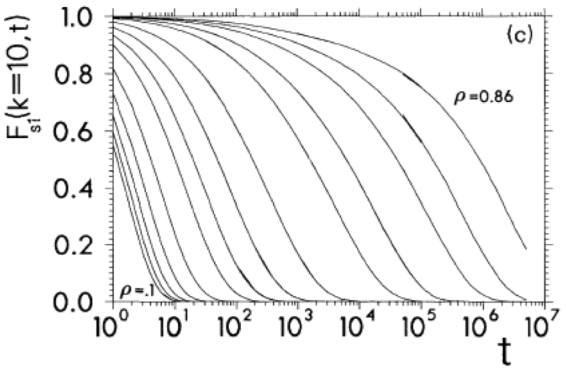

Figure 5.2: Intermediate self scattering function $F_s(k,t)$ as a function of time, for $L = 20$ and $k = 10$ and different values of the density ranging form $\rho = 0.1$ to $\rho = 0.86$. From Ref. [149].

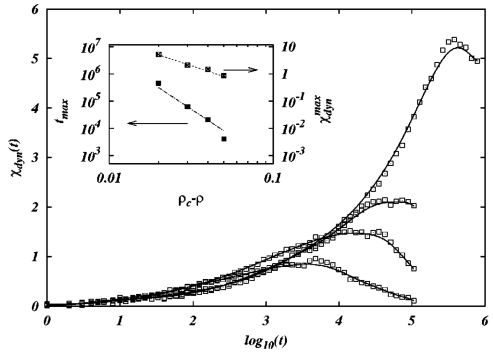

Figure 5.3: Dynamical susceptibilities in the KA model as a function of time for different densities. From to to bottom $\rho = 0.86, 0.85, 0.84, 0.83$. The inset shows the maximum values for the susceptibility and the relative time close to the transition of structural arrest; the lines are power laws fit with exponents 4 and 2 respectively. From Ref. [151].

for our work.

As the density increases, the dynamics rapidly slows down becoming sluggish and heterogeneous. In particular the self diffusion coefficient D, extrapolated by the long time behaviour of the mean squared displacement, is found to vanish in a critical way as the density approaches a threshold value, $\rho_{ka} \simeq 0.881$, which seems to depend weakly on the system size [149]. Fig. 5.1, where D is plotted as a function of $(\rho_{ka} - \rho)$, clarifies that at high density

data are well fitted by a power law: $D \propto (\rho_{ka} - \rho)^{\delta}$ with $\delta \simeq 3.1$

Fig. 5.2 shows the self-intermediate scattering function $F_s(k,t)$ as a function of time at a fixed value of k. Note that the dynamical correlation function does not show the two-step relaxation which is typical of glassy systems. The lack of the β relaxation was ascribed to the absence of particle rattling around their original position: in KA model all caged particles seems to be completely immobile until their cage fall apart [149]. However $F_s(k,t)$ markedly shows a non-exponential relaxation with a plateau which becomes longer and longer as the density increases. Rather than the β-relaxation, this plateau (which coincides with the intermediate or α-plateau in system with two step relaxation) is the very essential property of glass formers since it sets the time-scale for structural relaxation (see Sec. 3.1.5). In fact, from the time evolution of the self intermediate scattering function, Kob and Andersen extrapolated the relaxation time τ as the time such that $F_s(k,\tau) = 1/e$. As result, $\tau(\rho)$ also is found to diverge at a critical value compatible with ρ_{ka}: at high density τ behaves as $(\rho_{ka} - \rho)^{-\lambda}$ where the exponent λ is roughly comprised between 4 and 5 depending on the value of k. Thus, the behaviour of D and τ strongly suggests that ρ_{ka} is the locus of a dynamical transition of structural arrest of the kind provided by MCT.

Later it was proved [150] that for finite-dimensional KA models a true dynamical transition cannot exist in the thermodynamic limit , while it is actually present on Bethe lattice ($d = \infty$). In the standard KA model, what was confused with a transition at ρ_{ka} is just a sharp crossover interpretable as the *Ghost* of the infinite-dimensional transition. It was shown that this crossover is related to the emergence of a length-scale Ξ which sharply increases with the density. The phase space of systems with linear size $L > \Xi$ is ergodic, while for $L < \Xi$ the phase space is non-ergodic, resulting decomposed in many disjoints parts. It is predicted that for the standard KA Ξ diverges at the trivial density value $\rho = 1$ as a double exponential function, $\Xi(\rho) \propto exp[exp[c(1-\rho)]^{-}1]$. Similar fits work well also for $D(\rho)$ and $\tau(\rho)$ in the thermodynamic limit, i.e. provided $L > \Xi(\rho)$. Such a rapid increase explains why numerical investigations of ergodic system ($\rho > \rho_{ka}$) are not available at high density due to computational limitations.

As a matter of fact, the observed phenomenology is compatible with a glass transition at ρ_{ka}, making investigations of KA model a very intriguing task. In particular, several works [151, 152] have shown the presence of DHs, whose behaviour strongly resembles those found in real supercooled liquids. This is proven in Fig. 5.3 for the case of the dynamical susceptibility studied in Ref.[151] : χ_4^* and t^* are compatible with power law fits diverging at ρ_{ka} with exponents about 2 and 4 respectively.

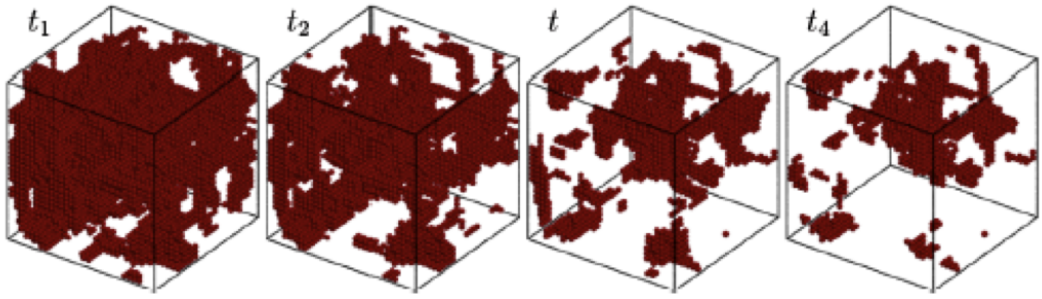

Figure 5.4: Persistent particles in a numerical simulations of the Kob–Andersen model at $\rho = 0.85$, at times $t_1 = 3.5{\cdot}10^5$, $t_2 = 7.5{\cdot}10^5$, $t_3 = 1.6{\cdot}10^6$, and $t_4 = 2.1 \cdot 10^6$.

5.1.3 Simulation details

Our simulations of the KA model spans a set of density values ranging over up $\rho = 0.87$. We have investigated a wide range of system size from $L = 8$ up to $L = 50$. Data reported in the following concerns a system size $L = 30$, where we have performed the largest statistics: for each density values, the results are averaged on at least 10^2 over up 10^4 runs. The runs at higher density values lasts up 10^8 Monte Carlo sweeps.

5.2 Dynamical correlation function

In order to monitor the dynamics of our system, we must chose an observable field $\phi_i(t)$ (see Sec. 3.1.5). We focus on the lattice site observable

$$\phi_i(t) = \frac{n_i(t)}{\rho}, \tag{5.1}$$

where $n_i(t)$ is known as 'persistence', and it is $n_i(t) = 1(0)$ if site i is (is not) persistently occupied by a particle in the interval of time $[0, t]$. Note that formally $\phi_i(t)$ does not explicitly show the two-time structure of Eq. 4.8 . By contrast, it is even more than a two-time function, since it keeps trace of the whole history in the interval $[0, t]$: in fact, it can be written as multi-time function, $n_i(t) = \Pi_{t'=0}^{t'=t} m_i(t)$, where $m_i(t)$ is the usual occupation number of site i at time t. The bulk quantity Φ defined in Eq.4.9 can be written as the fraction of persistent particles:

$$\Phi(t) = \frac{p(t)}{\rho} \tag{5.2}$$

where $p(t) = \frac{1}{V}\sum_{i=1}^{V} n_i(t)$ is the global density of persistent particles at time t.

The quantity $p(t)$ describes the relaxation of the system in a very direct way: initially $p(0) = \rho$ but as time proceeds, particles eventually move from their original positions and $p(t)$ decreases. This process is represented in Fig. 5.4 which shows the persistent particles in the system at different times of the same run. Note that as few and few persistent particles remain, spatial correlations between them seems to emerge. The normalized average value of $p(t)$ is our control parameter for relaxation, $C(t) = \frac{\langle p(t)\rangle}{\rho}$. Fig. 5.5a shows that $\frac{\langle p(t)\rangle}{\rho}$ has the same qualitative behaviour found for $F_s(k,t)$ in Ref. [149] (Fig.**??**). In a large time window and for $\rho \leq 0.85$, the decay of the dynamical correlation function is well described by the von Schweidler law:

$$\frac{\langle p(t)\rangle}{\rho} = f_0 - (t/\tau), \tag{5.3}$$

with $b \simeq 0.3$ and $f_0 \simeq 1$, whereas for larger time a stretched exponential fit works better. The relaxation time τ is still defined such that $\frac{\langle p(t)\rangle}{\rho} = 1/e$. Fig. 5.8b shows τ to diverge approaching the transition of structural arrest, $\tau(\rho) \propto (\rho_{ka} - \rho)^{-\lambda_\tau}$, with $\lambda_\tau \simeq 4.7$ consistent with the result of Ref. [151].

5.2.1 Persistance, overlap and scattering functions

Another advantage which motivates the use of $\frac{\langle p(t)\rangle}{\rho}$ as dynamical correlation function is that it may be related to the self intermediate scattering function $F_s(k,t)$ by an approximated expression which works very well for our model.

We start by illuminating the relation between the (total) experimentally measured intermediate scattering function (see. Sec. 3.1.5), $F(k,t)$,

$$F(k,t) = \frac{1}{N}\langle \Phi(k,t)\rangle, \tag{5.4}$$

where,

$$\Phi(k,t) = \sum_{i,j=1}^{N} e^{ik\cdot[r_i(t) - r_j(0)]}. \tag{5.5}$$

and a different dynamical correlation function known as overlap function, $q(t)$,

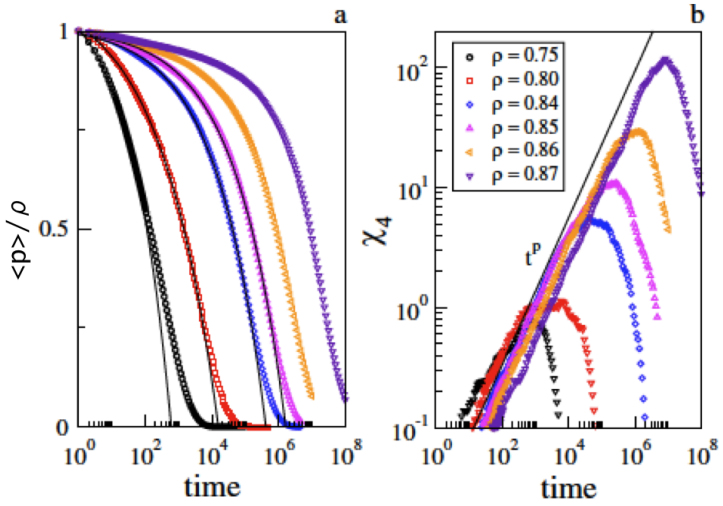

Figure 5.5: Normalized density of persistent particles $\langle p \rangle / \rho$ (panel a), and dynamical susceptibility χ_4 (panel b), for different values of the density, as indicated. For $\rho \leq 0.85$, $\langle p \rangle / \rho$ is well described by the von Schweidler law, $\langle p \rangle / \rho = f_0 - (t/\tau)^b$, with $f_0 = 1$ and $b \simeq 0.3$. At short times, the dynamical susceptibility grows as t^p, with $p \simeq 0.61$.

$$q(t) = \frac{1}{N} \sum_{i,j=1}^{N} \delta[r_i(t) - r_j(0)]. \tag{5.6}$$

Here the sum runs over the N particles of the system. The average of $q(t)$ is often used as dynamical order parameter to monitor the dynamics of glassy systems. Indeed, $q(t)$ has simple physical interpretation: suppose to take two snapshots of the same system at time 0 and time t respectively. $q(t)$ accounts for the number of pair of particles that overlap when the two snapshots are themselves overlapped, i.e. this occurs whenever a particle occupy at time t the same position occupied at time 0 by itself or by any other particle.

The average $\langle q(t) \rangle$ can be easily related to $F(k,t)$. In fact, $q(t)$ is the integral over the wave vectors k of the function $\Phi(k,t)$ defined in 5.5, as we show below:

$$q(t) = \frac{1}{N}\sum_{i,j=1}^{N}\delta[r_i(t) - r_j(0)] = = \frac{1}{N}\sum_{i,j=1}^{N}\int dk e^{ik\cdot[r_i(t)-r_j(0)]}$$
$$= \frac{1}{N}\int dk \sum_{i,j=1}^{N} e^{ik\cdot[r_i(t)-r_j(0)]} = \frac{1}{N}\int dk \Phi(k,t). \tag{5.7}$$

Thus, by averaging, we obtain:

$$\langle q(t)\rangle = \int dk F(k,t) \tag{5.8}$$

Moreover, for discrete systems, where particles overlap is forbidden, $q(t)$ may be easily expressed as a function of lattice site variables. In this case $\delta[r_i(t) - r_j(0)] = 1$ only if the particle i is a time t in the same lattice site h the particle j occupied at time 0, i.e. if $m_h(t)m_h(0) = 1$, where m_h is the usual occupation number. Then, we can turn the sum over particles in a sum over sites to obtain:

$$q(t) = \frac{1}{N}\sum_{h=1}^{V} m_h(t)m_h(0). \tag{5.9}$$

More interesting for our scopes, it is that analogous considerations hold for the self part of the overlap $q_s(t)$

$$q_s(t) = \frac{1}{N}\sum_{i}^{N}\delta[r_i(t) - r_i(0)], \tag{5.10}$$

also called self-overlap. $q_s(t)$ only gets contribution by the particles that at time t occupy the same position they occupied at time 0. Performing a calculation analogous to Eq. 5.7 it is found that:

$$\langle q_s(t)\rangle = \int dk F_s(k,t), \tag{5.11}$$

where the self intermediate scattering function $F_s(k,t) = \frac{1}{N}\sum_{i=1}^{N} e^{ik\cdot[r_i(t)-r_j(0)]}$. For discrete systems $q_s(t)$ may be written as:

$$q_s(t) = \frac{1}{N}\sum_{h=1}^{V}\left[\sum_{i=1}^{N} m_h^i(t)m_h^i(0)\right], \tag{5.12}$$

where we have introduced the VN occupation numbers $m_h^i(t) = 1(0)$ if (if not) the particle i stays in the site h at time t. Note that $m_h^i(t)m_h^i(0) = 1$

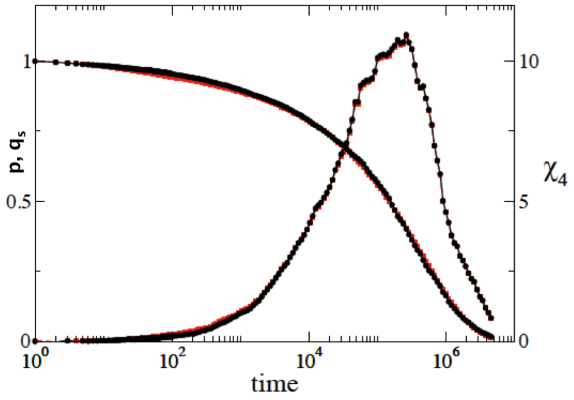

Figure 5.6: Fraction of persistent particle p (red) and self overlap q_s (black), and the dynamical susceptibilities computed by their respective fluctuations.

only if 1) the particle i has never moved from the site h until time t, i.e. if i is a persistent particle or if 2) the particle i starting from the site h has explored the system and then goes back at the initial position just at time t. The first contribution coincides with the persistence, while the latter is expected equal 1 with probability of the order $o(1/V)$, if rattlers are negligible and the system is ergodic. Then we can write:

$$q_s(t) \simeq 1/N \sum_{h=1}^{V} n_h(t) = \frac{p(t)}{\rho}, \tag{5.13}$$

which finally states that the self-overlap is approximated by the fraction of persistent particles. We have explicitly computed $q_s(t)$ in order to check to what extent this approximation works for our model. Fig. 5.6 clearly confirms that $q_s(t)$ and $p(t)/\rho$ have a very similar behaviour at any time-scale. The same holds for their fluctuations as evidenced by the dynamical susceptibilities. In conclusion, we can state that $\frac{\langle p(t) \rangle}{\rho} = \int dk F_s(k,t)$ and that $q_s(t)$ and $p(t)/\rho$ gives essentially the same results if used to investigate DHs [131].

5.3 Dynamical Heterogeneities

In order to quantify the correlation emerging in Fig. 5.4, we investigate the behaviour of DHs as defined by the persistence. In particular, we compute the correlation function between persistent particles,

$$g_4(r,t) = \langle n_i(t) n_j(t) \rangle - \langle n_i(t) \rangle \langle n_j(t) \rangle, \;\; r = |r_i - r_j|, \tag{5.14}$$

which represents our four-point correlation function, and, the dynamical susceptibility,

$$\chi_4(t) = \frac{V}{\rho} \left(\langle p(t)^2 \rangle - \langle p(t) \rangle^2 \right). \tag{5.15}$$

$g_4(t)$ and $\chi_4(t)$ are related by the following expression (see Sec. 4.1.2):

$$\chi_4(t) = \frac{1}{\rho V} \sum_{i,j}^{V} g_4(r,t). \tag{5.16}$$

From the data obtained for $g_4(r,t)$ we can estimate the dynamical correlation length $\xi_4(t)$.

Then, we are able to directly measure the time where $\xi_4(t)$ is maximum and we will use the notation t^*_ξ and t^*_χ in order to distinguish the times where $\xi_4(t)$ and $\chi_4(t)$ have their respective maxima.

Four-point correlation function

In Fig. 5.7a we show $g_4(r,t)$ at different times as a function of r. It is evident that the spatial extension of the correlation function grows until an intermediate time then decreasing at larger time, while its $r = 0$ value goes as $g_4(0,t) = \langle p(t) \rangle (1 - \rangle p(t) \langle)$, as determined by Eq. 5.14 .

Even though we find difficult to determine a precise functional form, the behaviour of $g_4(r,t)$ is consistent with a scaling form such as:

$$g_4(r,t) = A(t) \frac{e^{r/\xi_4(t)}}{r^{d-2+\eta}}, \tag{5.17}$$

where $\xi_4(t)$ is the dynamical correlation length (whose behaviour will be discussed in the next session) and $A(t)$ is the amplitude.

Fig. 5.7b shows $g_4(r,t)$ normalized by its value at $r = 0$ as a function of r for different densities and at intermediate time (roughly of the order of t^*_χ). As expected, g_4 becomes increasingly long ranged when the transition of structural arrest is approached.

5.3.1 Dynamical correlation length

From the data relative to $g_4(r,t)$, we have extracted the correlation length $\xi_4(t)$ via an exponential fit of the initial decay.

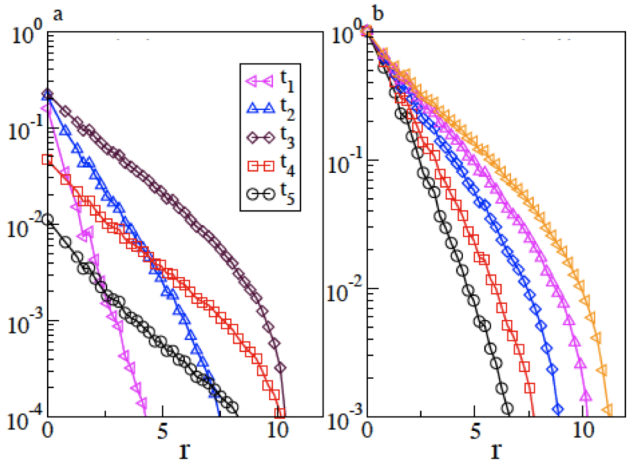

Figure 5.7: (Color online) Panel a: Correlation function between persistent particles $g_4 r, t$ as a function of the distance r at $\rho = 0.85$ amd for different times $t_1 = 10^2$, $t_2 = 5.3 \cdot 10^3$, $t3 = t^*_\chi = 5.6 \cdot 10^5$, $t_4 = 2.8 \cdot 10^6$, $t_5 = 4.6 \cdot 10^6$. Panel b: $g4(r, t \simeq t^*_\chi$ as a function of the distance r at different values of the density.

The behaviour of $\xi_4(t)$ is illustrated in Fig. 5.8a for different values of the density, and is well described by

$$\xi_4(t) \propto t^a \exp\left(-at/t^*_\xi\right). \tag{5.18}$$

Accordingly, at short times $\xi(t)$ grows as t^a with $a \simeq 0.156$, and then it decreases after reaching its maximum value ξ^*_4 at time t^*_ξ. We find that the time diverges as $t^*_\xi \propto (\rho_{ka} - \rho)^{-\lambda_{t^*_\xi}}$, with $\lambda_{t^*_\xi} = 3.8 \pm 0.1$. Then Eq. 5.18 predicts that the maximum dynamical correlation diverges as $\xi^*_4 \propto t^{*a}_\xi \propto (\rho_{ka} - \rho)^{-\nu}$, with $\nu = a\lambda_{t^*_\xi} \simeq 0.54$, in very good agreement with the data(Fig. 5.9) . Note here a very important result: contrary to what is expected, we find that, τ and t^*_ξ are not proportional but diverge with different exponents, $\lambda_\tau > \lambda_{t^*_\xi}$, approaching the transition of structural arrest. Moreover, as matter of fact, we find that at low density $t^*_\xi >> \tau$, but increasing the density τ grows faster then t^*_ξ, so that the two time-scales cross at intermediate density, and $t^*_\xi << \tau$ in the high density limit.

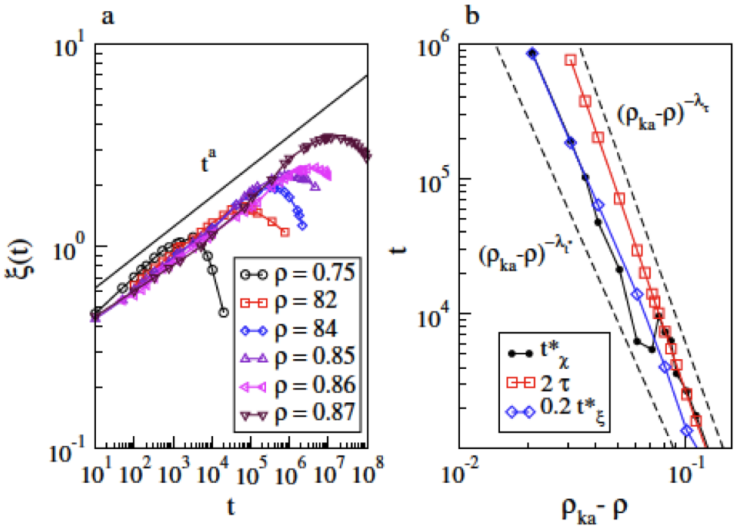

Figure 5.8: Panel a: dynamical correlation length for different values of the density. Panel b: divergence of the relaxation time τ, of the time where the correlation length acquires its maximum value t^*_ξ, and of the time where the dynamical susceptibility acquires its maximum value, t^*_χ. At low density, $t^*_\chi \propto \tau$, while at high density $t^*_\chi \propto t^*_\xi$. Errors on t^*_ξ and t^*_χ are of the order of 5%.

5.3.2 Dynamical Susceptibility

The emergence of an increasingly heterogeneous dynamics is clearly signaled by the dynamical susceptibility $\chi_4(t)$, shown in Fig. 5.5b for different values of the density. Qualitatively the behaviour of $\chi_4(t)$ appears similar to the one observed for $\xi_4(t)$, initially growing as $\chi_4(t) \propto t^p$, with $p \simeq 0.6$ and then decreasing after reaching its maximum value χ^*_4 at a time t^*_χ.

The decoupling between t^*_ξ and τ strongly influences $\chi^*_4(\rho)$ and the time $t^*_\chi(\rho)$, leading to a complex behaviour. In fact, inspired by Eq. 5.16 and Eq. 5.17 we find that $\chi_4(t)$ is well approximated by the expression:

$$\chi_4(t) \propto A(t)\xi(t)^{2-\eta} = \left[\langle p(t)\rangle(1-\langle p(t)\rangle)\right]\xi(t)^{2-\eta}, \qquad (5.19)$$

where we have estimated $A(t) = g_4(0,t)$ and $\eta \simeq 0$ consistent with [153]. Accordingly, the behaviour of the susceptibility is essentially given by the product of two competitive factors, the amplitude and the correlation length. Indeed, at low densities $t^*_\xi \gg \tau$, the amplitude dominates and Eq. 5.19 predicts $t^*_\chi \propto \tau$. By contrast, at high density $t^*_\xi \ll \tau$, and the maximum of the susceptibility χ^*_4 occurs at $t^*_\chi \propto t^*_\xi$. Such behavior of t^*_χ is apparent in

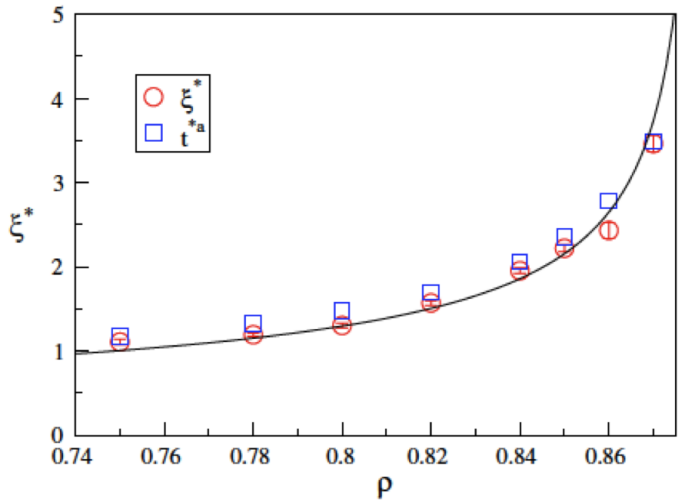

Figure 5.9: Dynamical correlation length at $t = t^*$, and prediction of the diffusing defect picture, $\xi^* \propto t^{*a} \propto \tau^q$, $q = a\lambda_\tau/\lambda_{t^*_\xi}$. The full line is a $(\rho_{ka} - \rho)^{-\nu}$, $\nu \simeq 0.54$ (we find $\rho_{ka} = 0.881$ as estimated from the divergence of the relaxation time).

Fig. 5.8: at intermediate density t^*_χ shows a clear crossover separating the two asymptotic regimes, where t^*_χ scales as τ in the limit of low-density and as t^*_ξ in the limit of high density.

In addition, when $t^*_\chi \propto \tau$, the maximum of the susceptibility scales as $\chi^*_4 \propto \tau^{2a} \propto (\rho_{ka} - \rho)^{-\gamma}$, with $\gamma = 2a\lambda_\tau$, in agreement with our results. Conversely, when $t^*_\chi \propto t^*_\xi$, we have $\chi^*_4 \propto t^{*2a}_\xi \propto \xi^{*a}_4 \propto (\rho_{ka} - \rho)^{-q}$, with $q = 2a\lambda_{t^*_\xi}$.

5.4 Geometrical interpretation

5.4.1 Diffusing defects

The results described so far are rationalized in the diffusing defects paradigm [106, 153, 157], where the relaxation is ascribed to the presence of possibly extended diffusing defects, with density ρ_d. since the KA model exhibits the typical handmark of cooperative KCMs, defects are expected to become extended and complex objects as much as the density is increased . As explained in Sec. 4.2.2, at short times the correlation length grow as $\xi_4(t) \propto t^{1/x}$, where d_f and $1/x$ are the fractal dimension and the diffusion exponent characterizing the defect walk. The number of distinct sites visited by a defect

grows as $n_v(t) \propto t^{d_f/x}$, so that the total number of distinct sites visited by the defects at time t is proportional to $\rho_d n_v(t)$. These assumption are expected to hold at least at short times, i.e. before defects interact. Under this condition, each site visited by a defect corresponds to a particle which first moves from its original position. Thus, we expect that at short times the the total number of distinct visited sites scale as the density of particles which have already relaxed at that time(the non-persitent particles), $1-\frac{\langle p(t)\rangle}{\rho}$. From the decay observed for the density of persistent particles, we can infer $1 - p(t)/\rho = (1/\tau)^b t^b \propto \rho_d n_v(t) \propto \rho_d t^{d_f/x}$. Therefore this picture reproduces the von Schweidler law, and relates the density of defects ρ_d with relaxation time [1], $\rho_d \propto \tau^{-b}$. By comparing the correlation length scaling provided by diffusing defect picture with the observed short time grows $\xi_4(t) \propto t^a$ (Fig. 5.9), we can conclude $1/x = a$ and $d_f = b/a \simeq 2$ Then we find that defects have a sub–diffusive nature, although they conserve the same fractal dimension of usual random walkers. We suggests this may be ascribed to defects that behave as random walkers, although characterized by a fat–tail waiting time distribution and, possibly, by weak spatial correlations which slows down the diffusion. In fact, it has been proved that these factors do not affect the fractal dimensions of the walks [158, 159].

Concerning with the susceptibility, the diffusing defect picture predicts that at short times, $\chi_4(t) \propto \rho_b n_v(t)^2 \propto t^{2b}$, which compared with our result allows to correctly estimate $p = 2b$.

5.4.2 Reverse dynamical percolation of persistent particles

Looking for a geometrical interpretation of the relaxation process, we were inspired by the analogy with chemical gels. The mechanical rigidity of chemical gels, in fact, arises from a percolating network of polymers which acts as a backbone in a liquid media (cfr Sec. 2.2.3). Since the bond of such network are of a chemical nature, relaxation cannot spontaneously occur and the system is solid at any time-scale. However relaxation may be induced by external factors, such as diffusing enzymes able to cut the bonds they meet [160, 161]: in this case, the system stays solid until the network survives, but it relaxes and becomes liquid at larger time-scale, when the network disappears.

In our case the glass former may be though as rigid on time scale smaller than the relaxation time τ. We suppose that during this time a percolating

[1] We are assuming that the diffusion coefficient of defects $D_d(\rho)$ varies slowly in the range of density we are dealing with

cluster of persistent particles plays the role of the physical backbone in gels; here the bonds are of a dynamical kind, i.e. we consider that two particles i and j are bonded in the interval $[0, t]$ if they are nearest neighbours and $n_i(t) = n_j(t) = 1$. Defects, instead, play the role of enzymes and progressively destroy the cluster. A reverse dynamical percolation transition is expected for time-scales of the order of the relaxation time. In fact, as the absence of the percolating cluster leads to the loss of rigidity, we expect that this transition is related to the relaxation process.

Data shown in Fig. 5.10 confirm our hipotesys. For density high enough to make glassy phenomena sensible, a cluster of persistent particles always spans the system at short times. We indicate with $P(t)$ its strength, i.e. the density of persistent particles belonging to such cluster. $\langle P(t)\rangle$ vanishes at a time t_{per} which is found to scale with the relaxation times τ as the density increases (Fig. 5.10 inset) .

The figure also reveals that the cluster strength overlaps with the total density of persistent particles, $\langle P(t)\rangle \simeq \langle p(t)\rangle$, for a long time. This means that in this interval the percolating cluster is the only cluster present. At larger time $p(t)$ slowly decays, while $P(t)$ vanishes. This is due to the onset of finite clusters with a broad size distribution, that give contributions to $p(t)$, but not to $P(t)$. This circumstance may explain the crossover observed for the dynamical correlation function (see Fig. 5.5a): at short time, the decay of $\langle p(t)\rangle/\rho$ is characterized by a single relaxation time, which is the life-time of the percolating cluster, and this leads to the von Schweidler law. By contrast, the broad spectra of finite cluster life-time determine the stretched exponential decay at large times.

To better understand the geometrical properties of this process, we investigate the behaviour of the length-scale $\xi_{per}(t)$ which characterizes percolation phenomena [162]. $\xi_{per}(t)$ is defined by the percolative correlation function $g_{per}(r, t)$:

$$g_{per}(r,t) = g_{pc}(r,t) - \langle P(t)\rangle^2 = \langle n_i(t) n_j(t)\rangle - \langle P(t)\rangle^2, \;\; r = |r_i - r_j| \;\; i, j \; connected, \tag{5.20}$$

where the *pair-connected* correlation function $g_{pc}(r, t)$ is limited to the pairs of particles that belong to the same dynamical cluster. $g_{pc}(r, t)$ can be also expressed as $g_{pc}(r, t) = P^f_{i,j}(r, t) + P^\infty_{i,j}(r, t)$ where $P^f_{i,j}(r, t)$ and $P^\infty_{i,j}(r, t)$ are the probabilities that two sites i and j belong to the same finite cluster, or to the percolating cluster (also called "infinite" cluster, inspired by the thermodynamic limit) respectively. Accordingly, if the percolating cluster is absent $g_{per}(r, t) = P^f_{i,j}(r, t)$ and $\xi_{per}(t)$ measures the typical size of finite clusters. Conversely, if finite clusters are negligible, then

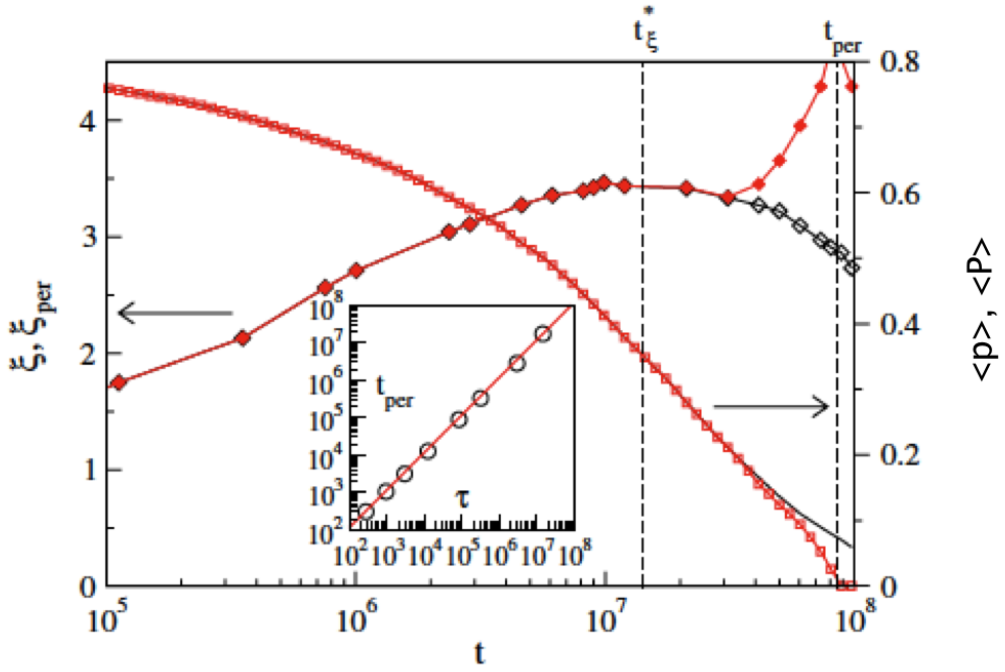

Figure 5.10: Percolation transition at $\rho = 0.87$. Left axis: dynamical correlation length ξ_4 (empty diamonds) and percolation correlation length ξ_{per} (full diamonds). Right axis: density of persistent particles $\langle p \rangle$ (full line) and strength of the percolating cluster $\langle P \rangle$ (squares). The vertical dashed lines mark t^*_ξ and t_{per}, which is proportional to τ (inset).

$$g_{per}(r,t) = P^{\infty}_{i,j}(r,t) - \langle P(t) \rangle^2 \tag{5.21}$$

measures the extension of the density fluctuations within the infinite cluster.

In our case, at short time, $\langle P(t) \rangle \simeq \langle p(t) \rangle$ and $P^{\infty}_{i,j}(r,t) \simeq \langle n_i(t) n_j(t) \rangle_{|i-j|=r}$, because almost all persistent particles belong to the percolating cluster, making the connectedness condition negligible [163]. Inserting these equalities in Eq. 5.21 and comparing with the definiton of the four point correlation function $g_4(r,t)$ of Eq. 5.14, we find that $g_{per}(r,t) \simeq g_4(r,t)$, and consequently $\xi_{per}(t) \simeq \xi_4(t)$

Fig. 5.10 confirms this prediction, showing that the dynamical and the percolative correlation length coincides in the same time interval where $\langle P(t) \rangle$ and $\langle p(t) \rangle$ overlap. The figure also indicates that we are dealing with an unusual percolation characterized by a non-monotonic percolative length.

In fact $\xi_{per}(t)$ is affected by the two time scales characterizing the glassy dynamics, the time t_ξ^* , where it has a relative maximum corresponding to the peak of the dynamical length, and the percolating time $t_{per} \propto \tau$, where it diverges in the thermodynamic limit as provided by standard percolation theory.

5.4.3 Some remarks

We have shown that in the KA model the relaxation process and the dynamical heterogeneities are characterized by two different timescales τ and t_ξ^*, which implies that they are less tangled than expected. We explain this feature in the diffusing defect picture, where we relate the relaxation process to a reverse percolation transition, and obtain a geometrical interpretation of the relaxation process and of the different timescales. Accordingly to their definitions, τ occurs when a given large fraction of all sites has relaxed, while t_ξ^* occurs when the correlations between the persistent particles decreases. Note that in principle our finding is not surprising: in facts, nothing forbids that these correlations may decrease before a large fraction of all sites has relaxed, $t_\xi^* < \tau$.

In models of defects behaving as perfectly random walkers, one finds that $\tau \propto t_\xi^*$ [106]. Therefore, one may speculate that, in our case, the decoupling between the two timescales is due to a complex nature of defects. For instance, they may be non conservative and characterized by birth and death rate with a constant average number, or they may not diffuse as random walkers.

Chapter 6

Jamming of sheared frictional grains

Friction, which characterize macroscopic particles such as granular materials, is also known to influence the jamming transition [23, 65, 66, 69, 167, 168, 169]. Its role has been deeply investigated at zero applied shear stress, $\sigma = 0$, where it changes the features of the jamming which occurs on compression. Indeed, studies of frictionless systems showed that these jam at a reasonably operatively well defined density value ϕ_c, the J-point (see Sec. 3.2.1), identified with the random close packing volume fraction ϕ_{rcp}. and only recently demonstrated to be weakly protocol dependent [48, 49, 50, 51]. Frictional systems, on the contrary, may jam at a volume fraction which may vary in a relatively large range [65, 66, 167, 168]. In presence of friction, the jamming density depends both on the compression protocol and on the friction coefficient (see Sec. 3.2.2). At finite shear stress, $\sigma > 0$, the jamming transition of frictional systems has been investigated to a much smaller extent, but for the case of granular particles on an inclined plane, where both the normal and the shear stress change with the angle of inclination, and where hysteretic effects have been reported [170]. However, there is not a systematic study of the jamming transition of frictional systems in the paradigmatic constant volume and constant shear stress 'ensemble' [1, 3].

Here, we report a comprehensive numerical investigation of the jamming transition of frictional systems at constant volume and constant applied shear stress, and show that friction controls the emergence of new dynamical regimes. Indeed, while in absence of friction a system is either fluid-like or jammed, in the presence of friction a system may reach a steady flowing state ('Flow' regime), may jam after flowing with a constant velocity for a long time ('Flow & Jam' regime), may jam after a small slip ('Slip & Jam' regime), or may respond as a solid ('Jam' regime). These features lead to the

jamming phase diagram illustrated in Fig. 6.8, where we introduce friction as a relevant control parameter [164]. We characterize the structural changes across the different jamming transition lines, and consider the possibility that granular systems jammed at finite shear stresses display a fragile behaviour [165].

This chapter is organized as follows. We start describing the investigated systems and the numerical procedure in Sec. 6.1. Then we illustrate in Sec. 6.2 the different dynamical regimes, and show how to define their transition lines. The dependence of these lines on the friction coefficient leads to the jamming three-dimensional jamming phase diagram described in Sec. 6.3. The mechanical properties of the jammed states and the concept of fragile matter are investigated in Sec. 6.4, and used to characterize the structural changes occurring across the transition lines in Sec. 6.4.3. Concerning the intriguing dynamical regimes present in the phase diagram, we named 'Flow & Jam' behavior, we discuss dynamical mechanism based on the concept of impeded dilatancy [166]. In Sec. 6.6 we describe finite size effects and the role of the numerical protocol.

6.1 Model system and numerical details

6.1.1 Investigated system

Our analysis is based on Molecular Dynamics (MD) simulations of soft-core spherical grains of mass M and diameter D, enclosed between two rough plates of size $l_x = l_y = 16D$, and $l_z = 8D$, as illustrated in Fig. 6.1. Each plate is made by a collection of particles that move as a rigid object. The bottom plate is fix (infinite mass). The top plate has a mass equal to the sum of the masses of the constituent particles. Periodic boundary conditions are used along x and y. The system is subject to a constant shear stress, $\sigma = \sigma_{xz}$, imposed by a shear force acting on the top plate, in absence of gravity. Periodic boundary conditions are used in the other directions.

The size of the vertical dimension l_z is chosen to be comparable to that of recent experiments [61, 62, 63]. We have investigated the effect of the finite size considering values of l_z up to $32D$, as described in Sec. 6.6.1.

6.1.2 Numerical model

We have used a standard model for the grain–grain interaction [171]. Two particles i and j, in positions $\mathbf{r}_i$ and $\mathbf{r}_j$, with linear velocities $\mathbf{v}_i$ and $\mathbf{v}_j$, and angular velocities ω_i and ω_j, interact when their separation distance

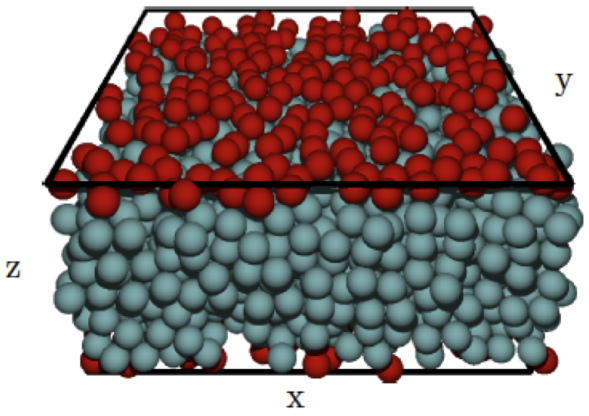

Figure 6.1: The investigated system. Grains are confined between two rough plates (red/dark particles) at a fixed vertical distance. A shear stress is fixed applying a force to the top plate; the bottom plate is fixed.

$\mathbf{r}_{ij} = \mathbf{r}_i - \mathbf{r}_j$ is smaller than their diameter, i.e. when the penetration length $\delta_{ij} = D - |\mathbf{r}_{ij}| \geq 0$. The interaction force has a normal and a tangential component, both having an elastic and a dissipative component.

The normal component is given by:

$$\mathbf{F}_{\mathbf{n}_{ij}} = -k_n \delta_{ij} \mathbf{n}_{ij} - \gamma_n m_{eff} \mathbf{v}_{\mathbf{n}_{ij}},$$

where k_n is the elastic modulus of the particles, $\mathbf{n}_{ij} = \mathbf{r}_{ij}/|\mathbf{r}_{ij}|$, $\mathbf{v}_{n_{ij}} = [(\mathbf{v}_i - \mathbf{v}_j) \cdot \mathbf{n}_{ij}]\mathbf{n}_{ij}$. The effective mass is $m_{eff} = M_i M_j / 2(M_i + M_j)$.

The tangential component is given by:

$$\mathbf{F}_{\mathbf{t}_{ij}} = -k_t \mathbf{u}_{\mathbf{t}_{ij}} - \gamma_t m_{eff} \mathbf{v}_{\mathbf{t}_{ij}},$$

where $\mathbf{u}_{\mathbf{t}_{ij}}$ is the elastic tangential displacement, and $\mathbf{v}_{\mathbf{t}_{ij}} = \mathbf{v}_{ij} - \mathbf{v}_{\mathbf{n}_{ij}}$. $\mathbf{u}_{\mathbf{t_{ij}}}$, set to zero at the beginning of a contact, measures the shear displacement during the lifetime of a contact. Its time evolution is fixed by $\mathbf{v}_{\mathbf{t}_{ij}}$, ω_i and ω_j, as described in Ref. [172]. Torques are given by $\tau_{ij} = -1/2 \mathbf{r}_{ij} \times \mathbf{F}_{t_{ij}}$. The shear displacement is set zero at the beginning of each contact, and is truncated to enforce the Coulomb condition $|\mathbf{F}_{\mathbf{t_{ij}}}| \leq |\mu \mathbf{F}_{\mathbf{t_{ij}}}|$ if needed. Here μ is the coefficient of static friction.

We use the value of the parameters of Ref. [172]: $k_n = 2 \times 10^5$, $k_t/k_n = 2/7$, $\gamma_n = 50$, $\gamma_t/\gamma_n = 0$. Different values of the friction coefficient are investigated. Lengths, masses, times and stresses are measured in units of $d_0 = D$, $m_0 = M$, $t_0 = \sqrt{M/k_n}$, $\sigma_0 = k_n/D$. We solve the equations of

motion of the system, $m\ddot{\mathbf{r}}_i = \sum_j \mathbf{F}_{\mathbf{n}_{ij}} + \mathbf{F}_{\mathbf{t}_{ij}}$ and $I\dot{\omega}_i = \sum_j \tau_{ij}$ via a velocity Verlet scheme, with an integration timestep $\delta t = 10^{-4}$.

When the applied shear stress is $\sigma \geq 2 \times 10^{-3}$ (the minimum value we have considered), the system reaches its steady state after a time of the order of $T = 10^6$ timesteps in all regions of the phase diagram, but for the 'Flow & Jam' regime (see below). In this regime, simulations with $T = 5 \times 10^8$ integration timesteps are needed. In $24h$, we simulate approximately a time 10^3, depending on the number of particles. We have performed simulations lasting up to 50 days. For each considered ϕ, σ, μ point, data are averaged at least over 10 independent runs. In the 'Flow & Jam' regime we have performed 100 runs for each considered ϕ, σ, μ point to properly evaluate the mean jamming time.

6.1.3 Volume fraction

The volume fraction ϕ is equal to the volume occupied by the grains divided by the volume of the container. Here, we have defined the volume fraction introducing a term which takes into account the effect of the rough plates protruding into the system. Due to the boundaries, the volume accessible to the grains is not $V_0 = l_x l_y l_z$, but $V = V_0 - \Delta V$, where ΔV is an unknown corrective term. Since ΔV is much smaller than V_0, we have:

$$\phi(N) = \frac{N v_0}{V_0 - \Delta V} \simeq \frac{N v_0}{V_0} \left(1 + \frac{\Delta V}{V_0}\right), \tag{6.1}$$

where N is the number of enclosed grains, we change to control the value of ϕ, and $v_0 = \pi/6D^3$ is the volume occupied by a single grain.

We have estimated ΔV evaluating the number of grains N_{rcp} corresponding to the jamming transition, i.e. such that the generated configurations have a finite pressure for $N > N_{rcp}$. Imposing $\phi(N_{rcp}) = \phi_{rcp}$, we have determined ΔV using Eq. 6.1.

6.1.4 Preparation protocol

We prepare the initial state using the protocol of Ref. [168]: randomly placed small particles are grown to their final size via molecular dynamics frictionless simulations, in the presence of a small viscous damping force. After inflating the particles, the system is allowed to relax until the kinetic energy vanishes. With this protocol, the jamming volume fraction at zero applied shear stress results to be $\phi_{rcp} \simeq 0.645$ [66]. Friction is introduced after these steps. Introducing friction after the inflation procedure allows for the generation of dense packings of frictional systems. Experimentally, these high

density states can be generated via more complex procedures such as vertical tapping, continuous high-frequency small amplitude vibrations [173], or thermal cycling [174]. The effect of different preparation protocols on the reported phenomenology is described in Sec. 6.6.2.

6.2 Dynamical regimes

6.2.1 Overview

When the Coulomb friction coefficient μ is set to zero, our system reduces to an assembly of frictionless particles which either flow, or responds as a solid to an applied external stress. The transition between these two regimes is assumed to occur along a well defined jamming line, $\phi_J(\sigma)$. In making this assumption, one is considering the system large enough for finite size effects to be negligible [24], and neglects the recently observed dependence of $\phi_J(0)$ on the protocol [48, 49, 50]. In our investigation these assumptions are reasonable, as we report a phenomenology occurring on volume fraction ranges which are greater than those of the intederminacy of $\phi_J(0)$ due to finite size effects, and to the protocol dependence. At finite applied shear stress $\sigma > 0$, assuming the presence of a single jamming line $\phi_J(\sigma)$ means to neglect hysteretic inertial effects [68].

Our simulations at constant volume and constant shear stress show that this scenario drastically changes in the presence of friction. Indeed, we have found four different dynamical regimes, 'Flow', 'Flow & Jam', 'Slip & Jam' and 'Jam' [1] , which are easily identified in Fig. 6.2, where we illustrate the time evolution of the top plate position (upper panel) and velocity (lower panel).

The behavior of the system in the different regimes can be summarized as follows. At low density, in the 'Flow' regime, the system flows and reaches a stationary velocity. For ϕ larger than a threshold $\phi_{J_1} = \phi_{J_1}(\sigma, \mu)$, the system enters the 'Flow & Jam' regime. Here the system first flows with a stationary velocity (reached after a transient), but eventually enters by chance a microscopic configuration which is able to sustain the applied shear stress, and jams. The 'Flow & Jam' region is limited by a jamming line $\phi_{J_2} = \phi_{J_2}(\sigma, \mu)$. Above ϕ_{J_2} steady flow is never observed, and the system jams after a small slip. This 'Slip & Jam' region is limited by the line $\phi_{J_3}(\sigma, \mu)$

[1] Another regime may be found at very high shear stresses, characterized by the ordering of the particles in planes parallel to the shearing direction [175, 176, 69, 177], causing a reduction of the shear viscosity. We do not describe this ordering transition in our diagram as it occurs at shear stresses which are higher than the ones we consider.

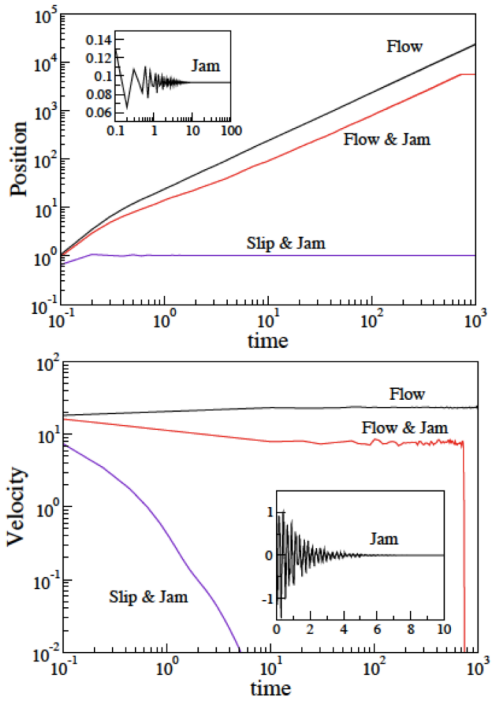

Figure 6.2: Position (upper panel) and velocity (lower panel) of the shearing top plate for $\sigma = 0.5$ and $\mu = 0.8$, and different volume fractions representative of the different flow regimes: $\phi = 0.578$ ('Flow'), 0.596 ('Flow & Jam'), 0.629 ('Slip & Jam') and 0.655 ('Jam'). In the 'Flow' regime the system flows with a steady velocity; in the 'Flow & Jam' regime the system first flows with a steady velocity, but then jams after a time t_{jam}; in the 'Slip & Jam' regime the system slips of a distance ΔL, never reaching a steady velocity, and then jams. In the 'Jam' regime the system responds as a solid to the applied shear stress.

above which the system does not slip, but responds as a solid to an applied external stress.

In the following, we describe how to quantitatively define the different transition lines.

6.2.2 Jamming line ϕ_{J_1}

The line ϕ_{J_1} marks the transition between the 'Flow' and the 'Flow & Jam' regime. In the 'Flow & Jam' regime, the system stops flowing when a jamming configuration has been selected, after an average time t_{jam}. We find

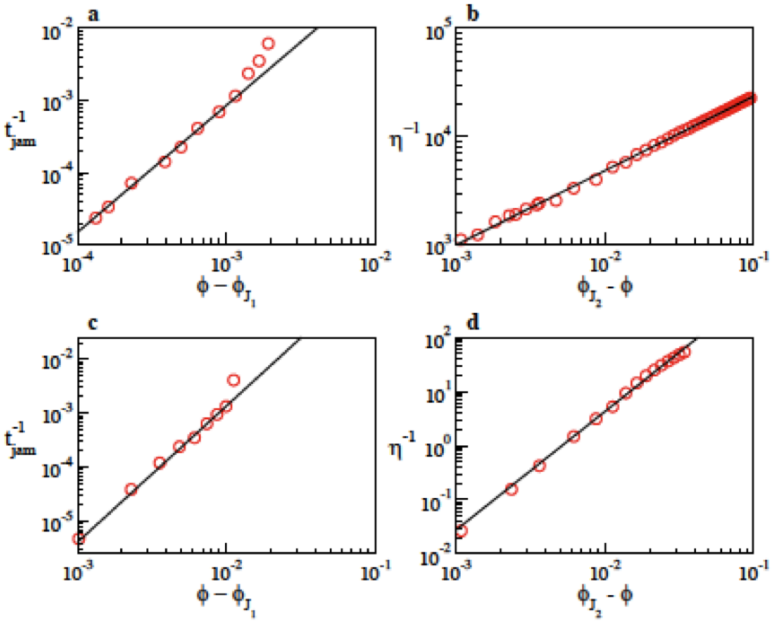

Figure 6.3: The jamming time t_{jam} and the viscosity η have been fitted by power laws, $t_{jam} \sim (\phi - \phi_{J_1})^{-\alpha}$, $\eta \sim (\phi_{J_2} - \phi)^{-\gamma}$, for any given value of σ and μ. Panel a) and b) show data corresponding to $\sigma = 2 \times 10^{-3}$ and $\mu = 0.1$, where $\alpha = 1.75$, $\phi_{J_1} = 0.622$, $\gamma = 0.75$ and $\phi_{J_2} = 0.625$. Panel c) and d) show the same quantities for $\sigma = 5 \times 10^{-3}$ and $\mu = 0.8$. In this case $\alpha = 2.4$, $\phi_{J_1} = 0.598$, $\gamma = 2.1$ and $\phi_{J_2} = 0.612$.

this jamming time to grow as the volume fraction decreases, in agreement with the expectation that, the lower the volume fraction, the smaller the number of configurations able to sustain the applied stress. Indeed, when the volume fraction is too small, no such configuration exists, and t_{jam} is infinite, as in the 'Flow' regime. We therefore define ϕ_{J_1} as the volume fraction where t_{jam} diverges on decreasing the volume fraction, and determine it via a numerical extrapolation. Our numerical data, shown in Fig. 6.3a,c for different values of the parameters, suggest a power law divergence of the jamming time, $t_{jam} \sim (\phi - \phi_{J_1})^{-\alpha}$, with α not universal.

6.2.3 Jamming line ϕ_{J_2}

When the system reaches a steady flowing state, in the 'Flow' regime, it is possible to define the shear viscosity $\eta(\phi, \sigma, \mu)$, as the ratio between shear stress σ and shear rate v_s/h, where h is the distance between the two plates,

and $v_s(\phi, \sigma, \mu)$ the velocity of the shearing plate. This definition is meaningful as we observe a linear velocity profile. The viscosity increases on increasing the volume fraction. We define ϕ_{J_2} as the volume fraction where the extrapolated viscosity diverges. We find η to diverge as a power law, $\eta \sim (\phi_{J_2} - \phi)^{-\gamma}$, with an exponent γ which appears not to depend on the shear stress, but to depend the friction coefficient. Results for the divergence of t_{jam} and of η are shown in Fig. 6.3. We always find $\phi_{J_2} > \phi_{J_1}$, as expected considering that the system flows with a finite shear rate at $\phi = \phi_{J_1}$.

Note that it is also possible to measure the shear viscosity in the 'Flow & Jam' regime, as for $t < t_{jam}$ the system flows in an apparently steady state. We have used values of the viscosity in this regime to reduce the error on the estimation of ϕ_{J_2}.

6.2.4 Jamming line ϕ_{J_3}

The line ϕ_{J_3} marks the end of the 'Slip & Jam' regime, where the system slips a distance $\Delta L(\phi, \sigma)$ before jamming. We therefore define ϕ_{J_3} as the volume fraction where ΔL vanishes. To measure ΔL one needs to consider that the total displacement of the top plate in a jammed configuration of the 'Slip & Jam' regime includes, beside the slip distance ΔL, a contribution due to the deformation induced by the shear stress. This additional deformation disappears when the shear stress is set back to zero. We have therefore defined the slip ΔL as the residual displacement of the top plate in a stress cycle: after preparing the system we slowly increase the stress to its final value σ, and then decrease it to zero. Figure 6.4 (top panel) shows the displacement of the top plate position as a function of the shear stress for $\sigma = 5 \times 10^{-3}$ and $\mu = 0.8$. Different curves refer to different values of the volume fraction, as indicated. At small ϕ, the initial and final positions of the top plate do not coincide, and the residual displacement is $\Delta L > 0$, while at high ϕ we find $\Delta L \simeq 0$.

Precisely, when the shear stress is small, the residual displacement decreases as a power law as the volume fraction increases, which allows to estimate ϕ_{J_3} via a numerical fit of $\Delta L(\phi)$ at each σ and μ, as illustrated in Fig. 6.4 (bottom panel). At high values of the shear stress, ΔL does not vanish on increasing the volume fraction, as the system deforms plastically in a stress cycle. When this is the case the dependence of ΔL on ϕ shows a clear crossover from a slip-dominated regime to a plastic-dominated regime, as shown in Fig. 6.5. When such a crossover is seen, we define ϕ_{J_3} as the inflection point of $\Delta L(\phi)$.

The crossover from the elastic to the plastic regime is due to the increase of the number of contacts that break as the strain increases. At small σ,

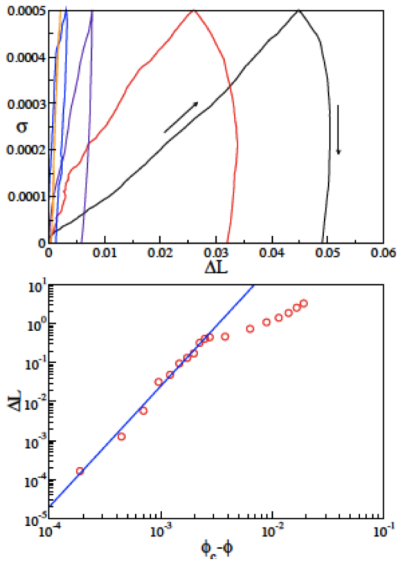

Figure 6.4: Top: displacement of the top plate in a stress cycle. The stress is first increased to its final value σ, and then decreased to zero. The residual displacement is our definition of the slip ΔL. From left to right, $\phi = 0.6488$, 0.6482, 0.6480, 0.6477, 0.6475. Bottom: for a fixed value of the shear stress ($\sigma = 5 \times 10^{-3}$), the slip decreases on increasing the volume fraction, and vanishes at a volume fraction ϕ_{J_3}, which depends on σ and μ. The straight line is a power law $\Delta L = a(\phi - \phi_{J_3})^b$, $b \simeq 1.2$ and $\phi_{J_3} \simeq 0.6495$.

the strain of the system is small, and contacts do not break. At higher σ, the strain of the system is large, and contacts break. Contact breaking appears therefore to be the microscopic origin of the plastic response. Indeed, memory of the tangential force between two grains is lost when the Coulomb threshold is reached.

The line ϕ_{J_3} can also be defined as that where the jamming time t_{jam} vanishes on increasing the density. Within numerical errors, the resulting estimate coincides with the one obtained investigating the residual slip.

6.3 Jamming phase diagram

The location of the jamming lines depends on the model parameters. Their dependence on the applied shear stress is illustrated in Fig. 6.6, for two different values of the friction coefficient. As the shear stress increases, all transitions move to higher volume fractions. The dependence on the friction

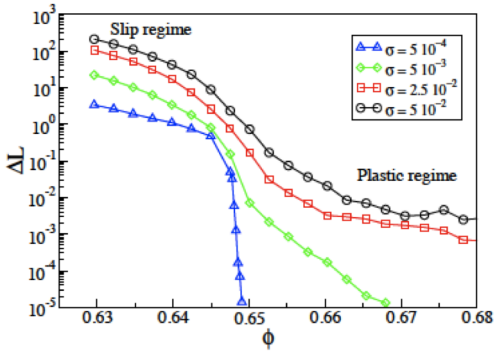

Figure 6.5: Dependence of the slip ΔL on the volume fraction ϕ, for different values of σ, at $\mu = 0.8$. When σ is small, ΔL decreases on increasing ϕ, and ϕ_{J_3} is defined as the volume fraction where ΔL vanishes, as illustrated in Fig. 6.4. Conversely, at high σ, ΔL does not vanishes, but shows a crossover from a slip-dominated regime to a plastic-dominated regime. In this case ϕ_{J_3} is defined as the inflection point of $\Delta L(\phi)$.

coefficient of ϕ_{J_1}, ϕ_{J_2} and ϕ_{J_3} is illustrated in Fig. 6.7, for $\sigma = 2 \times 10^{-3}$. The dependence of ϕ_{J_3} on μ is very small, and only appears at high ϕ or σ, where the system behaves plastically due to the breaking of frictional contacts. The dependence of ϕ_{J_1} and ϕ_{J_2} on μ is similar to that of different jamming thresholds found via particle inflating algorithms [66, 167], or via experiments [178] and simulations [64] of sedimentation.

Extrapolating our high friction estimate of ϕ_{J_1} to the limit of zero applied shear stress, we found $\lim_{\sigma \to 0} \phi_{J_1}(\sigma) \simeq 0.585$. This estimate is close to the smallest volume fraction at which jammed states have been found via particle inflating protocols in no gravity [66]. Looser states have been found experimentally in the presence of gravity [179, 178], as well as numerically in no gravity via particle deflating procedures [180]. We prefer not to link this loose density state with the random loose packing volume fraction, as this lacks an accepted theoretical definition, and is operatively defined via a different protocol (sedimentation) [179, 178, 181].

The dependence of the jamming lines on friction finally leads to the schematic jamming phase diagram for frictional particles of Fig. 6.8, characterized by three axis: the inverse density, the shear stress and the friction coefficient. In this phase diagram, the surfaces $\phi_{J_1}(\sigma, \mu)$, $\phi_{J_2}(\sigma, \mu)$ and $\phi_{J_3}(\sigma, \mu)$ enclose regions of different flow properties. In this diagram, we have assumed the jamming surfaces to meet in the $\mu = 0$ plane along a well defined jamming transition line, $\phi_J(\sigma)$, in agreement with the absence of results showing the

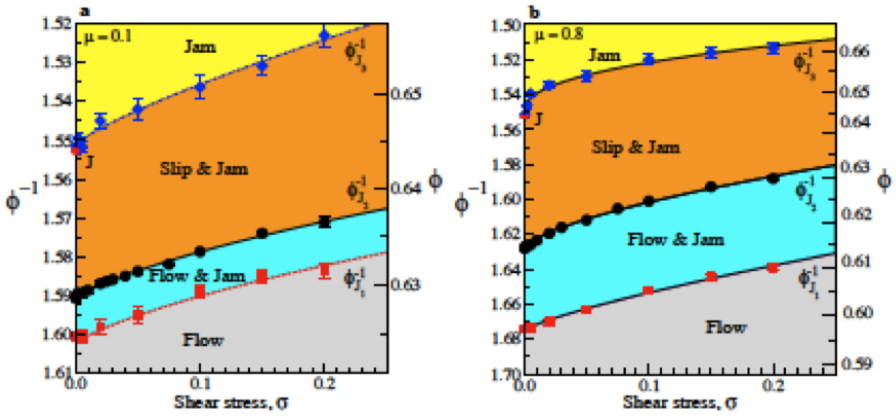

Figure 6.6: (Color online) Location of the different flow regimes in the inverse density, applied stress space, for $\mu = 0.1$ (panel a) and $\mu = 0.8$ (panel b).

presence of the 'Flow & Jam' phenomenology in frictionless systems. However, as already mentioned, at zero friction neither the J–point [48, 49, 50] nor the jamming transition line [68, 182] are uniquely defined, which suggests the possible existence of an extremely small volume fraction range where the 'Flow & Jam' and the 'Slip & Jam' regime persist [183].

The phase diagram of Fig. 6.8 clarifies the intuitive expectation that, when a frictional system jams after flowing, then it is possible to unjam it not only varying the density or the shear stress, but also by changing its friction coefficient, for instance changing humidity, temperature, or introducing lubricants [184, 185].

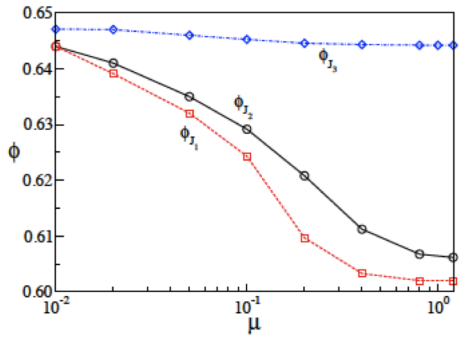

Figure 6.7: (Color online) Friction dependence of the different jamming lines, for $\sigma = 2 \times 10^{-3}$. Lines are a guide to the eyes.

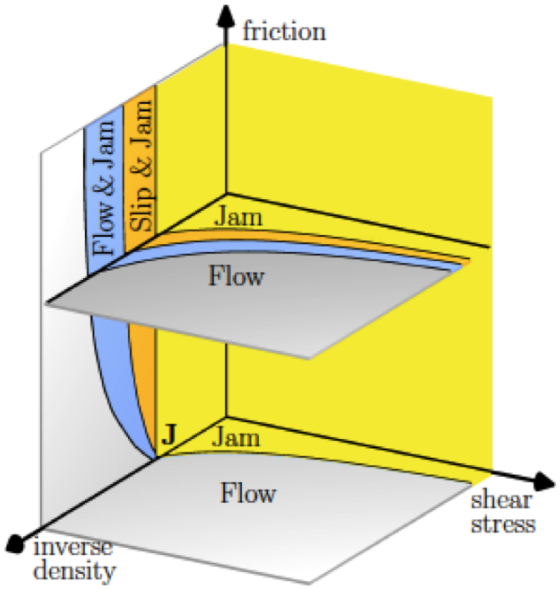

Figure 6.8: The jamming properties of frictional systems are illustrated in a diagram with axis the inverse density, the shear stress and the friction coefficient. At zero friction the jamming phase diagram is characterized by a 'Flow' and by a 'Jam' region, while in the presence of friction two new regions appear: the 'Flow & Jam' region and the 'Slip & Jam' region.

6.4 Mechanical Response and Fragility

The concept of *fragile matter* has been introduced by Cates et al. [23], following earlier numerical results concerning the shear viscosity of particle suspensions [72], and concerns systems jammed under the action of a shear stress (see Sec. 3.2.3). In these systems, the stress is supported by an anisotropic structure. It was speculated that this anisotropy influences the mechanical properties of the system, which may depend on the relation between the perturbing stress and the pre–existing one. In particular, the system is expected to behave as a solid in response to compatible perturbations, which are those not changing the principal stress axis. Conversely, perturbations changing the principal stress axis are expected to unjam the system.

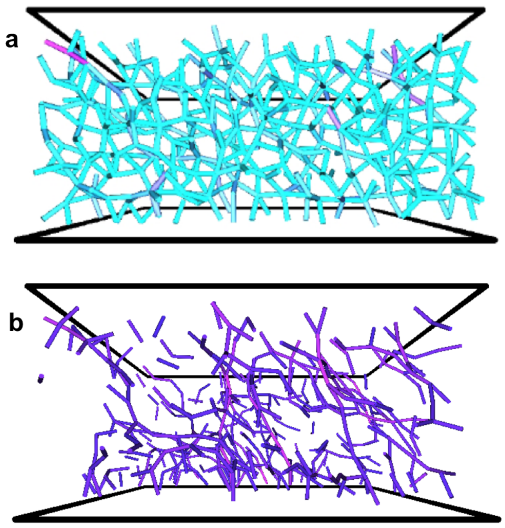

Figure 6.9: Panel a) Network of contact forces in a system jammed under the effect of a constant shear stress. Each segments marks the direction of the force acting between a pair of grains in contact. A color scale is used to represent the force intensities. Panel b) The picture only shows the strongest contacts (10% of all contacts) of the network.

6.4.1 Network of contact force

A simple model for a fragile system [23] consists in a series of force chains directed along the principal stress axis, supporting the applied stress and living in a sea of spectators. In our system, one does observe force chains preferentially aligned along the principal stress axis, as illustrated in Fig. 6.9a. These force chains belong to a percolating cluster of particles, which comprehends all of the particles but for a few rattlers. Indeed, due to the repulsive force acting between contacting particles, two particles can be in contact only if they both belong to a percolating cluster. This cluster provides the support for a network of force chains. Finite clusters, except single particles, called rattlers, are not allowed, since, due to repulsive force acting between contacting particles, a cluster not hold by the confining plates breaks.

Between all contact forces, it may be interesting to localize the stronger ones and to study the structure of their resulting network. The network of course will depend on how one defines a bond between two neighbours particles. So far we have considered two particles being connected if in contact, namely if the penetration length is positive. By introducing a threshold one

can consider two particles bonded if the penetration length is larger than a given threshold. Higher thresholds select larger stressed bonds. In Fig. 6.9b we show that the network found for high values of the threshold, although more complex and branched, strongly resembles the minimal model by *Cates et al.*, as it appears highly anisotropic, with the stronger forces being directed along the principal stress axis. By contrast, the largest network (Fig. 6.9a), where all the stressed bonds are taken into account, are more isotropic and less 'fragile'. Thus, we could expect that the response to stress applied in different direction share the same anisotropy, reflecting the structure of the underlying network of contact forces. However the 'fragility' property is expected to stem not only by the large stressed bonds but by the entire network, with an appropriate weight for each bond.

A more quantitative inspection of this point can be achieved by measuring the shear modulus of the system, as we discuss in the next section.

6.4.2 Shear modulus

Here we describe the measure of the shear modulus G. This is a quantity of interest both to characterize the jamming transitions, as well as to investigate whereas granular systems jammed at a finite value of the shear stress are fragile as speculated [23]. To measure the shear modulus G of a system jammed under the action of an existing shear stress σ_{xz}, we have introduced a perturbing shear stress. The non-zero components of this perturbing stress are $\delta\sigma_{xz}$ and $\delta\sigma_{yz}$, we fix in such a way that $\delta\sigma_{xz}^2 + \delta\sigma_{yz}^2 = \delta\sigma^2$. The perturbing shear stress is therefore conveniently expressed in terms $\delta\sigma$ and of $\theta = \arctan(\delta\sigma_{yz}/\delta\sigma_{xz})$.

Fig. 6.10 shows the displacement $\delta\mathbf{r} = (\delta x, \delta y)$ of the top plate position for different values of ϕ at fixed σ and $\delta\sigma$ (left), and for different values of $\delta\sigma$ at fixed σ and ϕ (right). Each curve is obtained by first applying a perturbing shear stress at $\theta = 0$, and then increasing θ from 0 to 2π. The figure clarifies that systems jammed under shear are elastic, as each curve describes a close path. Accordingly, even though their mechanical rigidity originates from an underlying force network which is highly anisotropic, these systems are not fragile as speculated [23], at least in their response to the small stress perturbations we have considered.

The absence of fragility can be rationalized in terms of the properties of the energy landscape of the system. Indeed, fragile jammed systems can be associated with saddle points, as their elastic energy may increase or decrease, depending on the direction of the perturbation, respectively leading to an elastic response, or to an instability. Since dissipative systems do not spontaneously arrest in an unstable point of their energy landscape, we

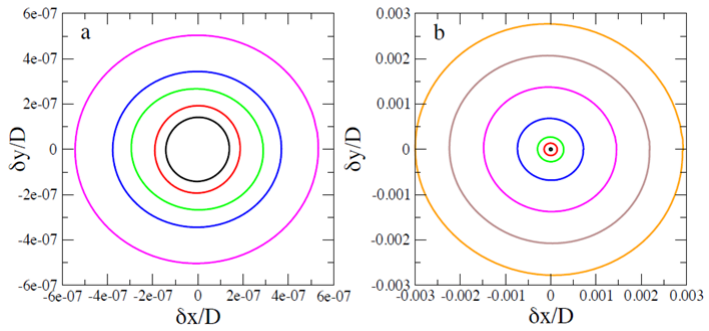

Figure 6.10: Response of a jammed system to a small perturbing shear stress. Panel (a) shows the response of systems jammed under the action of a stress $\sigma = 10^{-2}$, to a perturbing stress $\delta\sigma = 10^{-4}$, for different values of the volume fraction (from the inside, $\phi = 0.655$, 0.630, 0.617, 0.613 and 0.610). Panel (b) shows the response of system with volume fraction $\phi = 0.617$, jammed under the action of a shear stress $\sigma = 10^{-2}$, to different perturbing stresses (from the inside, $\delta\sigma = 10^{-3}$, 5×10^{-3}, 10^{-2}, 2.5×10^{-2}, 5×10^{-2}, 7.5×10^{-2}, 10^{-1}). The friction coefficient is $\mu = 0.8$.

expect them to arrest in a true energy minimum. Systems that jam under the action of an applied stress are therefore not expected to be fragile. Of course, a fragile behavior may appear in the response to large stress variations.

The curves of Fig. 6.10 resemble perfect circles, suggesting the presence of an isotropic response. We have verified that this is the case investigating the parameter

$$\xi(\theta) = \frac{[\delta x^2(\theta) + \delta y^2(\theta)]^{1/2} - \overline{\delta r}}{\overline{\delta r}}, \tag{6.2}$$

where $\overline{\delta r} = \langle [\delta x^2(\theta) + \delta y^2(\theta)]^{1/2} \rangle_\theta$. As illustrated in Fig. 6.11, the anisotropy of the system is small, being $|\xi(\theta)| < 4\%$.

Due to the elastic and isotropic response of the system, we are allowed to defined the shear modulus as $G = \lim_{\delta\sigma \to 0} \delta\sigma/\epsilon$, where ϵ is the shear strain induced by $\delta\sigma$. Its behavior is described in the next section.

6.4.3 Structural changes across the jamming lines

Here we consider how the structural properties of the system change across the jamming transitions. In particular, we focus on the variation of the mean contact number Z, of the normal pressure on the confining walls P, and of the shear modulus G. In Fig. 6.12, we illustrate their volume fraction dependence

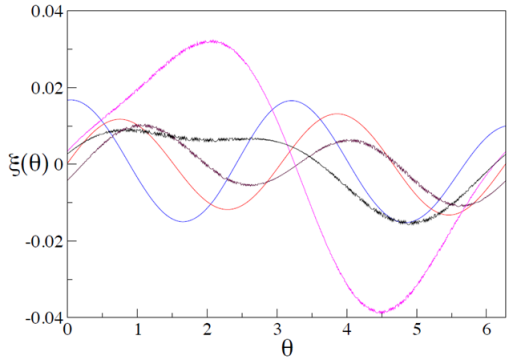

Figure 6.11: Anisotropy in the response to a small perturbing shear stress of a system jammed under the action of a large shear stress. Different curves refer to different values of the volume fraction.

for $\mu = 0.8$ and $\sigma = 5 \times 10^{-3}$. In the flowing regime (full circles) Z and P increase with ϕ, while G is zero. In the jammed regime (full diamonds) Z, P and G are roughly constant for $\phi < \phi_{J_3}$, while they increase as power laws for $\phi > \phi_{J_3}$, where a continuous transition occurs. Measures in the flowing state in the range ϕ_{J_1}–ϕ_{J_2} (open circles) are taken for $t < t_{jam}(\phi)$. Compared to previous numerical studies [169, 66, 167] conducted at $\sigma = 0$, our findings show that there is a whole volume fraction range where frictional granular systems may have the same mechanical properties. This volume fraction range can be identified with a constant Z line of the Z-ϕ diagram of Ref. [169].

6.5 'Flow & Jam' regime

In the 'Flow & Jam' region the system exhibits a very intriguing phenomenology, whereby it first flows with a constant velocity as in a steady flowing phase, but then suddenly jams(see Fig. 6.2). As we discuss in Sec. 6.2 this occurs after an average time tj, which diverges as a power-law by approaching the line ϕ_{J_1}, as shown in Fig.6.3. In this section we focus on the dynamics of this regime in order to clarifies the mechanisms originating such a complex behaviour.

6.5.1 Jamming times

Fig. 6.13 compares the velocity $v_s(t)$ of the upper plate as a function of time for three simulations at $\phi = 0.627$ and $\sigma = 2\ 10^{-3}$, clarifying that the

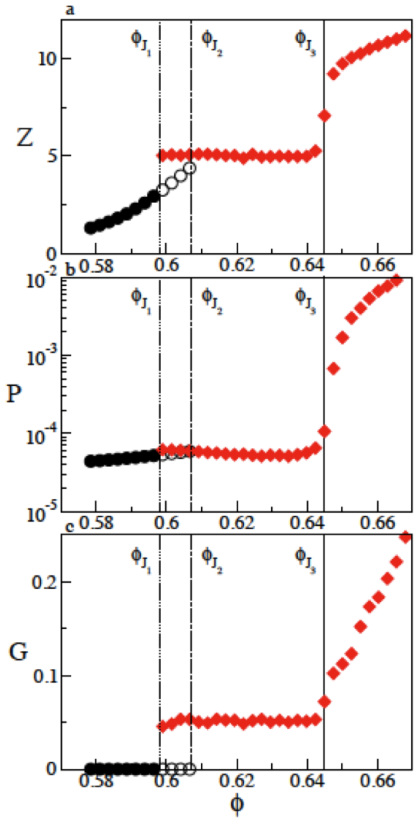

Figure 6.12: Mean contact number Z (a), normal pressure on the shearing plate P (b), and shear modulus G (c) as a function of ϕ, for $\sigma = 5 \times 10^{-3}$ and $\mu = 0.8$. The vertical lines mark ϕ_{J_1}, ϕ_{J_2}, and ϕ_{J_3}, as indicated. Full circles are measures taken when the system flows, while full diamonds are measure taken in jammed configurations. Open circles in the range ϕ_{J_1}–ϕ_{J_2} are measures taken in the flowing regime for $t < t_{jam}(\phi)$, before the system jams.

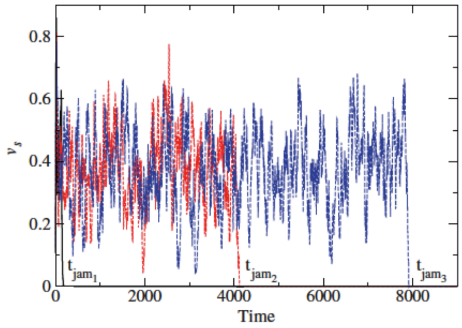

Figure 6.13: Velocity of the upper plate v_s as a function of time for three simulations at $\phi \simeq 0.627$ and $\sigma = 2 \cdot 10^{-3}$. We marked the values of the jamming times, t_{jam}, which differ by more than three decades.

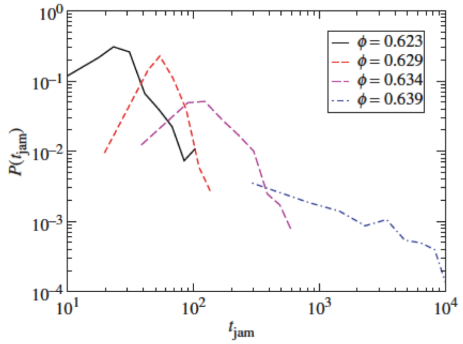

Figure 6.14: Probability distribution $P(t_{jam})$ of the jamming time for $\sigma = 2 \cdot 10^{-3}$ and different values of the volume fraction, as indicated.

jamming time is subject to large fluctuations. In facts, the three simulations shown in Fig. 6.13 jam at very different times, even though they differ only in the initial configuration. Such an observation suggested to study the sample fluctuations of the jamming time, which we show in Fig. 6.14 for $\sigma = 2 \cdot 10^{-3}$ and four different values of the volume fraction. While at high volume fractions $P(t_{jam})$ is peaked, meaning that the jamming time is well defined, on decreasing the volume fraction the distribution moves to larger times, and at the same times changes shape, becoming well described by a power law.

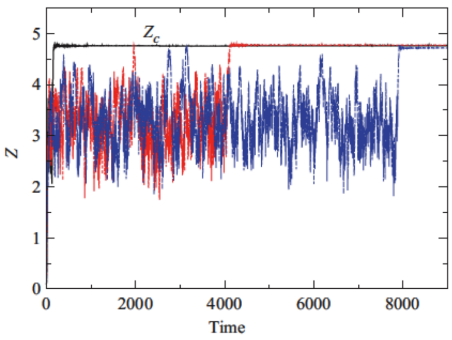

Figure 6.15: Mean number of contacts per grain Z as a function of time, for the simulations shown in Fig.6.13. The system jams when Z reaches a critical value Z_c.

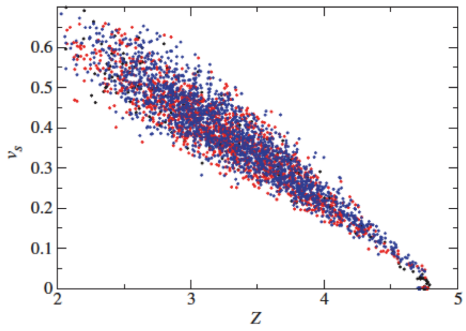

Figure 6.16: Parametric plot of the velocity of the top plate versus the mean number of contacts, obtained from the data shown in Fig.s 6.13 and 6.15. The collapse indicates the existence of a correlation between Z and v_s: the higher Z, the slower the system.

6.5.2 Fluctuations of the micro-structure of the system

Figure 6.15 illustrates the time evolution of the mean number of contacts per grain, $Z(t)$, for the same simulations considered in Fig. 6.13. At the beginning of the simulations, as a consequence of the considered preparation protocol, $Z(t = 0) = 0$. $Z(t)$ rapidly increases as the system start flowing, and then fluctuates around a constant value in the following steady flowing phase. A comparison between Fig. 6.13 and Fig. 6.15 suggests the presence of a correlation between the shear velocity $v_s(t)$ and the mean contact number $Z(t)$, whereby large values of Z occurs when the shear velocity is small, and

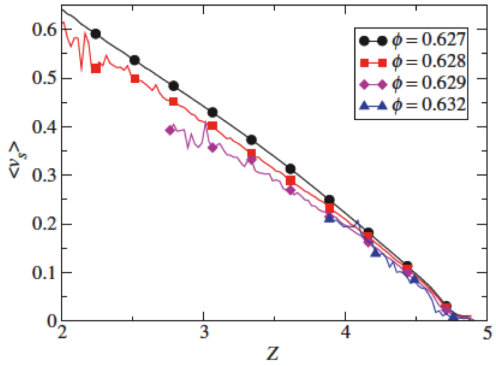

Figure 6.17: Dependence of the average shear velocity $\langle v_s \rangle$ as a function of the mean number of contacts per grain at $\sigma = 2 \cdot 10^{-3}$, for the indicated values of the volume fraction.

conversely. An analogous correlation is found between $v_s(t)$ and the pressure on the confining walls (not shown).

These correlation are evidenced in Fig. 6.16, which shows a parametric plot of $v_s(t)$ versus $Z(t)$ for the same simulations considered in Fig. 6.13 and Fig. 6.15. In such a representation, data sets characterized by very different jamming times display a very similar behaviour. Note that the fluctuations of the shear velocity decreases as the mean number of contacts increases, suggesting the presence of a well defined critical mean number of contacts Z_c at which jamming occurs, in agreement with the results of Fig. 6.15.

We plot in Fig. 6.17 the averaged shear velocity as a function of the mean number of contacts, $\langle v_s(Z) \rangle$ for the indicated values of the volume fraction. The figure suggests that Z_c is almost independent on the volume fraction, consistently with the previous finding (see Sec. 6.4.3) of a volume fraction range where granular systems with equal mechanical properties can be prepared.

On the contrary, as shown in Fig.s 6.18a,b Z_c increases with the applied shear stress. Considering that the shear modulus is expected to increase with the mean contact number [24], this result suggests that the shear modulus of frictional jammed systems does not simply depend on its volume fraction, but also on the applied stresses which caused jamming, i.e. on the history of the system.

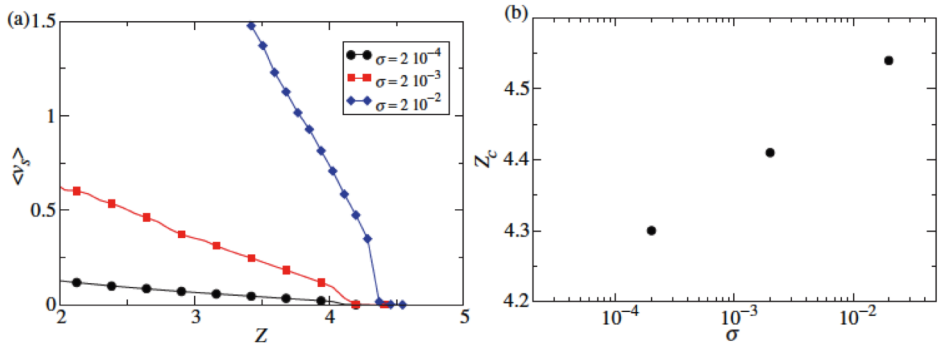

Figure 6.18: At $\phi = 0.629$, **a)**: average shear velocity $\langle v_s \rangle$ versus mean number of contacts per grain for the indicated values of the shear stress, and **b)**: jamming critical mean contact number Z_c as a function of the applied shear stress.

6.5.3 Jamming mechanism

Here we propose a qualitative mechanism to explain the origin of the 'Flow & Jam' phenomenology, based on the behavior of the shear velocity $\langle v_s(t) \rangle$ and of the mean contact number $Z(t)$, as well as on the dependence of t_{jam} and Z_c on the control parameters.

The starting point is the well known *dilatancy phenomenon* [186, 187, 188]. , which is the tendency of a particulate system to expand when flowing. Dilatancy has been mainly investigated at constant pressure and constant shear strain rate, whereby a dilation is actually observed, the larger the greater the shear velocity [189]. By contrast, at constant volume, which is the case considered here, dilation is by definition forbidden and we speculate that such an impeded dilatancy could be at the origin of the phenomenology observed in the 'Flow & Jam' region.

While flowing, the system visits different microscopic configurations, each one having a typical mean number of contact Z. When Z is small, particles exert a small resistance to the applied stress, the shear rate increases and the system tends to dilate. This leads to a configuration with a larger mean number of contacts, exerting a larger resistance, which causes the system to decelerate: this is the constant volume counterpart of the dilation observed at constant pressure.

The existence of such a feedback mechanism is suggested by the correlations between Z and v_s illustrated in Fig. 6.16. The impeded dilatancy appears therefore responsible for the fluctuations of the mean number of contacts. The flowing system jams as a result of a large fluctuation of the mean

number of contacts Z, which reaches the critical value Z_c corresponding to configurations able to sustain the applied stress.

How frequent are these fluctuations? We expect these fluctuations to be more rare when the volume fraction is small, simply because there are fewer configurations able to sustain the applied stress (i.e. with $Z = Z_c$): this explains why the jamming time increases as the volume fraction decreases. Also, one expects that when the volume fraction is smaller than a threshold value, there are no configurations with $Z = Z_c$, which explains why the jamming time diverges decreasing the volume fraction.

6.6 Checking the robustness of the results

6.6.1 Finite size effects

In this section, we discuss the robustness of the jamming phase diagram on the system size. We have performed this investigation keeping the size of the system in the transverse directions fixed, $l_x = l_y = 16D$, and varying the vertical size l_z. We compare the results for $l_z = 8$, described in Sec. **??**, with results obtained with $l_z = 16$ and $l_z = 32$. Data refer to $\sigma = 5 \cdot 10^{-3}$ and $\mu = 0.8$.

Finite size effects at ϕ_{J_1}

The jamming volume fraction ϕ_{J_1} is that where the time $t_{\rm jam}$ a system flows in a steady state before jamming diverges on decreasing the volume fraction. The numerical identification of ϕ_{J_1} is difficult because it involves a diverging timescale, and because $t_{\rm jam}$ widely fluctuates from run to run. This implies that a large number of runs are required to reliably estimate $t_{\rm jam}$ at each value of σ, ϕ and μ. The computational cost required to assess the presence/absence of finite size effects at ϕ_{J_1} is therefore prohibitive; accordingly, while we have observed the phenomenology at all values of the system size we have considered, and also when $l_z = 64D$, we cannot exclude that this phenomenology disappears in the infinite system size limit (where it could be that $\phi_{J_1} = \phi_{J_2}$).

Nevertheless, here we show data clarifying that $\phi_{J_1} < \phi_{J_2}$ in very large systems, even larger than those considered in many experiments of sheared granular particles [61, 62, 63]. This clarifies that the reported phenomenology is experimentally relevant.

Practically, we have determined the probability p that a simulation jams in a given time T as a function of ϕ, for different values of l_z. The probability

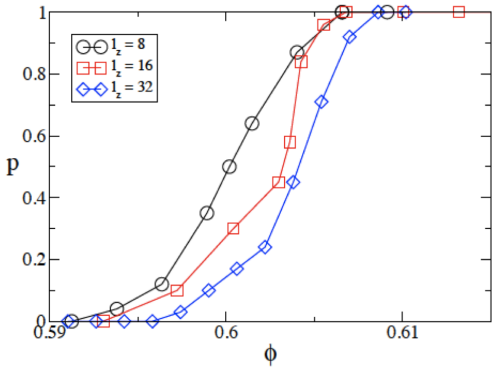

Figure 6.19: Volume fraction dependence of the fraction of simulations (over 100) jamming in a time $T = 100$, for different values of l_z.

is computed over 100 runs with different initial conditions, while the simulation time is fixed to $T = 100$. The results, which are shown in Fig. 6.19, clarify that the 'Flow & Jam' phenomenology is observed up to $l_z = 32$. Note that this data cannot be used to infer the fate of the ϕ_{J_1} line in the thermodynamic limit, as one should also consider the $T \to \infty$ limit.

Finite size effects at ϕ_{J_2}

For each value of l_z, we have measured the shear viscosity η in the steady state, which is found to diverge as a power law at a size independent ϕ_{J_2} value, as shown in Fig. 6.20. Data of different system sizes can be reasonably scaled on the same curve, which indicates that our system is large enough for finite size effects at ϕ_{J_2} to be negligible.

Finite size effects at ϕ_{J_3}

At the jamming line ϕ_{J_3}, defined as the volume fraction at which the 'slip' vanishes, structural quantities have cusps, as shown in Fig. 6.12. To investigate the dependence of the line ϕ_{J_3} on the system size, we have studied the size dependence of the location of the cusp in the pressure. As shown in Fig. 6.21, the cusp occurs at the same volume fraction regardless of the system size, implying that the line ϕ_{J_3} is not affected by finite size effects.

6.6.2 Preparation protocols

Due to the presence of frictional forces, the response of granular systems to applied perturbations may depend on the particular protocol used to pre-

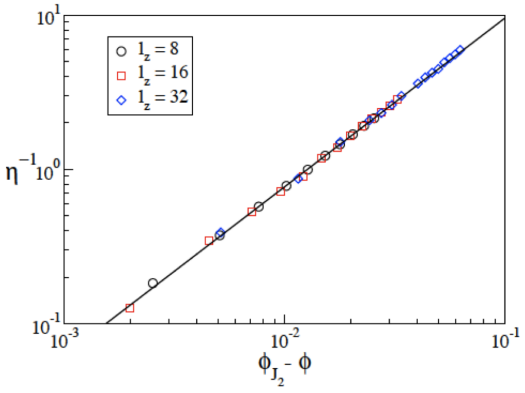

Figure 6.20: Log-log plot of the inverse shear viscosity η^{-1} versus $\phi_{J_2} - \phi$, for different system sizes. The data collapse on the same curve ($\eta^{-1} \simeq (\phi_{J_2} - \phi)^{\gamma}$, $\gamma \simeq 1.1$), indicating that finite-size effects are negligible.

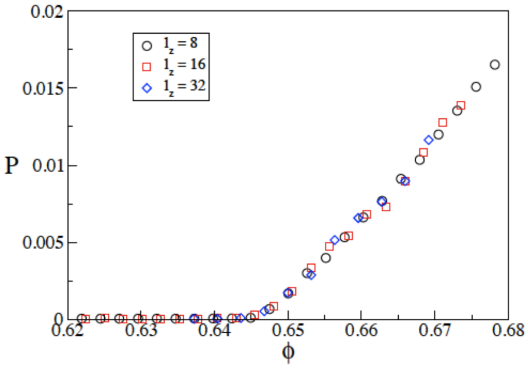

Figure 6.21: Normal pressure acting on the top confining plate as a function of the volume fraction, for different system sizes.

pare the initial state. The phenomenology described so-far is observed when frictional forces are introduced after the system has reached a state of zero kinetic energy at the desired volume fraction. This memoryless protocol give access to the whole zero pressure jamming phase diagram [169].

Here, we consider how our findings change when the initial packing is prepared using a different and popular protocol (see, for instance, Ref.s [66, 190]), where friction is always taken into account. Frictional grains, initially placed in random positions with small radii, are inflated until they reach their final size. We use the same inflation rate Γ both when using the protocol considered in the manuscript ('no friction protocol'), as well as when using

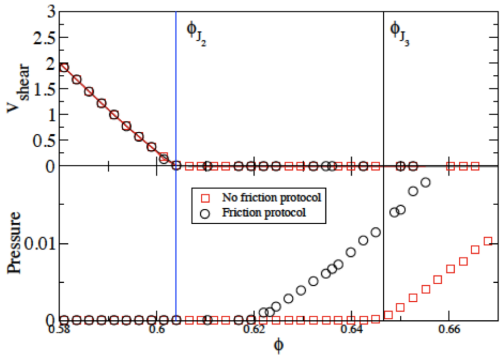

Figure 6.22: (Color online) Location of the jamming transition lines as found using different protocols to prepare the initial state. ϕ_{J_1} and ϕ_{J_2} are protocol independent, while the line ϕ_{J_3} depends on the protocol. Our estimate for ϕ_{J_3} is an upper bound for all possible estimations obtained using different protocols.

the modified protocol ('friction protocol'). In Fig. 6.22 we compare, for $\sigma = 5 \cdot 10^{-3}$ and $\mu = 0.8$, the velocity of the shear plate (upper panel), and the pressure (lower panel) obtained using the two protocols. The pressure is normal force acting on the top plate divided by its surface.

The shear velocity is the same regardless of the initial protocol, in agreement with the expectation that flowing systems do not remember their initial state. Accordingly, the line ϕ_{J_2}, where the viscosity diverges (the velocity vanishes), is protocol independent. The same is true for the line ϕ_{J_1} (not show), which is determined from the divergence of the jamming time, also measured when the system flows.

The pressure, which is shown in the bottom panel, has a cusp at ϕ_{J_3} (at small σ). Fig. 6.22 clarifies that the line ϕ_{J_3} depends on the preparation protocol. The line obtained with the 'no friction' protocol used in this work is an upper bound with respect to the lines obtained using other preparation protocols.

Chapter 7

Conclusions

In this Thesis we have studied two different aspects of the Jamming transition, the glassy dynamics in a model of supercooled liquid and the rheology of a frictional granular material under shear stress.

In supercooled liquids, upon lowering temperature, the relaxation time dramatically increases and clusters of particles dynamically correlated, known as Dynamical Heterogeneities (DHs), appear. We are interested to clarify structure and dynamics of DHs and their relation with the the structural relaxation process.

To this aim, we have investigated, via Monte Carlo simulations, the 'Kob-Andersen model'. In this kinetic constrained model for glassy dynamics, the density plays the role of an inverse temperature, and a transition of structural arrest appears to occur to at density $\rho_{ka} \simeq 0.88$. The simple properties of the Kob-Andersen model allows us a detailed inspection of DHs, which is more difficult in other models.

We find that:

- Contrary to common belief, structural relaxation and DHs are characterized by different time-scales and therefore they appear less tangled than expected.

- On the one hand, the emergence of DHs is well described by the diffusion of mobile elements, the defects, which allow the relaxation of nearby regions. In particular, the diffusing defects scenario correctly predicts the exponents we find to characterize the behaviour of DHs in our systems. On the other hand, the structural relaxation process can be interpreted in terms of a reverse dynamical percolation transition. This geometrical interpretation clarifies that the system relaxes when the percolating cluster disappears, while DH is maximum when spatial correlations between persistent particles

start to decrease: in our case this events are characterizd by different time-scales.

For systems of soft frictional spheres at zero temperature and zero applied stress, the Jamming transition is sharply defined and it has well defined signatures in mechanical and geometrical properties. Moreover, if a finite (but small) shear stress is applied the system behaves as a solid or as liquid, depending on the value of the control parameters. The introduction of inter-particle friction, which is an essential feature of real-world granular materials, makes the jamming phenomenology much more complex. In particular, the state of the system may depend on the time-scale of observation.

Via molecular dynamic simulations of a system of soft frictional spheres, we have investigated the effect of friction on the Jamming transition in the constant volume and constant shear stress ensemble.

We find that:

- The presence of friction leads to the onset of complex regimes characterized by novel dynamical and structural properties. In particular, frictional granular systems may flow in an apparently steady state for a long time, before they suddenly jam. We have proposed a mechanism to describe this dynamical jamming transition, using the concept of impeded dilatancy.

- The rich observed rheology is conveniently described in terms of a 3-dimensional jamming phase diagram with axes volume fraction, shear stress and friction coefficient. This diagram comprises four different regions dived by three transition line. These lines coincide at zero friction, where only two regions exist.

- The observed dynamical regimes have a clear counterpart in geometrical and mechanical properties of jammed states. In particular, when a system jams after flowing, the resulting mean contact number, pressure and shear modulus appear to depend on the applied shear stress, and not on the volume fraction. Moreover, we do not observe 'fragile' behavior in response to small perturbations, contrary to previous suggestions found in the literature.

Perspectives

In model of defects behaving as perfectly random walkers, one finds that the relaxation time and time of maximum dynamical correlation length scale in the same way, $\tau \propto t^*_\xi$. However in cooperative kinetic constrained model, such

as Kob-Andersen model, defects are expected to have a complex structure. A problem ahead is to unveil the structure of these defects and how this structure changes on approaching the transition of structural arrest. In fact, one may speculate that the decoupling between τ and t^*_ξ may be due to a more complex nature of defects, such as the non-conservation of defects characterized by birth and death rates with a constant average number, or the presence of heterogeneous defects. A second open question is to check whether the insights found for the Kob-Andersen model can be extended to continuous model of glass former.

Concerning granular materials, open questions ahead include the relation of the observed jamming transitions with phenomena seen at constant shear rate, where Jamming is by definition precluded. In addition, the role of other parameters which are expected to control the jamming transition of frictional systems, as the confining pressure, should be investigated. Future plans also include the investigation of the role of temperature in the jamming of frictional thermal particles. For example, large colloidal particles, with a size of roughly $1\mu m$, are in fact at the same time small enough for temperature to influence their dynamics, and large enough to be characterized by frictional forces.

Bibliography

[1] A. J. Liu and S. R. Nagel, Nature 396, 21 (1998).

[2] Van Hecke J. Phys.: Condens. Matter 22, 033101 (2010).

[3] V. Trappe, V. Prasad, Luca Cipelletti, P. N. Segre, D. A. Weitz, Nature 411 (2001).

[4] P.G. Debenedetti and F. H. Stillinger, Nature 410, 259 (2001).

[5] C.A. Angell, J. Non-Cryst. Solids, 102, 205 (1998).

[6] A. Cavagna, Phys. Rep. 476, 51 (2009).

[7] R. A. L. Jones, Soft condensed matter, Oxford University Press (2002).

[8] P. J. Lu, E. Zaccarelli, F. Ciulla, A. B. Schofield, F. Sciortino, D. A. Weitz, Nature 453 (2008).

[9] P. N. Pusey and W. Van Megen, Nature 320 (1986).

[10] E. Del Gado, A. Fierro, L. de Arcangelis , and A. Coniglio, EuroPhys. Lett., 63 (1), pp. 1[U+FFFD] (2003).

[11] P. N. Pusey, E. Zaccarelli, C. Valeriani, E. Sanz, W. C. K. Poon, and M.E. Cates, Phil. Trans. R. Soc. A 367, 1909 (2009).

[12] P.J. Flory, The Physics of Polymer Chemistry (Cornell University Press, Ithaca, 1954).

[13] P.G. de Gennes, Scaling Concepts in Polymer Physics (Cornell University Press, Ithaca, 1993).

[14] D. Stauffer, A. Coniglio, and M. Adam, Adv. Polym. Sci. 44, 103 (1982).

[15] P G de Gennes and L Leger, Ann. Rev. Phys. Chem. Vol. 33: 49-61 (1982).

[16] R. Hohler, S. Cohen-Addad, Rheology of liquid foam. J. Phys: Condens. Matter 17, R1041 (2005).

[17] T. G. Mason, Current Opinion in Colloid and Interface Science 4 (1999) 231-238.

[18] S. Tcholakova, N. D. Denkov K. Golemanov K. P. Ananthapadmanabhan and A. Lips, Phys. Rev. E 78, 011405 (2008).

[19] R. Lespiat, S. Cohen-Addad and Reinhard Hohler, Phys. Rev. Lett. 106, 148302 (2011).

[20] G. Katgert and M. van Hecke, EPL, 92, 34002, (2010).

[21] M. Jaeger, S. R. Nagel, B. Behringer, Rev. of Mod. Phys. 68, 1259 (2000).

[22] I. Aranson, L. Tsmiring, Rev. of Mod. Phys. 78, 641 (2006).

[23] M. E. Cates, J. P. Wittmer, J. P. Bouchaud, and P. Claudin, Phys. Rev. Lett 81, 1841 (1998).

[24] C. O'Hern, L. E. Silbert, A. J. Liu, and S. R. Nagel, Phys. Rev. E 68, 011306 (2003).

[25] W.T. Laughlin and D.R. Uhlmann, J. Phys. Chem. 76, 2317 (1972).

[26] C.A. Angell, J. Non-Cryst. Solids, 102, 205 (1998).

[27] C.A. Angell, Relaxation in Complex Systems, edited by K.L. Ngai and G.B. Wright (US Dept. Commerce, Springfield, 1985).

[28] T. Hecksher, A. I. Nielsen, N. B. Olsen, and J. Dyre, Nature Phys. 4, 737 (2008).

[29] W. Kauzmann, Chem. Review 43, 219 (1948).

[30] M. Goldstein, J. Chem. Phys. 51, 3728 (1969).

[31] J.-P. Hansen and I.R. McDonald, Theory of Simple Liquids (Academic Press, London, 1986).

[32] M.P. Allen and D.J. Tildesley, Computer Simulations of Liquids (Clarendon Press, Oxford, 1987).

[33] B. J. Alder and T. E. Wainwright, Phys. Rev. 127, 359 (1962).

[34] W. Kob, Supercooled Liquids, the Glass Transition and Computer Simulations, edited by J.-L. Barrat, M. Feigelman, J. Kurchan and J. Dalibard, Les Houches. Session LXXVII, 2002 (EDP Sciences, Les Ulis; Springer-Verlag, Berlin, 2003),199.

[35] D.L. Price and J.M. Carpenter, J. Non-Cryst. Solids 92, 153 (1987).

[36] G. Biroli, J.-P. Bouchaud, A. Cavagna, T. S. Grigera and P. Verrocchio, Nature Physics 4, 771 (2008).

[37] J. Cardy, Scaling and Renormalization in Statistical Physics, Cambridge University Press, Cambridge (1996).

[38] W. Kob and H.C. Andersen, Phys. Rev. Lett. 73, 1376 (1994).

[39] W. Kob and H.C. Andersen, Phys. Rev. E 52, 4134 (1995).

[40] T.B. Schroder, S. Sastry, J.C. Dyre, S.C. Glotze, J. Chem. Phys. 112, 9834 (2000).

[41] K. Binder and W. Kob, Glassy materials and disordered solids (World Scientific, Singapore, 2005).

[42] E. Rossler, Phys. Rev. Lett., 65, 1595, (1990).

[43] F. Fujara, B. Geil, H. Sillescu and G. Fleischer, Z. Phys. B 88, 195 (1992).

[44] I. Chang, F. Fujara, B. Geil, G. Heuberger, T. Mangel, H. Sillescu, J. Non-Cryst. Solids 248, 172 (1994).

[45] M.T. Cicerone and M.D. Ediger, J. Chem. Phys. 104, 7210 (1996).

[46] W. Kob and H.C. Andersen, Phys. Rev. E 51, 4626 (1995).

[47] A. J. Liu and S. R. Nagel, Ann. Rev. of Cond. Mat. Phys. 1, 347 (2010).

[48] M. Pica Ciamarra, A. Coniglio and A. de Candia, Soft Matter 6, 2975 (2010).

[49] P. Chaudhuri, L. Berthier and S. Sastry, Phys. Rev. Lett. 104, 165701 (2010).

[50] M. Hermes and M. Dijkstra, EPL 89, 38005 (2010).

[51] D. Vagberg, P. Olsson and S. Teitel, Phys. Rev. E 83, 031307 (2011).

[52] D.J. Durian, Phys. Rev. Lett. 75, 4780 (1997).

[53] J.A. Drocco, M.B. Hastings, C.J. Olson Reichhardt, and C. Reichhardt, Phys. Rev. Lett. 95, 088001 (2005).

[54] P. Olsson, S. Teitl, Phys. Rew. Lett. 99, 178001 (2007).

[55] M. Wyart, L.E.Silbert, S.R. Nagel and T.A. Witten Phys. Rev. E 72, 051306 (2005).

[56] W.G. Ellenbroek, M. van Hecke, W. van Saarloos, Phys. Rev. E 80, 061307 (2009).

[57] T. R. Kirkpatrick, D. Thirumalai, Phys. Rev. Lett. 58, 2091 (1987).

[58] C. Toninelli, G. Biroli, D. S. Fisher Phys. Rev. Lett. 92, 185504 (2004).

[59] J. Chalupa, P. Leath, G. R. Reich, J. Phys. C 12, L31 (1979)

[60] J.M. Schwarz, A.J. Liu, L.Q. Chayes, Europhys. Lett. 73, 560 (2006).

[61] D.J. Pine, contribution to KITP Program on Granular Physics, 2005, unpublished.

[62] J.-C. Tsai and J.P. Gollub, Phys. Rev. E 72, 051304 (2005).

[63] K.E. Daniels and R.P. Behringer, Phys. Rev. Lett. 94, 168001 (2005).

[64] L.E. Silbert, D. Ertas, G.S. Grest, T.C. Halsey, and D. Levine, Phys. Rev. E 65, 031304 (2002).

[65] H.A. Makse, D.L. Johnson, and L.M. Schwartz, Phys. Rev. Lett. 84, 4160 (2000).

[66] H.P. Zhang and H.A. Makse, Phys. Rev. E 72, 011301 (2005).

[67] E. Somfai, M. van Hecke. W.G. Ellenbroek, K. Shundyak, W. van Saarloos, Phys. Rev. E 75 020301 (R) (2007).

[68] M. Pica Ciamarra and A. Coniglio, Phys. Rev. Lett. 103, 235701 (2009).

[69] D.S. Grebenkov, M. Pica Ciamarra, M. Nicodemi and A. Coniglio, Phys. Rev. Lett. 100, 078001 (2008).

[70] M. E. Cates, J. P. Wittmer, J.-P. Bouchaud, and P. Claudin, Jamming and stress propagation in particulate matter, Phys. A 263, 35(1999).

[71] Soft and Fragile Matter. CRC Press. ISBN 0750307242.

[72] R.S. Farr, J.R. Melrose, and R.C. Ball, Phys. Rev. E 55, 7203 (1997); R.C. Ball and J.R. Melrose, Adv. Colloid Interface Sci. 59, 19 (1995); J.R. Melrose and R.C. Ball, Europhys. Lett. 32, 535 (1995).

[73] C. Goldenberg, Phys. Rev. Lett 89, 084302 (2002).

[74] M. D. Ediger, Annu. Rev. Phys. Chem. 51, 99 (2000).

[75] H. Sillescu, J. Non-Cryst. Solids 243, 81 (1999).

[76] A. S. Keys, A. R. Abate, S. C. Glotzer, and D. J. Durian, Nature Phys., 3, 260 (2007).

[77] E. R. Weeks, J. C. Crocker, A. C. Levitt, A. Schofield, and D. A. Weitz, Science, 287, 627 (2000).

[78] O. Dauchot, G. Marty, and G. Biroli, Phys. Rev. Lett., 95, 265701 (2005).

[79] F. Ritort and P. Sollich, Adv. Phys., 52, 219, (2003).

[80] C. B. Picallo, J. M. Lopez, S. Zapperi, M. J. Alava, Phys. Rev. Lett. 105, 155502 (2010).

[81] L. Laurson, M.C. Miguel and M.J. Alava, Phys. Rev. Lett. 105 , 015501 (2010).

[82] R. Kohlrausch, Ann. Phys. (Leipzig) 12, 393 (1847).

[83] G. Williams and D.C. Watts, Trans. Faraday Soc. 66, 80 (1980).

[84] C. A. Angell, K. L. Ngai, G. B. McKenna, P. F. McMillan and S. W. Martin, J. Appl. Phys. 88, 3113 (2000).

[85] D. Perera and P. Harrowell, Phys. Rev. E 54, 1652 (1996).

[86] W. Kob, C. Donati, S.J. Plimpton, P. H. Poole and S.C. Glotzer, Phys. Rev. Lett. 79, 2827 (1997).

[87] C. Donati, J.F. Douglas, W. Kob, S.J. Plimpton, P.H. Poole and S.C. Glotzer, Phys. Rev. Lett. 80, 2338 (1998).

[88] B. Doliwa and A. Heuer, Phys. Rev. Lett. 80, 4915 (1998).

[89] W.K. Kegel and A. van Blaaderen, Science 287 290 (2000).

[90] L. Berthier, and W. Kob, J. Phys.: Condens. Matter, 19, 205130 (2007).

[91] E. Vidal Russell and N. E. Israeloff, Nature 408, 695 (2000).

[92] A. Widmer-Cooper, H. Perry, P. Harrowell, and D. R. Reichman, Nature Phys., 4, 711 (2008).

[93] S. F. Edwards and P. W. Anderson, J. Phys. F: Metal Phys. 5, 965 (1975).

[94] K. Binder and A.P. Young, Rev. Mod. Phys. 58, 801 (1986).

[95] E. R. Weeks, J. C. Crocker, and D. A. Weitz, J. Phys.: Condens. Matter 19, 205131 (2007).

[96] P.Mayer, H. Bissig, L. Berthier, L. Cipelletti,J. P. Garrahan, P. Sollich, and V. Trappe, Phys. Rev. Lett. 93, 115701 (2004).

[97] A. Duri and L. Cipelletti, Europhys. Lett. 76, 972 (2006).

[98] S. Franz, C. Donati, G. Parisi, and S. C. Glotzer, Philos. Mag. B 79, 1827 (1999).

[99] C. Bennemann, C. Donati, J. Baschnagel, and S. C. Glotzer, Nature 399, 246 (1999).

[100] N. Lacevic, F.W. Starr, T. B. Schroder, and S. C. Glotzer, J. Chem. Phys. 119, 7372 (2003).

[101] S. C. Glotzer, J. Non-Cryst. Solids 274, 342 (2000).

[102] L. Berthier, Phys. Rev. E 69, 020201(R) (2004).

[103] M. Vogel and S. C. Glotzer, Phys. Rev. E 70, 061504 (2004).

[104] L. Berthier, G. Biroli, J.-P. Bouchaud,W. Kob, K. Miyazaki, and D. R. Reichman, J. Chem. Phys. 126, 184503 (2007).

[105] L. Berthier, Phys. Rev. E 76, 011507 (2007).

[106] C. Toninelli, M. Wyart, L. Berthier, G. Biroli, and J.-P. Bouchaud, Phys. Rev. E 71, 041505 (2005).

[107] C. Donati, S.C. Glotzer and P.H. Poole, Phys. Rev. Lett. 82, 5064 (1999).

[108] C. Donati, S. Franz, S.C. Glotzer, G. Parisi, J. Non-Cryst. Solids 307, 215 (2002).

[109] P. Ballesta, A. Duri, and L. Cipelletti, Nature Phys. 4, 550 (2008).

[110] B. Doliwa and A. Heuer, Phys. Rev. E 61, 6898 (2000).

[111] L. Berthier, G. Biroli, J.-P. Bouchaud, W. Kob, K. Miyazaki, and D. R. Reichman, J. Chem. Phys. 126, 184503 (2007).

[112] S. Whitelam, L. Berthier, and J. P. Garrahan, Phys. Rev. Lett. 92, 185705 (2004).

[113] R. S. L. Stein and H. C. Andersen, Phys. Rev. Lett. 101, 267802 (2008).

[114] S. Karmakara, C. Dasgupta, and S. Sastry, Proc. Natl. Acad. Sci. USA 106, 3675 (2009).

[115] D. Chandler, J. P. Garrahan, R. L. Jack, L. Maibaum and A. C. Pan, Phys. Rev. E 74, 051501 (2006).

[116] F. Lechenault, O. Dauchot, G. Biroli, J. P. Bouchaud Europhys. Lett. 83, 46002 (2008).

[117] F. Lechenault, O. Dauchot, G. Biroli, J. P. Bouchaud, Europhys. Lett. 83, 46003 (2008).

[118] C. Heussinger, L. Berthier, and J.-L. Barrat, arXiv:1001.0914.

[119] C. Dasgupta, A.V. Indrani, S. Ramaswamy, M.K. Phani, Europhys. Lett. 15, 307 (1991) [Addendum: ibidem 467].

[120] G. Parisi, J. Phys. A: Math. Gen. 30, L765 (1997).

[121] L. Berthier and G. Biroli, Rev. Mod. Phys. 83, 587 (2011).

[122] S. Chandrasekhar, Rev. Mod. Phys. 15, 1 (1943).

[123] J.H. Gibbs, J. Chem. Phys. 25, 185 (1956).

[124] J.H. Gibbs and E.A. Di Marzio, J. Chem. Phys. 28, 373 (1958).

[125] G. Adam and J.H. Gibbs, J. Chem. Phys. 43, 139.

[126] M. Mezard, G. Parisi and M.A. Virasoro, Spin-Glass theory and beyond (World Scientific, Singapore, 1987).

[127] D.J. Gross and M. Mezard, Nucl. Phys. B 240, 431 (1984).

[128] T. Castellani and A. Cavagna, J. Stat. Mech. P05012 (2005).

[129] R. Zwanzig, Lectures in Theoretical Physics, edited byW.E. Britton, B.W. Downs and J. Downs (Wiley, NewYork, 1961), 135.

[130] H. Mori, Prog. Theor. Phys. 33, 423 (1965).

[131] A. Coniglio, T. Abete, A. de Candia, E. Del Gado, A. Fierro, R. Pastore and M. Pica Ciamarra, *Geometrical characterization of dynamical heterogeneities in chemical gels, colloidal gels and colloidal glasses*, accepted in Proceedings of the International School of Physics 'E. Fermi', Course CLXXVI - 'Complex materials in physics and biology'.

[132] E. Leutheusser, Phys. Rev. A, 29, 2765 (1984).

[133] W. Gotze and L. Sjogren, Rep. Prog. Phys. 55, 241 (1992).

[134] D. R. Reichman and P. Charbonneau , J. Stat. Mech. P05013 (2005).

[135] R. Kohlrausch, Ann. Phys. (Leipzig) 12, 393 (1847).

[136] T.B. Schroder, S. Sastry, J.C. Dyre, S.C. Glotze, J. Chem. Phys. 112, 9834 (2000).

[137] A.P. Sokolov, J. Non-Cryst. Solids 235-237, 190 (1998).

[138] L. Berthier, G. Biroli, J.-P. Bouchaud, W. Kob, K. Miyazaki, and D. R. Reichman, J. Chem. Phys. 126, 184504 (2007).

[139] T.R. Kirkpatrick and P.G. Wolynes, Phys. Rev. A, 35, 3072 (1987)

[140] T.R. Kirkpatrick, D. Thirumalai and P.G. Wolynes, Phys. Rev. A 40, 1045 (1989).

[141] C. Dalle-Ferrier, C. Thibierge, C. Alba-Simionesco, L. Berthier, G. Biroli, J.P. Bouchaud, F. Ladieu, D. L'Hote,, and G. Tarjus, Phys. Rev. E, 76, 041510 (2007).

[142] S. Capaccioli, G. Ruocco, and F. Zamponi, J. Phys. Chem. B, 112, 10652 (2008).

[143] X. Y. Xia and P. G. Wolynes, Proc. Natl. Acad. Sci. USA, 97, 2990 (2000).

[144] G. Biroli and J.P. Bouchaud, arXiv:0912.2542 (2009).

[145] J. D. Stevenson, J. Schmalian, and P. G. Wolynes, Nature Phys., 2, 268 (2006).

[146] D. Chandler and J. P. Garrahan, Annu. Rev. Phys. Chem. 61, 191 (2010).

[147] F. Ritort and P. Sollich, Adv. Phys. 52, 219 (2003).

[148] R. Pastore, M. Pica Ciamarra, A. de Candia and A. Coniglio, Phys. Rev. Lett. 107, 065703 (2011).

[149] W. Kob and H.C. Andersen, Phys. Rev. E 48, 4364 (1993).

[150] C. Toninelli, G. Biroli, D. S. Fisher, Phys. Rev. Lett. 92, 18 (2004).

[151] S. Franz, R. Mulet and G. Parisi, Phys. Rev. E 65, 021506 (2002).

[152] E. Marinari and E. Pitard, Europhys. Lett. 69, 2 (2004).

[153] L. Berthier, G. Biroli, J.-P. Bouchaud, and R. L. Jack, in Dynamical Heterogeneities in Glasses, Colloids, and Granular Media, edited by L. Berthier, G. Biroli, J.-P. Bouchaud, L. Cipelletti, and W. van Saarloos (Oxford University, New York, to be published).

[154] P. Ballesta, A. Duri and L. Cipelletti, Nature Physics 4, 550 (2008).

[155] S. C. Glotzer, V. N. Novikov and T, B. Schrøoder J. Chem. Phys. 112, 509 (2000).

[156] A. Fierro, A. de Candia and A. Coniglio, Phys. Rev. E 62, 7715 (2000).

[157] J.T. Bendler and M.F. Shlesinger, Journal of Statistical Physics 53, 531 (1988).

[158] S.B. Yuste, J. Klafter, and K. Lindenberg, Phys. Rev. E 77, 032101 (2008).

[159] A. Ordemann, G. Berkolaiko, S. Havlin, and A. Bunde, Phys. Rev. E 61, R1005 (2000).

[160] T. Abete, A. de Candia, D. Lairez and A. Coniglio, Phys. Rev. Lett. 93, 228301 (2004).

[161] V. Sidoravicius and A. S. Sznitman, Comm. Pure Appl. Math. 62, 831 (2009).

[162] D. Stauffer and A. Aharony, *Introduction to percolation Theory* (Taylor and Francis, London 1992).

[163] A. Coniglio A and R. Figari, J. Phys. A: Math. Gen. 16, L535 (1983).

[164] M. Pica Ciamarra, R. Pastore, M. Nicodemi and A. Coniglio, Phys. Rev. E 84, 041308 (2011).

[165] R. Pastore, M. Pica Ciamarra and A. Coniglio, *Mechanical response of jammed granular materials and the question of 'fragility'*, to appear in Granular Matter.

[166] R. Pastore, M. Pica Ciamarra and A. Coniglio, Phil. Mag. 91,13, 2006 (2011).

[167] K. Shundyak, M. van Hecke and W. van Saarloos, Phys. Rev. E 75, 010301 (2007).

[168] V. Magnanimo, L. La Ragione, J. T. Jenkins, P. Wang and H.A. Makse Europhysics Letters 81, 34006 (2008).

[169] C. Song, P. Wang and H.A. Makse, Nature 453, 629 (2008).

[170] J. Durian, Sands, Powders, and Grains, An Introduction to the Physics of Granular Materials, Springer, 2000.

[171] P. A. Cundall and O. D. L. Strack, Geotechnique 29, 47 (1979).

[172] L.E. Silbert et al. Phys Rev. E 64, 051302 (2001).

[173] G-J Gao, J. Blawzdziewicz, C. S. O'Hern and M. Shattuck, Phys. Rev. E 80, 061303 (2009).

[174] K. Chen et al., Nature 442, 257 (2006).

[175] J.-C. Tsai, G.A. Voth, and J.P. Gollub, Phys. Rev. Lett. 91, 064301 (2003).

[176] K.E. Daniels and R.P. Behringer, Phys. Rev. Lett. 94, 168001 (2005).

[177] M. Pica Ciamarra, A. Coniglio, D. De Martino, M. Nicodemi, Eur. Phys. J. E 24, 411 (2007).

[178] G.R. Farrell, K.M. Martini and N. Menon, Soft Matter 6, 2925 (2010).

[179] G.Y. Onoda and E.G. Liniger, Phys. Rev. Lett. 64, 2727 (1990).

[180] L.E. Silbert, Soft Matter 6, 2918 (2010).

[181] M. Pica Ciamarra and A. Coniglio, Phys. Rev. Lett. 101, 128001 (2008).

[182] C. Heussinger and J.–L. Barrat, Phys. Rev. Lett. 102, 218303 (2009).

[183] M. Pica Ciamarra, M. Nicodemi and A. Coniglio, Soft Matter 6, 2871 (2010).

[184] H. Yoshizawa, Y-L Chen and J. Israelachvili, J. Phys. Chem. 97, 4128 (1993).

[185] J. Crassous, L. Bocquet, S. Ciliberto and C. Laroche, Europhysics Letters 47, 562 (1999).

[186] O. Reynolds, Philos. Mag. 20, 469 (1885).

[187] O. Reynolds, Proc. Royal Inst. 2, 354 (1886).

[188] A.J. Kabla and T.J. Senden, Phys. Rev. Lett. 102, 228301 (2009).

[189] G.W. Scott Blair, Elementary Rheology, Academic Press, London (1969).

[190] E. Somfai, M. van Hecke. W.G. Ellenbroek, K. Shundyak, W. van Saarloos, Phys. Rev. E 75 020301 (R) (2007).